UNIVERSITY OF CALGARY

Apparatus to Investigate Rag Layer Growth

by

Jorge Luis Andrade Rios

A THESIS
SUBMITTED TO THE FACULTY OF GRADUATE STUDIES
IN PARTIAL FULFILMENT OF THE REQUIREMENTS FOR THE
DEGREE OF MASTER IN SCIENCE IN CHEMICAL ENGINEERING

DEPARTMENT OF CHEMICAL AND PETROLEUM ENGINEERING

CALGARY, ALBERTA
SEPTEMBER, 2009

UNIVERSITY OF CALGARY

FACULTY OF GRADUATE STUDIES

The undersigned certify that they have read, and recommend to the Faculty of Graduate Studies for acceptance, a thesis entitled " Apparatus to Investigate Rag Layer Growth " submitted by Jorge L. Andrade Rios in partial fulfillment of the requirements of the degree of Master in Science in Chemical Engineering.

Supervisor, Dr. H. W. Yarranton
Department of Chemical and Petroleum Engineering

Dr W.Y. Svrcek.
Department of Chemical and Petroleum Engineering

Dr. Brij Maini
Department of Chemical and Petroleum Engineering

Dr. Larry Lines
Department of Geoscience

Date

Abstract

During oil sands froth treatment, a rag layer, or dense packed zone, can build up between the oil and water interface, and prevent efficient water/oil separation. This rag layer is a relatively stable structure which contains a mixture of water, oil and solids. The objective of this work was the design and methodology for using a continuous separator to study rag layer growth.

The thesis presents the design and testing of a continuous separation apparatus as well as a rag layer growth model based on a mass balance on the water in the rag layer. This model balances the emulsified water entering the rag layer with the water exiting due to coalescence. A methodology to determine these coalescence rates from batch experiments is developed. The model is then tested on rag layer growth data from continuous separation experiments performed on the new apparatus.

All of the experiments were performed on model emulsions consisting of water emulsified into a toluene/*n*-heptane blend and partially stabilized with a surfactant. Batch experiments were performed in a beaker and the decrease in rag layer height and increase in free water height were measured over time. In continuous experiments, the increase in rag layer height over time was also measured. The decrease in rag layer height after shutting of the feed (a decay experiment) was also measured.

The coalescence rate was found to decrease with time, since the emulsions are polydisperse in drop size and larger droplets probably coalesce more rapidly giving a higher initial coalescence rate. The coalescence rate in the batch experiments was typically higher than in the decay experiments. It appears that an instantaneously formed rag layer (batch) coalesces more rapidly than a slowly accumulated rag layer (decay). Continuous rag layer growth could not be predicted from the batch or decay experimental data. However, the steady state rag layer height could be predicted from the decay

experiment data. These conclusions were also applicable to different surfactants and surfactant concentrations.

The predictive capability of the model was tested for different flow rates and separator geometries with the same emulsion system. The rag layer model successfully predicted the increase in rag layer height with an increase in flow rate. The model under-predicted the decrease in rag layer height when a separator with a smaller cross-sectional area was used. It appeared that the coalescence occurs primarily at the water-oil interface rather than throughout the rag layer, hence modifications to the model were made. These results represent a first positive step towards investigating rag layer growth in oil sand froths.

Acknowledgements

First and foremost, I am deeply indebted to my supervisor, Dr. H.W. Yarranton for his guidance, support and encouragement during my Master's degree program. His door was always open whenever I ran into a problem or had a question about anything. It was my privilege and pleasure to be a member of his team. I also wish to thank Ms. Elaine Stasiuk for her assistance and the great help that she provided during my masters research.

I am thankful to the Department of Chemical and Petroleum Engineering of The University of Calgary, NSERC, and Syncrude Canada Ltd. for their financial support throughout my Masters program.

I am grateful to the Asphaltene and Emulsion Research members at the University of Calgary, and fellow graduate students for their useful suggestions.

Finally, from the deepest of my heart, I would give special thanks to my family who are always there supporting me, reminding me and encouraging me. I am really grateful for their caring and understanding.

Dedicated to my Parents

Jorge Luis Andrade Cruz and Raquel Ríos González

TABLE OF CONTENTS

List of Tables

List of Figures

List of Symbols

A	Cross-sectional area (cm^2)
c	Constant
d_p	Droplet or particle diameter
d / D	Particle to column diameter ratio
g	Gravity acceleration (9.8 m/s^2)
h	Height of the rag layer
H	Total height of the dispersion
h_s	Height of sedimentation zone
h_p	Height of dense-packed zone
h_w	Height of free water
h^o	Initial rag layer height
k , k_p	Constants
k	Coalescence rate constant
k_o	Initial coalescence rate
k_s	Steady-state coalescence rate
$\dot{m}_{wo}$	Mass flow rate of free water exiting the rag layer
$\dot{m}_{wi}$	Mass flow rate of water entering the rag layer
M_w	Mass of water in the rag layer
n	Richardson-Zaki's parameter
Re_t	Reynolds number
t	Time
u	Hindered settling rate
V	Volume
V_e	Volume of emulsion layer

V_w^0 Volume of water in the whole mixture

V_w Volume of water layer

$\dot{V}_{in}$ Volumetric flow rate of feed

$\dot{V}_c$ Volumetric flow rate of the continuous phase

$\dot{V}_d$ Volumetric flow rate of the dispersed phase

$\dot{V}_d / A$ Volume flow rate of the dispersed phase per unit area

x Volume per area of the continuous phase

y Volume per area of the dispersed phase

Greeks letters

α_f Volume fraction of fluid or suspension voidage

μ Viscosity

ρ_p Density of the particle

θ Contact angle (°)

ϕ Space-average fraction

ϕ_0 Initial dispersed phase fraction

ϕ_d Dispersed phase fraction

ϕ_w Volume fraction of water in the rag layer

ϕ_w^o Fraction of emulsified water in the feed outlet to the separator

υ_t Terminal velocity of an insolated particle

ψ Volumetric coalescence rate per area

Subscripts

‘ 0 ’ Initial

‘c’ Continuous phase

‘d’ Dispersed phase

‘ *f* ’ Final

‘ *fw* ’ Free water layer

‘ *m* ’ Medium

‘o’ Oil

‘ *p* ’ Dense-packed layer

‘ *s* ’ Sedimentation zone

‘ *S* ’ Sphere or particle

‘ *w* ’ Water

Superscripts

‘ * ’ In the dense-packed zone

‘ 0 ’ Initial

Abbreviation

‘AOT’ Aerosol OT

‘Heptol’ Mixture of heptane and toluene

‘NEO-10’ Nonylphenol ethoxylate with 10 ethoxy groups in the molecule

‘NEO-15’ Nonylphenol ethoxylate with 15 ethoxy groups in the molecule

‘wvf’ Water Volume Fraction

CHAPTER 1 - INTRODUCTION

Most petroleum recovery processes require the separation of water and solids from the crude oil typically via gravity settling or centrifugation, often assisted by heating and chemical addition. During the separation, unresolved water-in-oil emulsions, oil-in-water emulsions, and solid particles sometimes accumulate between the oil and water interface to form a "rag" layer. If the rag layer grows too large, it may overflow into the oil or water outlet streams. If the rag material enters the oil stream, it introduces water and fine solids which may cause corrosion and fouling in downstream processes. If it enters into the water stream, oil recovery is reduced, necessitating further treatment (Saadatmand et at., 2008).

Figure 1.1 Photograph of a rag layer formed during the gravity separation of diluted bitumen froth in a continuous process (Moran, 2006).

Previous research in the Asphaltenes and Emulsions Research Group has focused on the factors that stabilize water-in-crude oil emulsions (Gafonova and Yarranton, 2001; Sztukowski and Yarranton, 2005). However, dynamic factors such as entrained solids can prevent close approach of droplets within the rag layer and contribute to rag layer growth (Saadatmand, 2008b). Also, oilfield emulsions do not coalesce instantaneously, but have a finite coalescence rate. If the settling rate exceeds the coalescence rate, rag layer growth is expected.

Rag layer formation can also occur during oil sands froth treatment (Czarnecki et at., 2007). Oil sands froth is a mixture of bitumen, water, sand, and clays and during froth treatment is diluted with a solvent such as naphtha or a mixture of paraffins (Romanova et at., 2004). Currently, naphtha diluted froths are centrifuged and paraffin diluted froths are gravity settled to achieve separation. In both cases, a rag layer can form that consists of unresolved water-in-oil emulsion and relatively fine solids that are likely intermediate to oil-wet (Chen et at., 1999).

The accumulation of a rag layer depends primarily on the settling rate of the droplets dispersed in the continuous phases and the coalescence rate of the concentrated emulsion. The coalescence rate depends on the interfacial properties of the droplets but may also depends on dynamic factors such as the accumulation of solid particles within the rag layer (Hirasaki et at., 2008).

Previously, batch experiments were performed to assess the effect of process variables on rag layers formed during centrifugation (Saadatmand et at., 2008). The next step is to examine rag layer growth during a continuous gravity settling process. The relationship between measured coalescence rates and rag layer growth has not been established. This study focuses on the design and methodology for using a continuous separator to examine rag layer growth. These results are intended to provide baselines and preliminary models prior to investigating the more complex oil sand froths. The understanding of factors that

contribute to the formation and accumulation of rag layer is required to guide future design choices in new froth treatment processes.

1.1 Objectives

There are three main objectives to this research:

- Develop a methodology to measure macroscopic coalescence rates of model emulsion rag layers (batch experiments).
- Construct a laboratory scale apparatus to study rag layer formation and accumulation (continuous growth and decay experiments where decay is the shrinkage of the rag layer after the emulsion feed is stopped).
- Measure rag layer growth and relate it to coalescence rates for model emulsion systems.

1.2 Thesis Structure

This thesis is distributed into five more chapters.

Chapter 2 defines the rag layer. Emulsions are reviewed including the role of surfactants and solids in emulsion formation, and emulsion destabilization mechanisms. Detailed characteristics of rag layers and a simple model of rag layer growth are reviewed. Finally, rag layers in the oil sands processes are discussed.

Chapter 3 describes the methods for model emulsion preparation and batch coalescence rate experiments. The design of a continuous water-oil separation apparatus is presented and the procedure for the continuous rag layer growth experiments is described.

Chapter 4 presents the derivations of both the batch and continuous material balances, from which a rag layer growth model is developed. This model relates the rag layer

height over time to the emulsion feed rate and the coalescence rate. Validation of some of the model assumptions is also discussed.

Chapter 5 presents the results and modeling of the batch and decay experiments. Data and modeling results are presented for the rag layer growth in the continuous separator. The effect of surfactant concentration and the type of surfactant are outlined. The prediction of the effect of flow rate and separator geometry on rag layer growth in the continuous separator is discussed.

Chapter 6 summarizes the conclusions of this study and suggests recommendations for further research.

CHAPTER 2-LITERATURE REVIEW

During the separation treatment of water and solids from crude oil or bitumen, an intermediate layer at the water/oil interface is formed. This intermediate layer has been described as a rag layer or dense packed zone. The rag layer typically consists of emulsified water, emulsified oil and fine solids suspended in a continuous oil phase. Figure 2.1 shows the formation of rag layer between the oil-water interface during a bottom water and solids spin test (reproduced from Schramm, 2000).

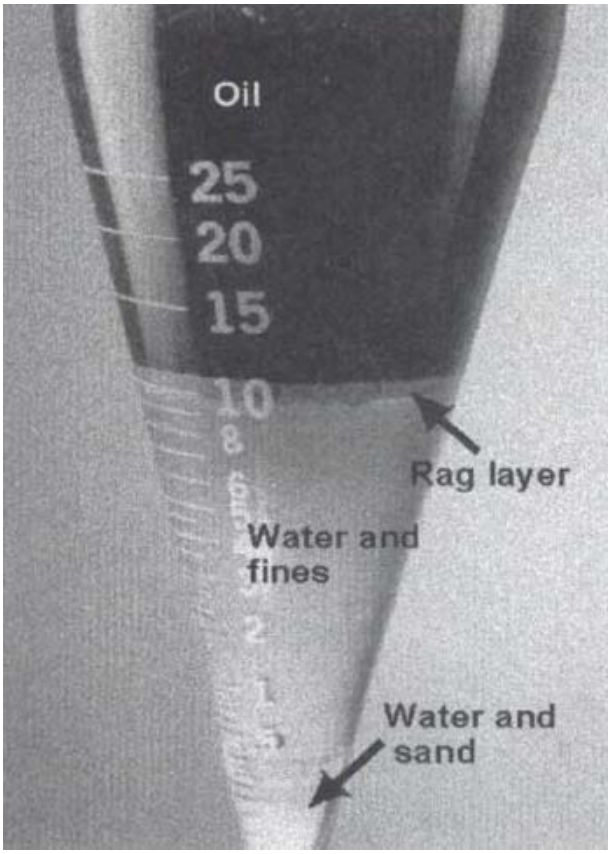

Figure 2.1 Visual observation of rag layer formation between the oil-water interface (reproduced from Schramm, 2000).

During normal operation in a separation treatment, the rag layer material coalesces at approximately the same rate as the water and oil droplets arrive at the interface so that a stable thickness is maintained. However, if the coalescence rate of the water droplets is lower than the accumulation rate, the rag layer can grow continuously until it fills the vessel and upsets the process (Saadatmand et at., 2008).

This thesis focuses on the role of coalescence in rag layer growth, hence it is necessary to first review emulsion fundamentals. The background concepts necessary to understand rag layer growth are presented, in particular emulsion stability with a focus on surface-active components and fine solids. Then, detailed characteristics of rag layers are reviewed along with previous models for rag layers. Finally, previous research on rag layers in oil sands froth treatment is discussed.

2.1 Emulsion Fundamentals

Emulsions may be found in many important areas, including foods, cosmetics, paints, agriculture, and the petroleum industry. An emulsion is defined as a mixture of two immiscible liquids containing droplets of one liquid dispersed in another (Binks, 1998). The droplets are referred to as the dispersed phase and the surroundings liquid is as the continuous phase. There are several classifications of emulsions as follows:

- Water in oil (w/o) emulsion for water droplets dispersed in an oil continuous phase.
- Oil in water (o/w) emulsion for oil droplets dispersed in water.
- Complex emulsions systems, such as a multiple emulsion. Two types are possible: water/in oil/in water (w/o/w) and oil/in water/in oil (o/w/o) (Manning, 1995). For example, w/o/w multiple emulsions consist of two aqueous phases separated by a middle oil layer which acts as a liquid membrane.

An emulsion is formed by agitation of an oil-water mixture so that one liquid breaks into droplets that are dispersed into the other liquid. Emulsions are thermodynamically unstable (Somasundaran, 2006) because molecules of each phase are forced into contact at the interface giving rise to excess energy in the form of interfacial tension. The interfacial tension can be considered as a driving force to coalesce the dispersed droplets in order to minimize the interfacial area between the two phases. Consequently, the reduction of the interfacial tension facilitates emulsion formation (Manning, 1995), because it reduces the amount of added energy needed to break up one liquid into droplets and spread the other liquid around them. Two pure immiscible liquids cannot form a thermodynamically stable emulsion (Rosen M, 2004), but can form a kinetically stable emulsion in the presence of an emulsifying agent (Swarbrick, 2007). An emulsifying agent, or emulsifier, adsorbs at the water/oil interface and creates a physical or electrostatic barrier that prevents droplets from recombining with each other (Vaclavik, 2007; Manning, 1995).

In summary, in order to form a stable emulsion, three basic requirements must exist:

1. Two immiscible liquids.
2. Sufficient agitation to disperse one liquid into the other.
3. The presence of an emulsifying agent or a combination of emulsifiers

2.1.1 Role of Surface Active Agents

Surfactants or surface active agents are the most common type of emulsifier. Surfactant molecules consist of two parts. One part of the molecule is a (water-loving) polar hydrophilic "head", which is orientated towards the aqueous phase and the other section is non-polar hydrophobic (water-fearing) "tail", oriented towards the oil phase, as shown in Figure 2.2.

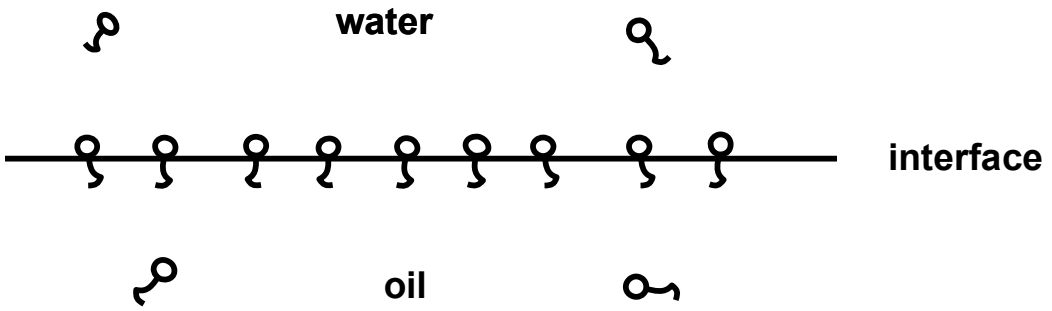

Figure 2.2 Surfactant molecules at the water-oil interface (adapted from Yarranton, 1997).

The hydrophilic group makes the surfactant soluble in polar solvents such as water and the hydrophobic group makes the surfactant soluble in non-polar solvents and oil (Somasundaran, 2006). The structure of the surfactant molecule determines many of its properties. For example, a molecule can have one hydrophilic head and one hydrophobic tail, one hydrophilic head and two hydrophobic tails, or one hydrophobic tail terminated at both ends by hydrophilic groups (Farn, 2006).

Depending on the nature of the charge of the surfactant, or the absence of ionization, surfactants are classified as anionic, cationic, nonionic, or amphoteric (Rosen, 2004).

1. Anionic. The surface-active portion of the molecule bears a negative charge, for example, alkylbenzene sulfonate ($RC_6H_4SO_3^-Na^+$).
2. Cationic. The surface-active portion bears a positive charge, for example, salt of a long-chain amine ($RN(CH_3)_3^+Cl^-$).
3. Amphoteric or zwitterionic. Both positive and negative charges may be present in the surface-active portion, for example, long-chain amino acid ($RN^+H_2CH_2COO^-$).
4. Nonionic. The surface-active portion bears no apparent ionic charge, for example monoglyceride of a long chain fatty acid ($RCOOCH_2CHOHCH_2OH$).

Surfactant molecules stabilize emulsion by adsorbing at the oil-water interface to form an interfacial film around the drops, as shown in Figure 2.3. These films can stabilize the emulsion by reducing the surface tension forces, thus decreasing the energy required to shear the dispersed phase into small droplets (Manning, 1995). Smaller droplets make more stable emulsions because the probability of collision and film rupture is lower. Lower surface energy also decreases the driving force for coalesce.

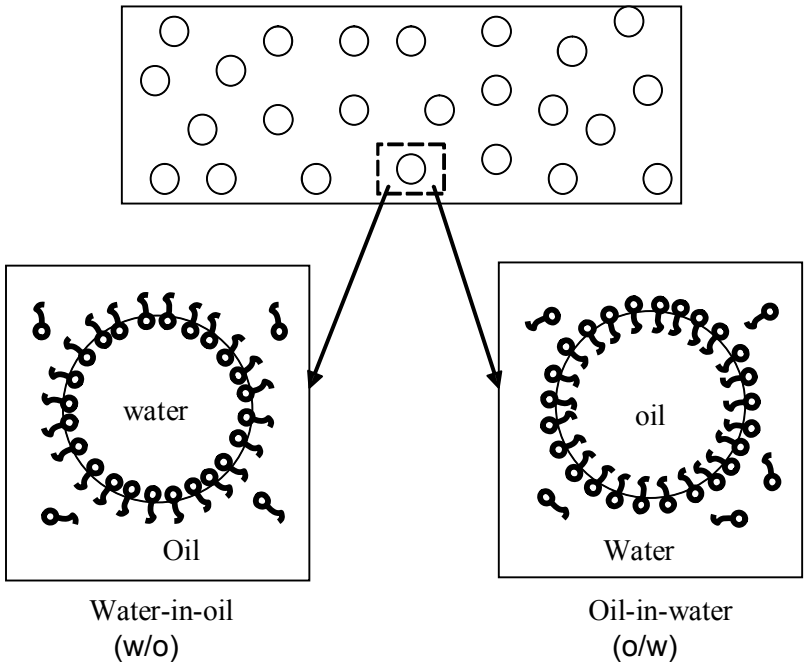

Figure 2.3 Structural principles of w/o and o/w emulsions. Surfactant molecules gather at the interface, where hydrophilic head group is orientated towards the water phase and the hydrophobic tail towards the oil phase.

For o/w emulsions, surfactants can also electrostatically stabilize emulsions. The adsorbed surfactant creates a surface charge on the droplets surfaces, which attracts the counter-ions from the water medium, but repells co-ions. The charge separation is termed the electrostatic double layer. If the counter ion layer is diffuse, the droplets appear to each other as similarly charged spheres and repel each other, stabilizing the emulsion. Electrostatic stabilization is significant only for oil-in-water emulsions since the electric double-layer thickness is much greater in water than in oil (Masliyah, 1994).

For the case of w/o emulsions, polymer surfactant molecules with a large tail can stabilize the dispersed phase. The polymer tails extend from the droplet surface to create a thick layer (Holmberg, 2003). As a result, adsorbed polymer surfactant particles can form a physical barrier against aggregation and coalescence. This barrier prevents the droplets from approaching closely enough to trigger coalescence.

2.1.2 Role of Solids

Fine solids can also act as emulsifiers. These insoluble particles adsorb on the interface and form a physical barrier that prevents coalescence by reducing droplet contact. In order to stabilize the emulsion, fine solids must be at least 100 times smaller in diameter than the emulsion droplet (Kitchner and Musselwhite, 1968). The stability of the emulsion also depends on the ability of the particles to adsorb at the interfacial region and remain there in a state of mechanical equilibrium (Tambe and Sharma, 1992).

When solid particles adsorb at the water/oil interface, a steric or rigid film is formed and coalescence of emulsion droplets is inhibited. At sufficiently high concentrations of fine solid particles, the interfacial region will tend to exhibit viscous and elastic properties. In addition, charged particles at the interface can impart a degree of electrostatic repulsion, which will further enhance the stability of the emulsion (Tambe and Sharma, 1992).

Solid particles that collect at an interface are “bi-wetted”, which means that the solids have both hydrophilic and hydrophobic areas. This condition implies that the solid must have a contact angle in the region of 90° at the three phase (oil / water / solid) contact line. Schulman and Leja (1954) observed that the angle at the oil-water-solid line of contact is slightly less than 90° tend to stabilize o/w emulsions but if the contact angle is slightly greater than 90°, the particles stabilized w/o emulsions, as shown in Figure 2.4. They also observed that emulsion stability increased as particle size decreased. (Schulman and Leja, 1954).

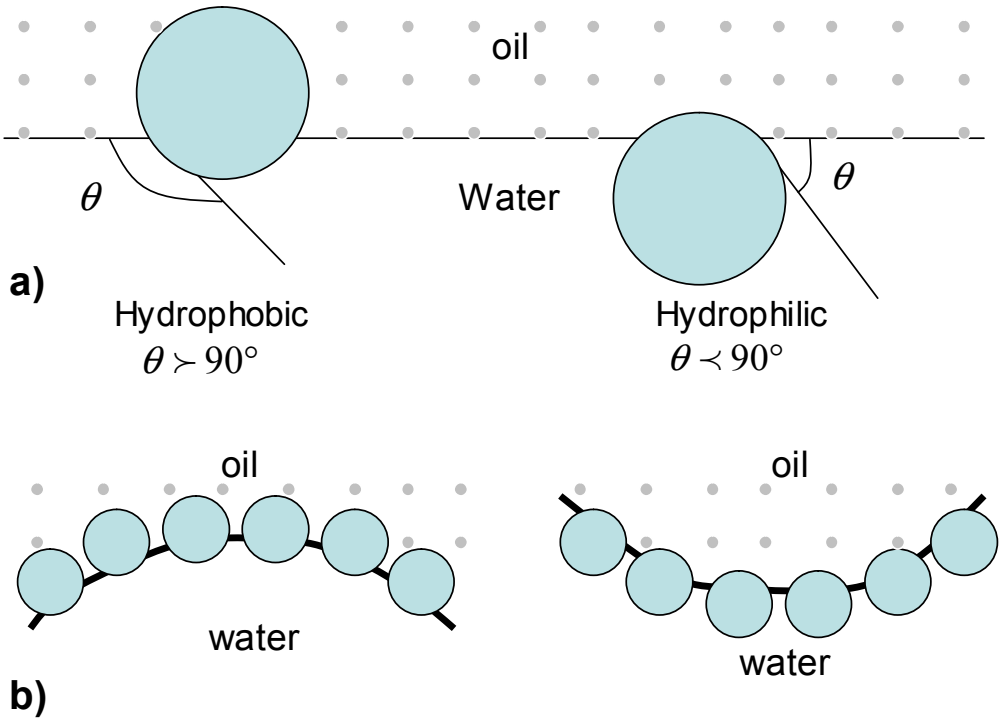

Figure 2.4 Preferential position of small particles at a (a) planar and (b) curved oil-water interface. For $\theta \prec 90°$ solid-stabilized o/w (right) emulsions may form. For $\theta \succ 90°$ solid-stabilized w/o (left) emulsions may form (modified from Binks and Horozov, 2006).

2.1.3 Emulsion Destabilization

Emulsions that are unstable separate into two bulk phases. Emulsion destabilization has three primary mechanisms that lead to instability: flocculation, sedimentation/creaming and coalescence as shown in Figure 2.5. First, droplets must approach each other, usually as a result of sedimentation and flocculation. Then, the droplets must coalesce to grow in size which will accelerate settling and eventually lead to complete phase separation.

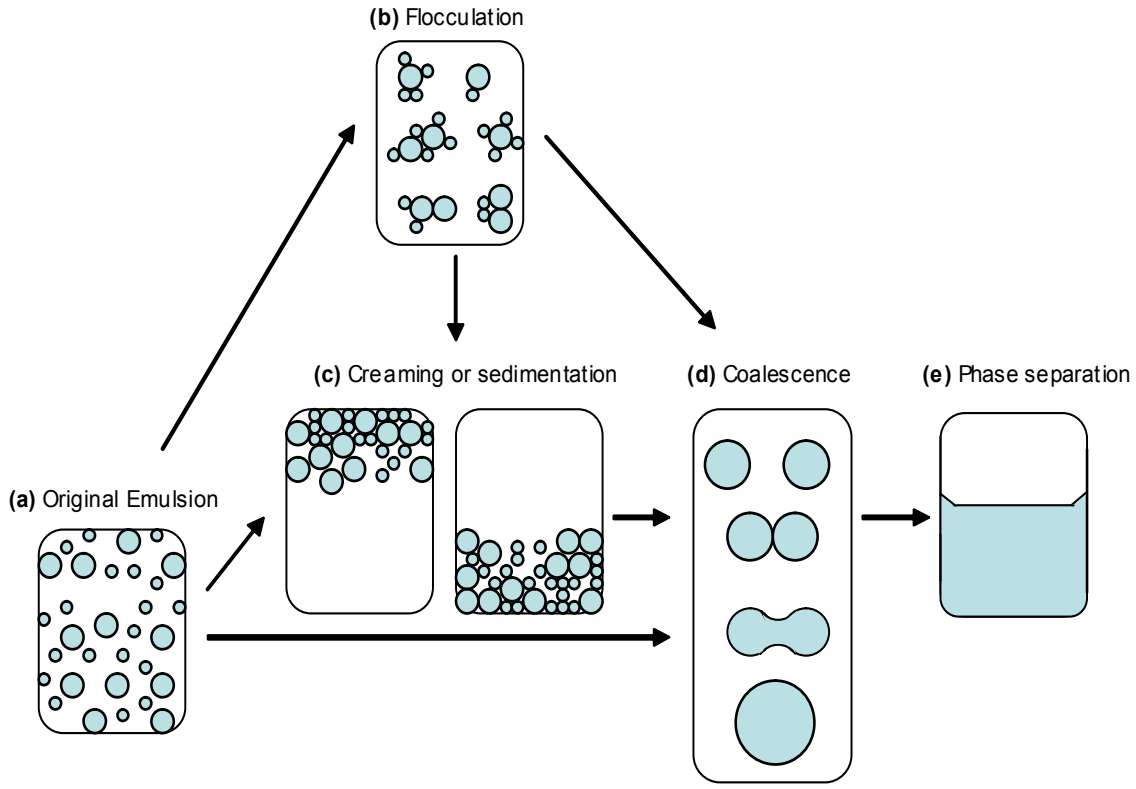

Figure 2.5 Emulsion destabilization mechanism (modified from Binks and Horozov, 2006).

2.1.3.1 Flocculation

Flocculation occurs when two or more droplets are attracted very close to each other, without the rupture of the stabilizing layer at the water-oil interface as shown in Figure 2.5b. As a result, the droplets form aggregates, the aggregates formed by flocculation enhance sedimentation since droplets settle faster as the droplet radius increases. Flocculation also increases the probability of coalescence because the droplets are brought closer together.

The flocculation of an emulsion is determined by the net interaction energy potential experienced over the interparticle distance (Stechemesser and B. Dobiáš, 2005). Derjiagin, Landau, Verwey, and Overbeck developed independently the DLVO theory, in which the total energy of interaction is the sum of the London-van der Waals attractive energy and the electrical double layer repulsive energy between the particles. A typical curve of the interaction energy versus interparticle distance is shown in Figure 2.6.

The total interaction curve in Figure 2.6 includes three important regions, two local minima and one local maximum. The primary and the secondary minima are locations where droplets can coagulate and flocculate, respectively (Swarbrick, 2007). The local maximum is a potential energy barrier which is produced by net electrostatic repulsion (Stechemesser and B. Dobiáš, 2005). Note, if the repulsive force between the droplets is weak, the energy barrier disappears so that there is a net attraction at all separation distances beyond the primary minimum. If the repulsive force is strong, there can be a net repulsion at all distances beyond the primary minimum; that is, no secondary minimum. Flocculation occurs in the second minimum, where the attractive forces are relatively weak and flocculates are easily separated by low energy agitation (Swarbrick, 2007). If the energy barrier is not too high, the droplets can jump to the primary minimum where coalescence can occur.

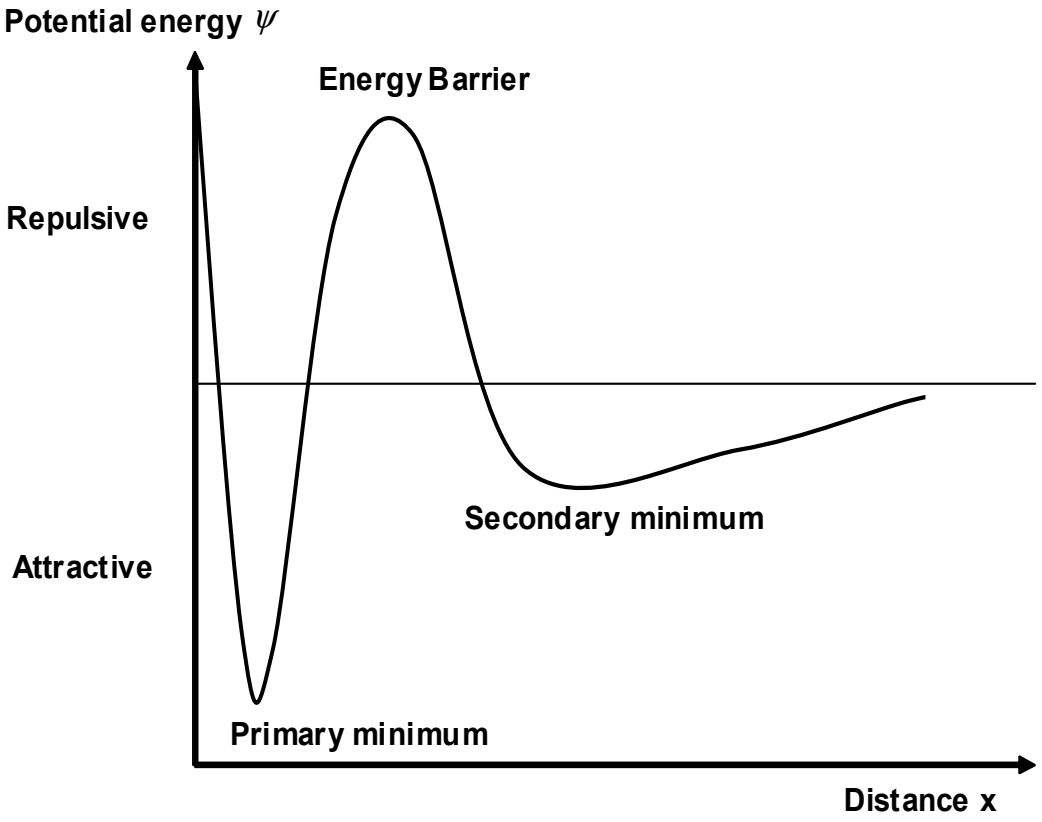

Figure 2.6 Diagram of the potential energy between two particles in dependence on the surface distance (adapted from Tropea et al., 2007).

2.1.3.2 Settling

Settling is the downward movement of dispersed droplets due to the difference in density between the dispersed and continuous phase, under the action of gravitational forces. Settling occurs in most w/o emulsions. If the dispersed phase is less dense than continuous phase, the equivalent process is called "creaming" in which droplets rise to the top (Binks, 1998) as shown in Figure 2.5c.

In 1851, George Stokes derived an expression for the viscous drag force acting on a single spherical particle in an infinite fluid. A particle falling freely under gravity forces accelerates until the drag force exactly equals the gravity force and a terminal velocity is attained. The terminal settling velocity υ_t of a spherical particle in laminar conditions is given by:

$$\upsilon_t = \frac{d_p^2(\rho_p - \rho_m)g}{18\mu_m} \qquad \textbf{Equation 2.1}$$

where ρ_p is the density of the particle, ρ_m is the density of the medium, d_p is the diameter of sphere or particle, μ_m is the viscosity of medium and g is the gravitational acceleration Equation 2.1 is known as Stokes' law.

Stokes' Law assumes that the droplet is isolated and that settling is not influenced by the presence of other particles. In concentrated dispersions, the settling rate of a droplet is affected by the wakes of the other droplets and the reduced settling rate is termed as "hindered settling" (Salamone, 1996). In this situation, Stokes' Law is modified as, for example, in the Richardson-Zaki equation:

$$u = u_t \alpha_f^n \qquad \textbf{Equation 2.2}$$

where u is the hindered settling rate, u_t is the terminal settling velocity of an isolated particle, α_f is the volume fraction of fluid or suspension voidage, and n is the Richardson-Zaki's parameter. The parameter n is a function of the flow regime, expressed by the terminal Reynolds number Re_t, and of the particle to column diameter ratio d/D, which can be determined either experimentally or by using the equations given by Richardson and Zaki, Table 2.1.

Table 2.1 Values of the parameters n (adapted from Richardson and Zaki, 1954).

Relation	Validity
$n = 4.65 + 19.5d / D$	$\mathrm{Re}_t \prec 0.2$
$n = (4.35 + 17.5d / D)\,\mathrm{Re}_t^{-0.03}$	$0.2 \prec \mathrm{Re}_t \prec 1$
$n = (4.35 + 18d / D)\,\mathrm{Re}_t^{-0.1}$	$1 \prec \mathrm{Re}_t \prec 200$
$n = (4.45\,\mathrm{Re}_t^{-0.1})$	$200 \prec \mathrm{Re}_t \prec 500$
$n = 2.39$	$\mathrm{Re}_t \prec 500$

2.1.3.3. Coalescence

Coalescence is the fusion of two or more droplets to form a single larger droplet, Figure 2.5d. For coalescence to occur, the two droplets must first approach each other. Then the droplets may deform and create a dimpling or a planar interface. The continuous phase between droplets starts to drain, when the film has thinned to some critical thickness, it ruptures and creates bridges between the two droplets which rapidly fuse into one droplet (Figure 2.7).

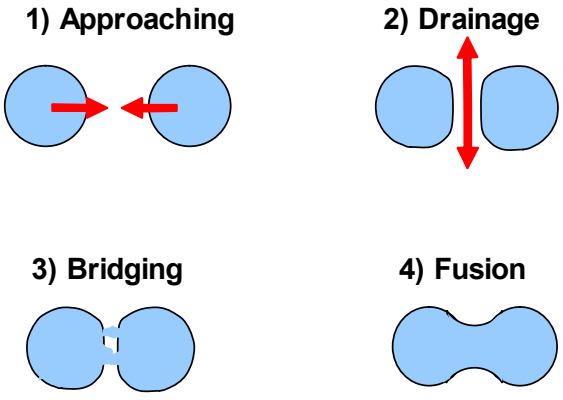

Figure 2.7 Illustration of the Coalescence Mechanism.

2.2 Rag Layers

2.2.1 Rag Layer Description

Rag layer formation in any settling vessel starts when droplets rise or sink to the interface as shown in Figure 2.8. In this case, oil droplets through the aqueous phase emulsion cream and water droplets settle through the oil phase. The droplets accumulate in the rag layer since their intermediate density forces them to stay between the two phases (Czarnecki et al., 2007).

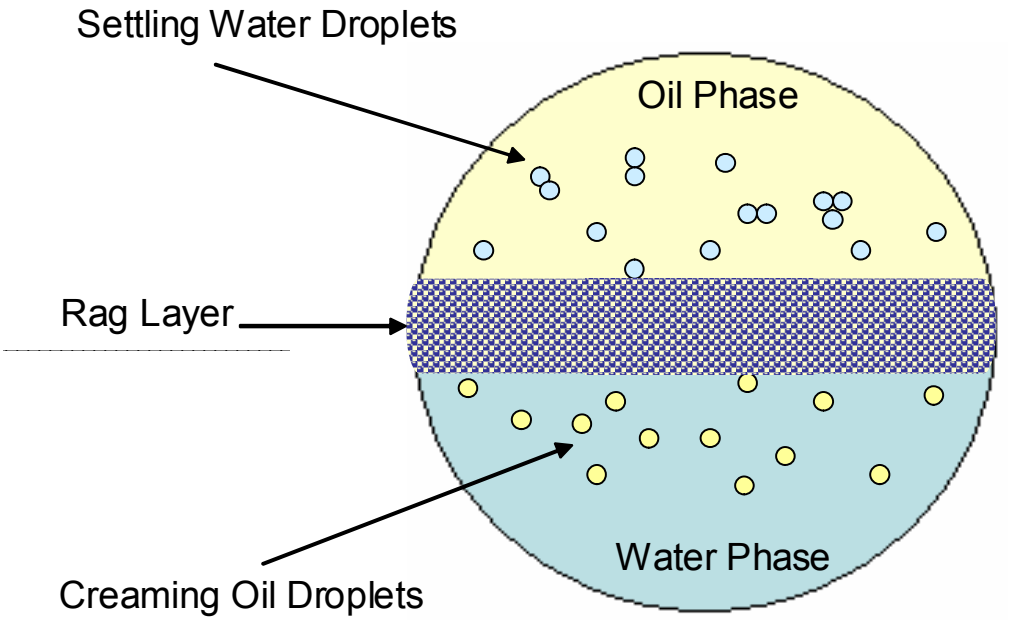

Figure 2.8 Rag layer formation during the rise of oil and sink of water droplets in a separation vessel.

In the rag layer, the dispersed droplets will form a close packed layer of dispersed droplets, where droplets can grow in size by drop to drop interactions (binary coalescence Figure 2.9a), and finally coalesce at the water-oil interface (interfacial coalescence Figure 2.9b).

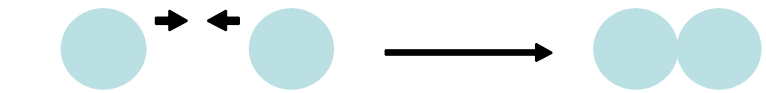

(a) Drop-drop coalescence

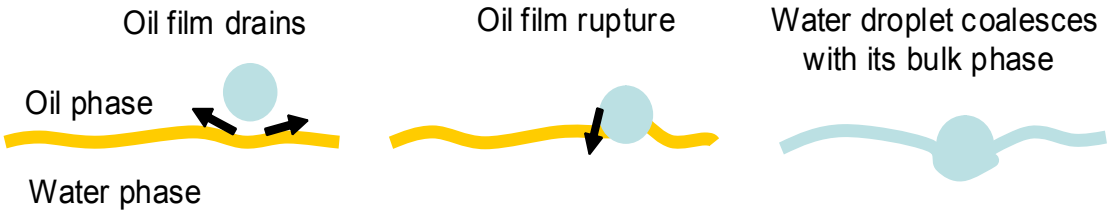

(b) Drop-interface coalescence

Figure 2.9 Disengagement of water-oil dispersion (adapted from Kankaanpaan, 2007).

The size of the rag layer depends on the ratio of the settling and coalescence rates. For example, if the rate of coalescence at the water-oil interface is high compared with the rate of sedimentation, the height of the packed layer will always be small. On the other hand, if the rate of coalescence is low compared with the sedimentation rate the packed layer height will occupy all the dispersion for most of the decay time (Hartland, 1979).

Also of importance in the rag layer is the coalescence time of a droplet, which is defined as the time between the arrival of the droplet at the interface and the rupture of the film separating the droplet from the interface. The interface may be that of a second drop

(binary coalescence), the bulk phase (interfacial coalescence) or a solid surface. The rate of approach of the drop is controlled by the rate of drainage of the film. At some point the film becomes sufficiently thin, it ruptures and coalescence occurs. The time taken for drainage of the film contributes considerably to the coalescence time (Ivanov, 1998).

In a steady state, the settling emulsion has three different zones (Figure 2.10): (I) Flocculation zone, (II) Sedimentation zone and (III) Packed zone (Hartland, 1979). These are described as follows:

- In the flocculation zone the droplets are attracted very close to each other, without the rupture of the stabilizing layer at the water-oil interface. This zone does not occur in all systems.
- In the sedimentation zone the dispersed phase fraction or hold up, varies about 0.5 to 0.75. The droplets move relative to each other and are deformed by inter-drop collisions.
- In the packed zone the dispersed phase fraction varies between 0.75 and 1. The droplets do not move relative to each other, except though inter-drop coalescence. Gravitational forces are transmitted from drop to drop.

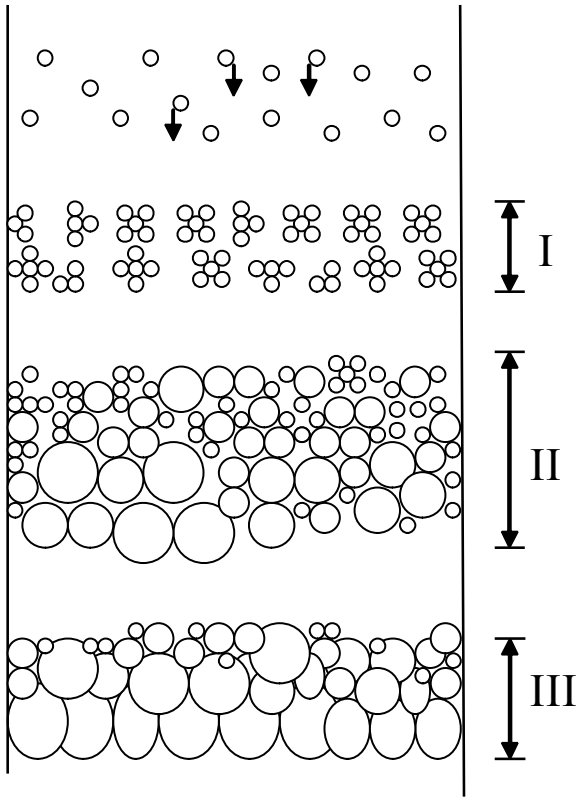

Figure 2.10 Structural arrangement of droplets in steady state close packed settling emulsion. I = flocculating zone, II = sedimenting zone, III = packing zone. (modified from Hartland, 1979).

Consider a batch dispersion of constant cross-sectional area decaying with time (Figure 2.11) due to simultaneous sedimentation and interfacial coalescence. The drops first sediment while they grow in size due to inter-drop (binary) coalescence. Then they enter the dense-packed zone and finally coalesce into their own bulk phase at the coalescing interface (interfacial coalescence). The height of the dense-packed zone initially increases when the sedimentation rate is faster than the interfacial coalescence rate and finally

decreases when sedimentation is complete and interfacial coalescence predominates (Hartland and Jeelani, 1988).

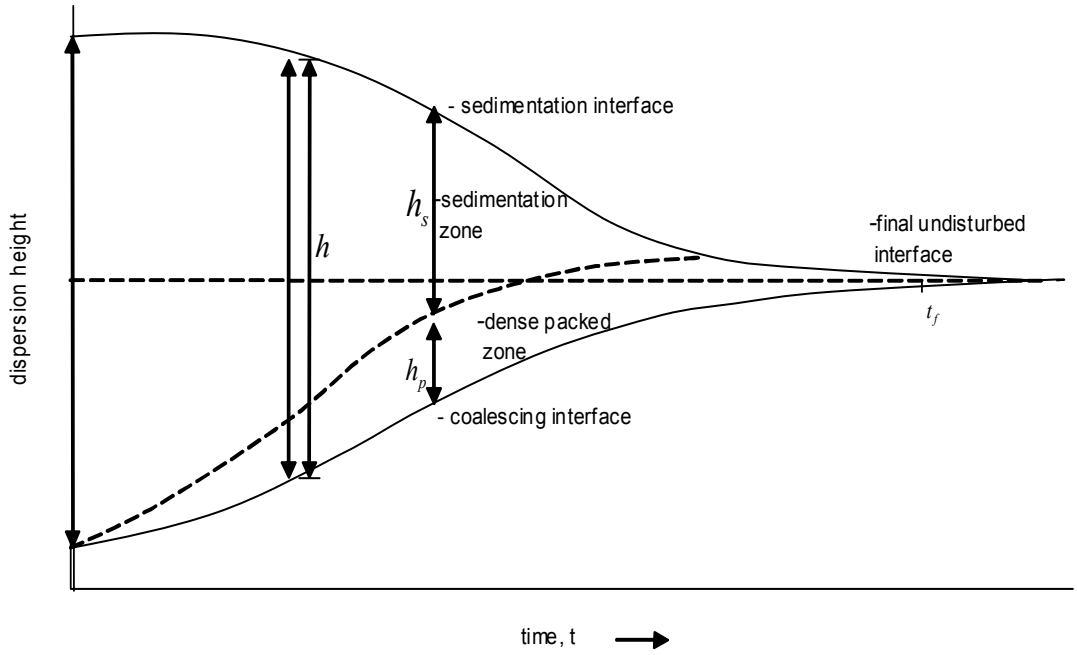

Figure 2.11 Schematic variation in the heights of sedimentation and coalescing interfaces h_s and h_p, with time t for a water-in-oil dispersion (adapted from Hartland, 1979).

If instead the dispersion is continuously fed into a gravity settler (Figure 2.12), the height of the dispersion increases with time until a constant steady-state value is reached. As with a batch separation, the drops entering into gravity settler first sediment, while they grow in size due to inter-drop (binary) coalescence, then they collect in a dense-packed layer adjacent to the coalescing interface and finally coalesce by interfacial coalescence. The dense-packed zone or rag layer forms if the sedimentation rate is faster than the interfacial coalescence rate during the growth period. For a given throughput (flow rate), the residence time of drops in the sedimentation and dense-packed zones is proportional to the height of the corresponding zone.

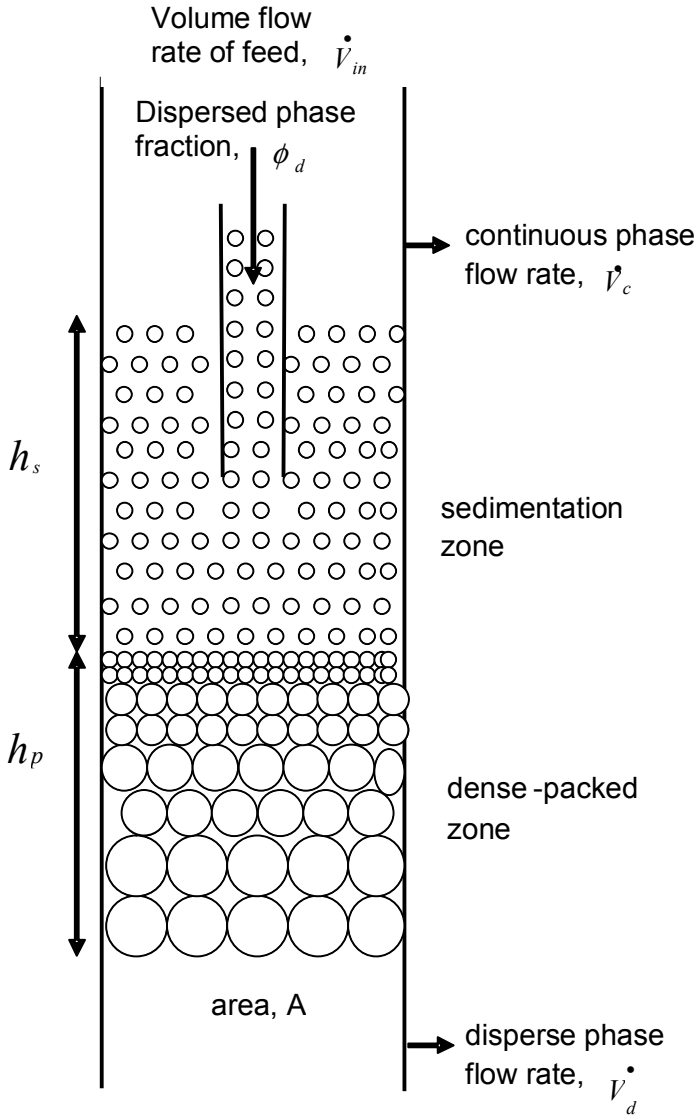

Figure 2.12 Schematic representation of sedimentation and dense-packed zones in a steady-state settler (adapted from Hartland, 1986).

At steady-state, the volume flow rate (throughput) of the dispersed phase equals the rate of interfacial coalescence. The steady-state height also increases with the specific volume flow rate of the dispersed phase per unit area, $\dot{V}_d / A$. In some cases the height of the sedimentation and dense-packed zones at steady-state conditions are approximately equal. In other cases one of the zones may be of negligible height relative to the others, where the interfacial coalescence rate depends only on the total dispersion height (Hartland and Jeelani, 1987). Consequently, different scenarios may occur, such as:

- One limiting case is when the drops in the dispersion feed are so large that their volume rate of sedimentation is greater than the dispersed phase throughput. In this case, the height of the sedimentation zone is insignificant at steady state and no residence time is available for the drops to grow in size through binary coalescence in the sedimentation zone.

- Another limiting case is when the drops in the dispersion feed are small (so that they sediment at a volume rate lower than the dispersed phase throughput), and coalesce immediately when they arrive at the coalescing interface. In this case, no dense-packed zone forms. Also, the residence time in the sedimentation zone is long enough for the drops to grow in size, so their volume rate of sedimentation becomes equal to the steady-state throughput.

- If the drops in the feed dispersion are moderately small, then both sedimentation and dense-packed zones exist, and there is sufficient residence time for drops to grow by binary coalescence.

2.2.2 Rag Layer Models

Several authors (Dalingaros, 1987; Hartland and Jeelani, 1985; Jeelani and Hartland, 1985, 1986a,b) developed theoretical models for rag layer growth based on the different mechanisms that controlled the separation of dispersions or emulsions. These models predicted the variation in steady-state dispersion height with throughput in continuous flow based on batch sedimentation and coalescence profiles.

Consider the batch settling process shown in Figure 2.11. Instantaneous volume balances on the dispersed and continuous phases of the dispersion give:

$$\phi_s V_s + \phi_p V_p = V_d \qquad \textbf{Equation 2.3}$$

$$(1-\phi_s)V_s + (1-\phi_p)V_p = V_c \qquad \textbf{Equation 2.4}$$

where ϕ is the space-average fraction, V is the volume, subscripts s and p denote the sedimentation and dense packed zones, respectively, and subscripts d and c denote the dispersed and continuous phase, respectively. For a constant cross-sectional are, Eq's 2.3 and 2.4 can be divided by the area to obtain:

$$\phi_s h_s + \phi_p h_p = y \qquad \textbf{Equation 2.5}$$

$$(1-\phi_s)h_s + (1-\phi_p)h_p = x \qquad \textbf{Equation 2.6}$$

where h_s and h_p are the heights of the sedimentation and dense packed zones, y is the volume per area of the dispersed phase, and x is the volume per area of the continuous phase.

A total volume balance gives:

$$h_s + h_p = H \qquad \textbf{Equation 2.7}$$

where H is the total height of the dispersion. Combining Eq. 2.7 with Eqns 2.5 and 2.6 gives the heights of the dense-packed and sedimentation zones:

$$h_p = \frac{y - \phi_s H}{\phi_p - \phi_s} \qquad \textbf{Equation 2.8}$$

$$h_s = \frac{\phi_p H - y}{\phi_p - \phi_s} \qquad \textbf{Equation 2.9}$$

The dispersed-phase fraction ϕ_s in the sedimentation zone is assumed to be constant and equal to the initial dispersed fraction, ϕ_0:

$$\phi_s = \phi_o = \frac{y_o}{H_o} \qquad \textbf{Equation 2.10}$$

During sedimentation, the dispersed fraction in the packed zone, ϕ_p, is also assumed to remain constant and equal to ϕ_p*, the dispersed fraction in the dense packed zone at time t* when sedimentation ceases and the whole dispersion become a dense-packed zone. The value of ϕ_p* is usually close to 0.75, the value pertaining to dense-packed spheres.

When the dense-packed zone occupies the whole of the dispersion so that $h_p = H$ and $h_s = H$, Equations 2.5 and 2.6 can be manipulated to show that *x* and *y* are related as follows:

$$x = \frac{(1-\phi_p)y}{\phi_p} \qquad \textbf{Equation 2.11}$$

In this case, ϕ_p is no longer constant and usually increases with time from ϕ_p* to a value near to unity when coalescence is complete.

The above material balances are functions of *x* and *y* which in turn depend on the coalescence rate and time. In a batch dispersion, the volume rate of coalescence of droplets at the coalescing interface is identical to the decrease in the dispersed phase volume:

$$\frac{dV_d}{dt} = -\psi A \qquad \textbf{Equation 2.12}$$

where ψ is the volumetric coalescence rate per area and *t* is time. Eq. 2.12 can be divided by the cross-sectional area to obtain:

$$\frac{d(\phi_s h_s + \phi_p h_p)}{dt} = \frac{dy}{dt} = -\psi \qquad \textbf{Equation 2.13}$$

If the water volume fractions and the coalescence rate are known over time, Eq's 2.7, 2.8, 2.9, 2.11, and 2.13 can be solved simultaneously to determine the height of the settling and dense packed zones. Typically, only steady state conditions are evaluated.

A special case occurs when there is only a dense packed one and coalescence is independent of drop size. Hartland (1979) showed that when drops are constrained, as in a close packed dispersion, the force pressing on each drop increased with dispersion depth if part of the net weight of each drop was transmitted to the drop below. The time for each drop to coalesce thus decreased with the dispersion depth; that is, the volume rate of coalescence at the disengaging interface increased with the height of packed dispersions. In this case, Hartland and Jeelani (1988) showed that Eq. 2.13 becomes:

$$\psi = k_p h_p^p \qquad \textbf{Equation 2.14}$$

where k_p is a constant. The values of k_p and p are obtained from a least squares fit of the correlation of $\psi(-dy/dt)$ with h_p.

Jeelani (1985, 1993) showed that the functional form of Eq. 2.14 can also be applied to the steady state condition for a continuous separator. At steady state, the coalescence rate is also identical to the volume flux of the dispersed phase:

$$\psi = \frac{\dot{V}_d}{A} \qquad \textbf{Equation 2.15}$$

where $\dot{V}_d$ is the volumetric flow rate of the dispersed phase. Introducing Eq. 2.15 to Eq. 2.14 gives:

$$h_p = k\left(\frac{\dot{V}_d}{A}\right)^p \qquad \textbf{Equation 2.16}$$

where k and p are experimentally defined constants, which depend on the dispersion characteristics (Mizrahi and Barnea, 1973). The constants are not necessarily the same as the batch settling system because the dense packed zone in the continuous settler is always replenished with fresh dispersion.

2.2.3 Rag Layers in Oil Sands

In oil sands froth treatment, rag layers can be form and are problematic because they do not separate easily. Rag layers in the oil sands industry typically consist of flocculated water droplets and multiple water-in-oil and oil-in-water emulsions stabilized by a sub-fraction of asphaltenic material, naturally occurring surfactants like sodium naphthenate and fine solids such as clays (Czarnecki et al., 2007).

The natural and added surfactants in oil sand froth can adsorb at the oil-water interface where they sometimes form an irreversibly adsorbed film or "skin." Such skin-like structures can prevent the coalescence of droplets with their respective bulk phase as well as coalescence between the droplets (Czarnecki et al., 2007). Furthermore, once the rag layer has formed, it can trap additional components that would otherwise have creamed or settled out of the way. This usually makes the rag emulsion even more intractable.

The presence of oil-wet fine solids can adsorb on the interface and can create a structural barrier that prevents water and solid particles from passing through (Chen et al., 1999). These solids also contribute to the stability of dispersed water droplets in the oil phase in froth treatment processes either through adsorption to form a steric barrier or simply impeding the approach of droplets (Sztukowski and Yarranton, 2005). Small asphaltene-coated w/o emulsion droplets accumulate at the interface, creating an oil-wet surface (Khadim and Sarbar, 1999). Also, hindered settling decreases the rate at which emulsion droplets and solid particles settle. If the settling rate is too slow, rag layers will form in a continuous process (Saadatmand, 2007b).

Saadatmand (2008) examined rag layer formation from diluted froths and showed that two possible mechanisms can form rag layers: a mechanical barrier and slow coalescence. If the froth contains oil-wet materials, they may accumulate at the interface and form a barrier that prevents water and solid particles from passing through. Where the emulsified water in froths is stabilized by a coating of asphaltenes (Khadim, 1999) and hence the surface must be oil-wet. These droplets may not settle through the interface

until they coalesce to large sizes or in effect coalesce with the free water layer. If the coalescence rate is slow, a rag layer may accumulate. Saadatmand did not specifically investigate the factors that triggered rag layer growth but did observe that more compact rag layers were found in heptane diluted froths as opposed to toluene diluted froths probably because the droplets flocculated more in heptane. He also found that larger rag layers formed in poorer quality froths perhaps due the increased amount of fine solids.

Recent research has focused on breaking rag layers. Guoxing Gu (2007) designed a semi-batch apparatus to separate water and bitumen in naphtha-diluted bitumen froth (NDBF) by a water washing technique to accelerate the separation and the build up of rag layer to be collected for further investigation of rag formation mechanisms. In the first step of bitumen froth cleaning, 1–5 mm diameter NDBF drops were introduced into an aqueous phase to allow the NDBF drops to rise to the top as the organic phase. In the second step, the top organic phase was then washed using the bottom aqueous phase by circulating the top organic phase back to the aqueous phase.

The technique was tested at 80 °C on two froths: one at a naphtha-to-bitumen mass ratio (N/B) of 0.7 and the other at an N/B of 7.0. A significant improvement in separation performance was achieved with the washing scheme. However, the formation of rag was intensified because the skin materials were left behind after the dispersed water droplets broke and migrating into the bulk aqueous phase. It appeared that, the higher the separation efficiency, the faster the rag built up between the top organic phase and the bottom aqueous phase.

The formation of rag layer during the water washing of NDBF was observed for both cases of N/B = 0.7 and 7. However, there was a clear distinction between the two cases with respect to the properties of the rag layer. In the case of N/B = 0.7, the rag layer was a loose mixture and settled partly to the bottom of the separation vessel without mechanical agitation and settled almost completely when the rag layer was slightly

agitated mechanically. However, in the case of N/B = 7, the rag layer was a viscous and dense mixture, behaving like a gel, and mechanical agitation did not make it sink.

The asphaltene content in the rag layer was calculated for the two naphtha-to-bitumen ratios. In the two cases, rag "asphaltene" contents are higher (23.7% for N/B=0.7 and 55.8% for N/B=7) than the asphaltene content of 17% in typical bitumen, indicating that asphaltenes concentrated in the rag layer during water washing. It is well known that asphaltenes are a key stabilizer of water-in-oil emulsions (Gafonova and Yarranton, 2001). The high asphaltene content in the rag layer at N/B=7 indicates that asphaltene precipitation occurred at this dilution and may account for the viscous properties of the rag layer at these conditions.

Hirasaki, Jiang T., and Miller (2008) developed a methodology for reducing or eliminating the rag layer for water-in-oil emulsions from diluted bitumen. The experimental procedure consisted of three steps for complete separation. The first step was to add a small amount of sodium silicate during initial emulsion formation to make the solids less oil-wet by enhancing clay solids dispersion and reducing bitumen clay coagulation. The second step was to proceed with treatment with a demulsifier and adding sodium hydroxide or sodium silicate with shaking to destroy the rag layer and form a relatively concentrated oil-in-water emulsion nearly free of solids. The third step was to add hydrochloric acid to break the oil-in-water emulsion. None of this work addresses the factors that contribute to rag layer growth in the first place.

2.3 Summary

Emulsions are often formed during oil production and are always present in oil sands froth treatment. These emulsions are usually concentrated using gravity settling or centrifugation. In the case of gravity settling, a rag layer of concentrated emulsion and solid particles can collect at the interface between the oil and water phase within the separation vessel. The presence of fine solids and natural and added surfactant increases the complexity of the rag layer, making it even more difficult to treat. This rag layer must be broken prior to transportation and refining due to viscosity and contamination issues, respectively.

Rag layer accumulation depends primarily on the settling rate of the droplets dispersed in the continuous phases and the coalescence rate of the concentrated emulsion. Most of the emulsion coalescence occurs within this layer. If the coalescence rate is too slow, the rag layer will accumulate droplets and eventually fill the vessel and upset the process. Models have been developed for rag layer growth but the coalescence rate must be determined experimentally. Coalescence rates in oil sands rag layers and the factors which control coalescence and rag layer growth, such as the role of fine solids, are still poorly understood.

CHAPTER 3
EXPERIMENTAL METHOD

The experimental methodology was to determine coalescence rates of model emulsions based on the decrease in rag layer volume over time in a batch experiment. Then rag layer growth was measured for continuously flowing emulsions made from the same model systems. This data is to be used to test a rag layer growth model for the continuous system. The model emulsions consisted of water emulsified into a toluene/heptane blend and partially stabilized with a surfactant.

This chapter provides details of emulsion preparation, batch coalescence rate experimental procedure, continuous apparatus design, and continuous rag layer growth experimental procedure.

3.1 Materials

Commercial *n*-heptane (98% purity) and toluene were purchased from Conoco Phillips Co. and Univar Canada Ltd, respectively. Toluene and *n*-heptane were used to prepare water-in-oil emulsions. Reverse osmosis (RO) water was supplied from the University of Calgary water plant.

Nonylphenol ethoxylate surfactants with 10 and 15 moles of ethylene oxide, NEO-10 and NEO-15, were provided by Champion Technologies, Ltd. Aerosol OT, or AOT, was 98% pure and was purchased from Aldrich Chemical Company, Inc. AOT is a short form descriptor of the chemical sodium bis (2-ethylhexyl) sulfosuccinate.

3.1.1 Preparation of Emulsions

To prepare the surfactant solutions used in the emulsions, the surfactant was weighed exactly on an analytical balance and then dissolved in a given mass of water using an

ultrasonic bath. The surfactant concentrations were set between 40 ppm and 80 ppm. All of the concentrations were below the critical micelle concentration.

The emulsions were prepared from an aqueous phase with 80 ppm of NEO-10 (nonylphenol ethoxylate with 10 ethoxy groups per molecule) and an oil phase of equal portions of heptane and toluene. To prepare the water-in-oil emulsion, 800 ml of each phase was placed in a 2000 mL glass beaker of 120 mm diameter, 165 mm high, equipped with two wall baffles of 11 mm wide. For batch experiments, the mixture was stirred for 30 minutes at a speed of 800 rpm using a IKA-RW20 digital, variable speed overhead mixer with a 4-blade impeller (43 mm diameter, 10 mm width, and 9 mm height). The mixer impeller was located just below the water–oil interface, as shown in Figure 3.1b. For continuous experiments the mixer was left running for the whole experiment. A water bath and circulator with 20 liters capacity was used to control the temperature of the apparatus at a set value within the range of 20 to 80°C.

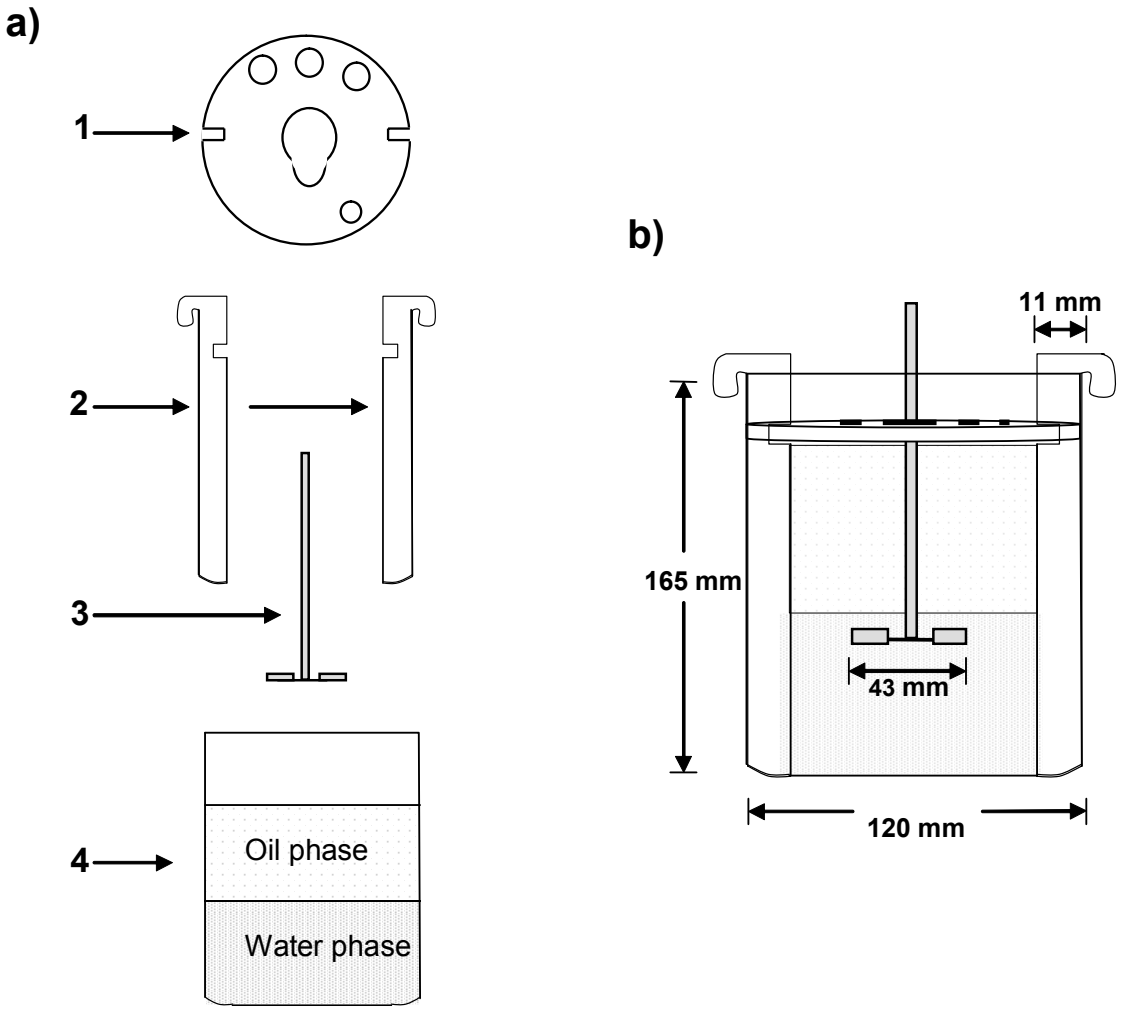

Figure 3.1 Apparatus for preparation of model emulsions. a) mixing components: 1- Teflon plate, 2- Teflon baffles, 3-impeller, 4-graduated glass beaker; b) mixing apparatus assembly.

3.2 Batch Coalescence Rate Experiments

To perform a batch coalescence rate experiment, the beaker was filled with equal volumes of oil and aqueous surfactant solution (1), as shown in Figure 3.2. The beaker was brought to the desired temperature and then the mixer was switched on. Once the emulsion was prepared (2), the mixer was turned off and immediately the height of the interfaces between the free organic phase, emulsion (rag), and water layers were measured over time (3).

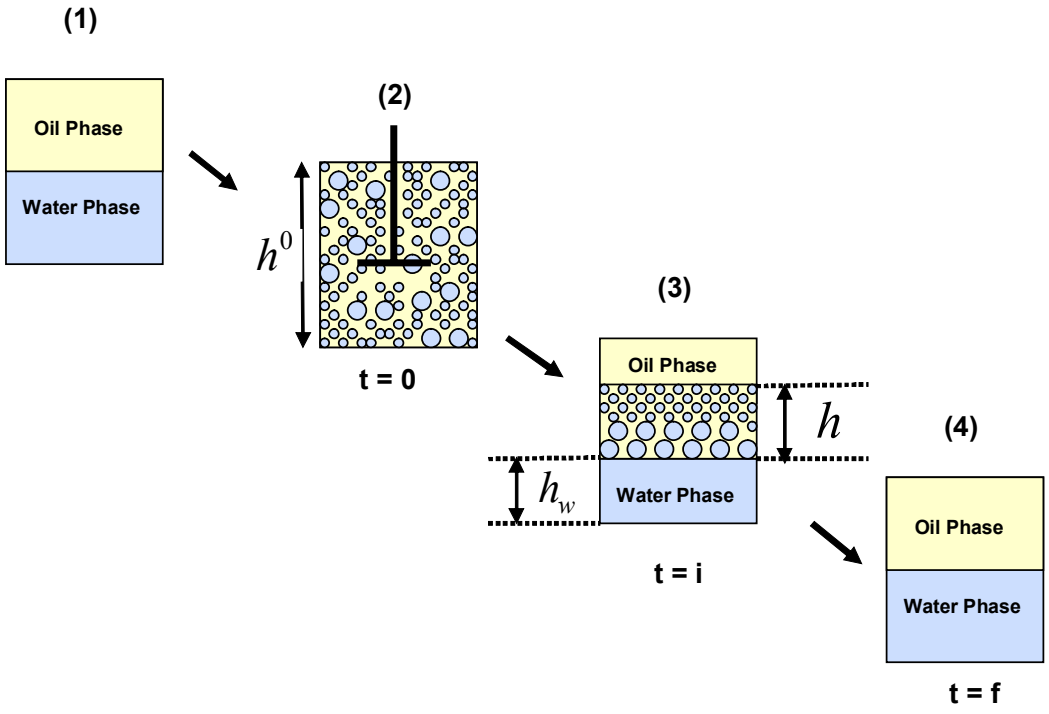

Figure 3.2 Steps of a batch experiment test

When the emulsions were prepared with 50% water, the dispersed water droplets formed a loose self-supporting network and no settling was observed. Hence, free organic and water phases only appeared as result of emulsion coalescence. Similarly, the height of rag layer decreased with time as coalescence progressed (4). The emulsions were tailored so that they would break over the course of 10 to 30 minutes during a batch experiment as

well as provide a measurable but finite steady state rag layer height in a continuous experiment (see Section 3.3.4 for details).

The macroscopic coalescence rate constant in the batch experiment is given by:

$$k = \frac{\dot{V}_w}{V_w} = \frac{\dot{V}_w}{\phi_w A h_w} \qquad \textbf{Equation 3.1}$$

where k is the coalescence rate constant, $\dot{V}_w$, V_w, and ϕ_w are the volumetric flow rate at which water coalesces, the volume of water and the volume fraction of water, respectively, in the emulsion layer, and A is the cross-sectional area of the beaker. The area of the beaker was known, the height of the water layer was measured directly, and the flow rate of the coalescing water and the water volume fraction were determined as described below.

Since there was no settling in these experiments, the rate at which water escaped from the rag layer was directly related to the height of the free water layer:

$$\dot{V}_w = A\frac{dh_w}{dt} \qquad \textbf{Equation 3.2}$$

where t is time. The water volume fraction in the rag layer was determined as follows:

$$\phi_w = \frac{V_w^o - V_w}{V_e} \qquad \textbf{Equation 3.3}$$

where V_w^o is the volume of water in the whole mixture, and V_e and V_w are the volumes of the emulsion layer and the water layer, respectively.

The absolute error for water volume fraction in the rag layer during batch experiment test was ±0.020. The absolute error for rag layer height during batch experiments was ±0.25 cm. The statistical error analysis is provided in Appendix C.

3.3 Continuous Rag Layer Growth Experiments

3.3.1 Continuous Emulsion Separation Apparatus

The components of the continuous apparatus included a beaker for emulsion preparation, a water bath, a peristaltic pump, and a cylindrical jacketed glass separator. A schematic of the apparatus is shown in Figure 3.3.

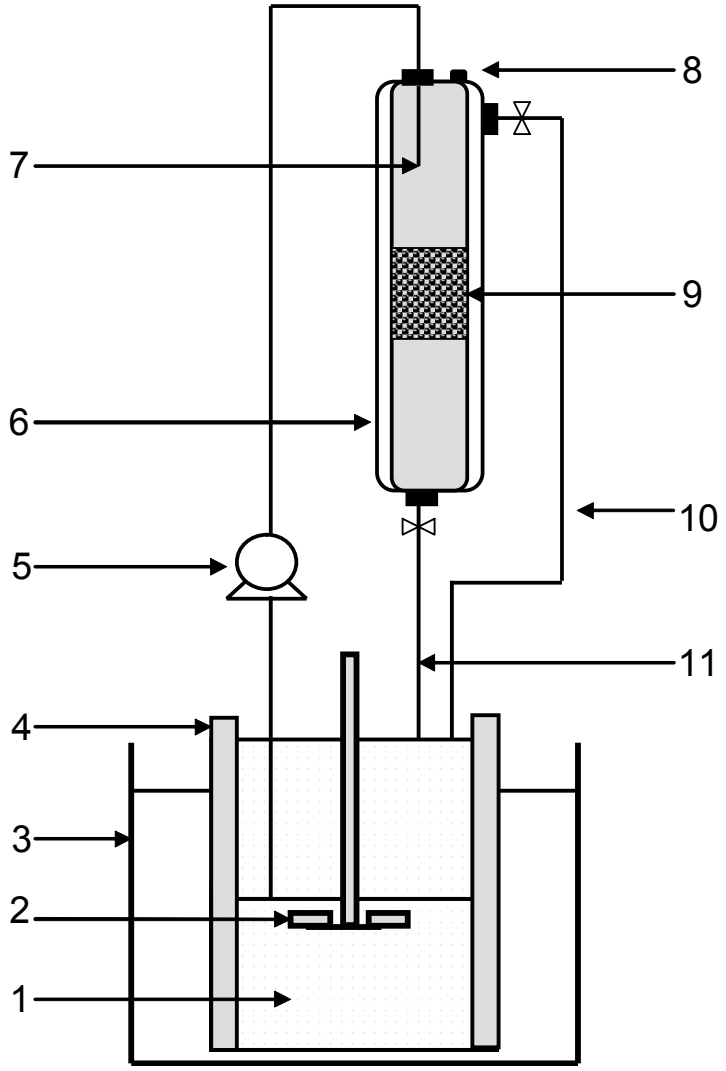

Figure 3.3 Schematic of the continuous apparatus. 1 - beaker, 2 – mixer impeller, 3 – water bath, 4 – baffle, 5 – pump, 6 – jacket glass cylinder, 7 – feed inlet, 8 – sampling port, 9 – rag layer, 10 – oil phase recirculated, 11 – water phase recirculated.

The 2000 mL beaker system, as shown in Figure 3.4, was modified slightly from the batch experiments and was composed of a graduated glass beaker (1), two Teflon baffles (2), and a Teflon plate (3) which was designed to work as a lid for the beaker and to connect the tubing system. The tubing system was composed of a water tubing outlet (4), oil tubing outlet (6), feed tubing inlet (7), and mixer impeller (5).

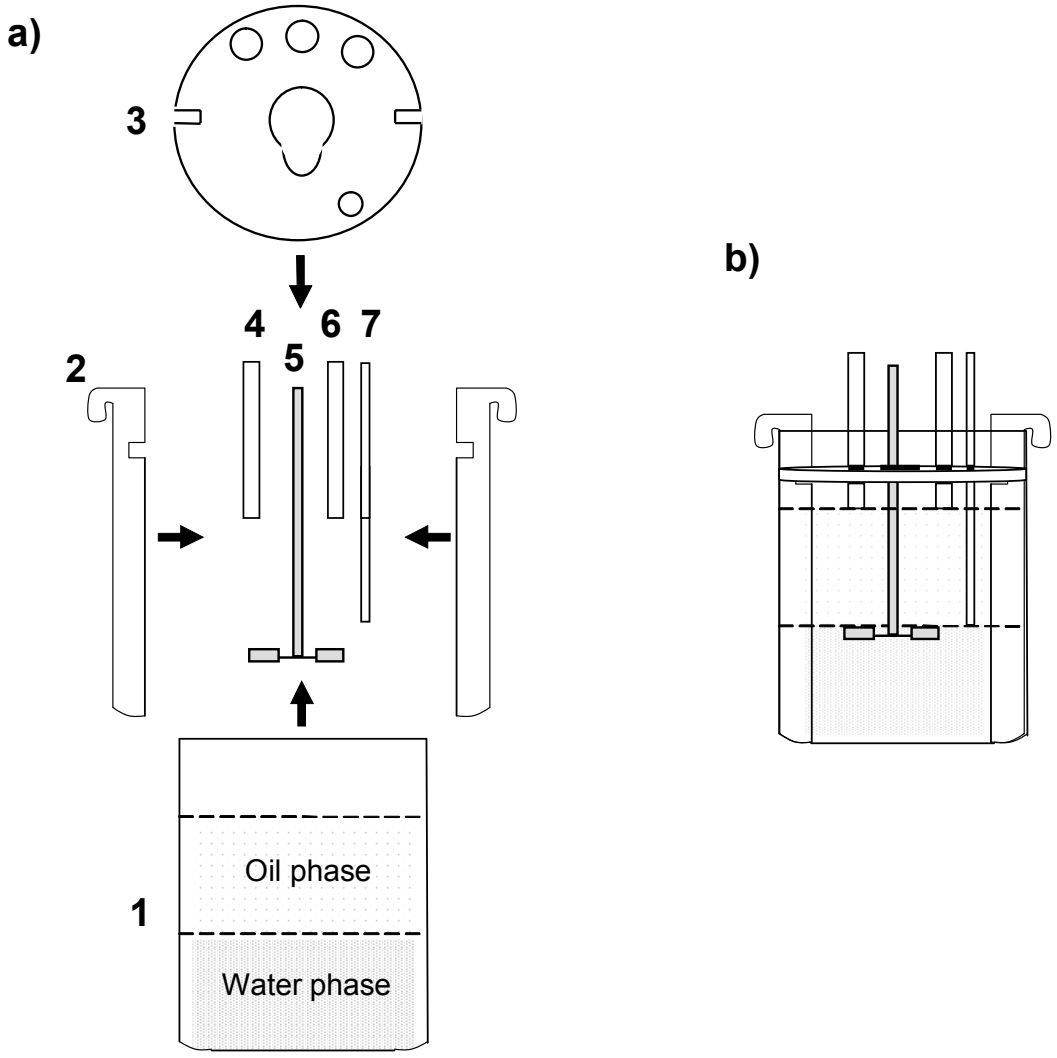

Figure 3.4 Continuous apparatus set-up: a) beaker system components: 1 – graduated glass beaker, 2 - baffle, 3 – plate, 4 – oil tubing outlet, 5 – mixer impeller, 6 –water tubing outlet, 7 – feed tubing inlet; b) beaker system set up.

A Masterflex LS peristaltic pump system was used to flow the emulsion from the beaker to the separator. The pump consists of an economy digital drive of 1.6 to 100 rpm and a Masterflex pump head L/S (Easy-Load II). Two different sizes of tubing were required. The Masterflex tubing-Viton #24, was used to connect the pump to the separator (130 cm length) and could accept flow rates from 5 to 280 cm^3/min (Figure 3.4a-7). The Masterflex tubing-Viton #36 was used to circulate water and oil from the separator to the beaker (Figure 3.4a-4.6).

The 250 mL glass separator was graduated in order to measure the phase volumes. An outer jacket was used for temperature control. The separator configuration had six ports, as shown in Figure 3.5. The feed port (1) injected the feed from the beaker to the inside of the separator (2). The feed outlet (2) was designed to operate with an adjustable height (3) without the need for any modification in the separator.

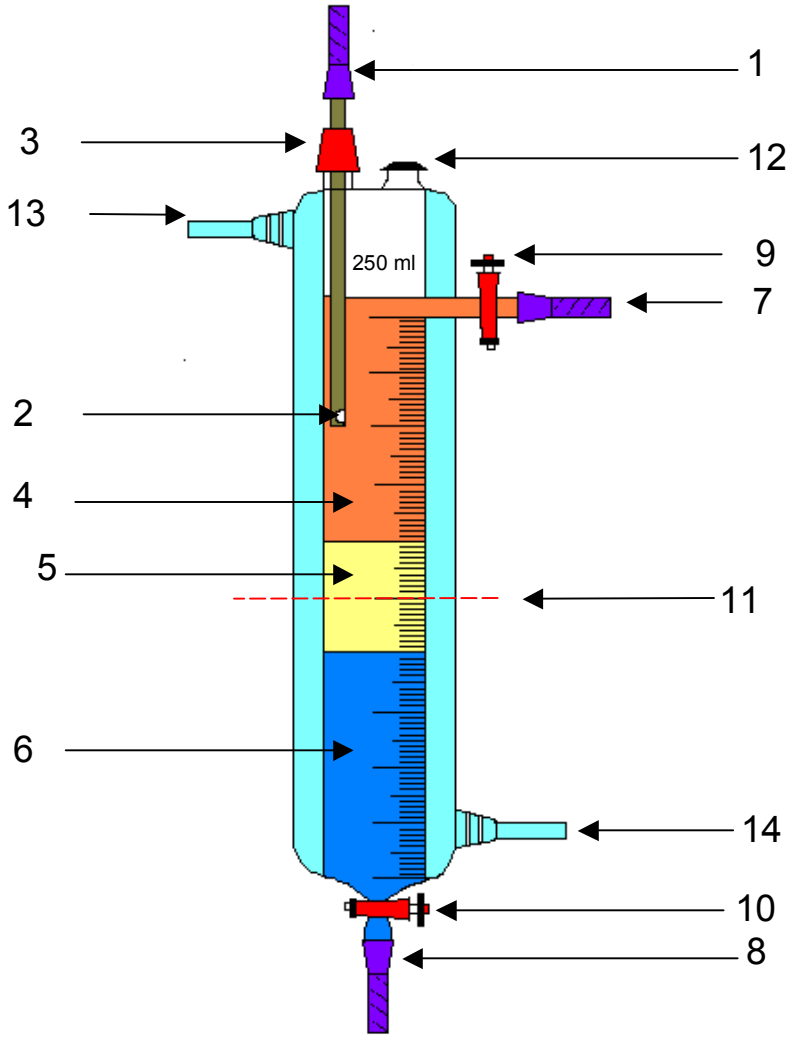

Figure 3.5 Separator system components: 1 - feed port, 2 – feed outlet, 3 – adjustable feed height, 4 – oil phase, 5 – rag layer, 6 – water phase, 7 – oil phase exit, 8 – water phase exit, 9 – oil valve, 10 – water valve, 11 – centerline, 12 – Sampling, 13 and 14 – water jacket ports.

Inside the separator the emulsion separated into three phases: oil phase (4), rag layer (5) and water phase (6). Port (7) was an exit for resolved oil and port (8) an exit for resolved water, controlled with valves (9) and (10), respectively, at a rate that maintained the total liquid height and the position of the centerline of the initial interface (11). Port (12) was

designed for sampling, which allowed the introduction of a pipette at any height inside the separator to collect a subsample for drop size distribution measurement. Port (12) was also used to measure temperature. Also, port (12) could be used to connect an external tubing for overflow or recalculating purposes. Port (13) and (14) are inlet and outlet water jacket ports, connected to a circulating water bath to maintain a constant temperature throughout the separator. A photograph of the apparatus is provided in Figure 3.6.

Figure 3.6 Photograph of the continuous apparatus.

3.3.2 Continuous Rag Layer Growth Experimental Procedure

To perform a continuous experiment, the separator was first filled with equal volumes of free aqueous and organic phases. The water jacket was connected to a circulating water bath to control the operating temperature. An emulsion was prepared in the beaker, as described previously. After 30 minutes of mixing, the emulsion was pumped from the beaker to the separator at a constant flow rate. The w/o feed entered the upper part of the separator and flowed through the oil phase until it reached the interface between the oil and water. Once flow started, the emulsion entered the separator and a dense-packed layer of dispersed droplets formed between the free oil and water phases. Free oil and free water were allowed to flow from the separator back to the emulsion preparation beaker where they were re-emulsified. The outlet flow rates were controlled such that the midpoint of the rag layer and the height of fluid in the separator were constant.

The mixing speed was maintained at 800 rpm during all the experiments. The temperature was held at 45°C and feed flow rates of 40 to 50 mL/min were used. Note, in order to take accurate and reproducible measurements, the beaker, tubing and separator system and accessories had to be rigorously cleaned for any batch and continuous experiment.

During an experiment, the height of the rag layer was measured over time to assess rag layer formation, growth, and as illustrated in the profile shown in the Figure 3.7. At the start of an experiment, the water droplets were fed to the interface at a rate faster than they coalesced and they accumulated to form a rag layer that grew in size (1). Eventually the rag layer volume became large enough that the coalescence rate equaled the water feed rate and the rag layer stopped growing; that is, the rag layer height became constant. Note, if the feed rate was too high relative to the coalescence rate, the rag layer overflowed the separator.

When the rag layer height appeared to reach a steady-state, condition (2), the flow to the separator was shut off and outlet valves for oil and water were simultaneously closed.

The height of the rag layer was again measured over time until the emulsion layer disappeared and two clear phases formed (3). Figure 3.8 shows a photograph of the three layers in a continuous separator experiment.

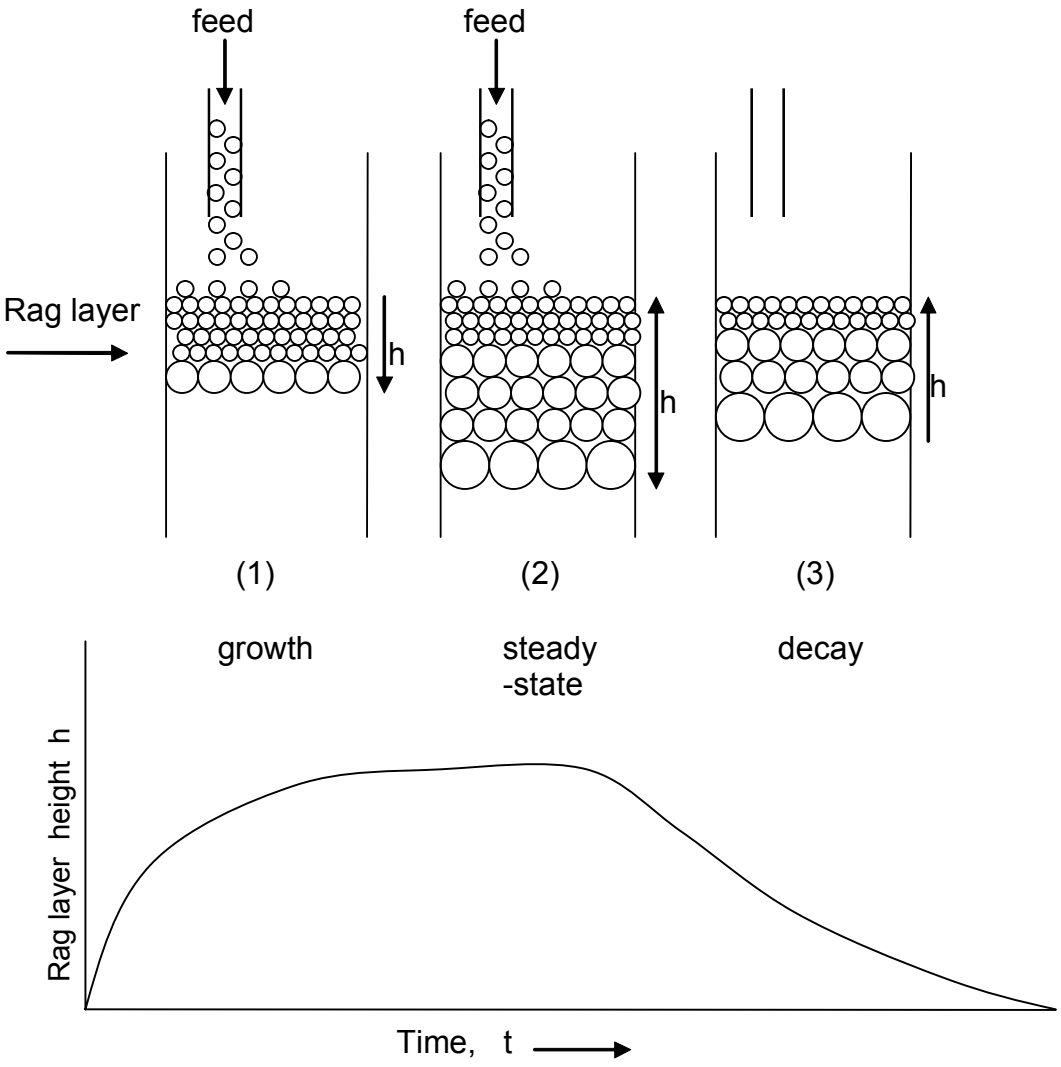

Figure 3.7 Variation of rag layer height with time: (a) increase during growth; (b) constant height at steady state; (c) decrease during decay.

Figure 3.8 Photograph of a continuous separator experiment. Three layers are visible in the column: oil phase (top), rag layer (center) and aqueous phase (bottom).

3.3.3 Repeatability Tests:

Two of the major challenges in the initial stages of the experimental work were poor repeatability and difficulty in reaching a steady state condition. It was found that this behavior was due to the accumulation of minor amounts of surfactant impurities within the apparatus. In order to take accurate and repeatable measurements, all the physical components had to be rigorously cleaned and placed in the same position for each experiment.

The following steps were taken to ensure the cleanliness:

1. The glass components (beaker and separator) were flushed twice with pure acetone.
2. The glass components and tubing system were cleaned with distilled water to remove surfactant impurities.
3. The glass components were flushed twice more with acetone.
4. All of the material was completely dried.
5. A new solution was used each time.
6. The Masterflex tubing was replaced approximately every 20 runs, because of tubing life time and accuracy of experiments.

Once these steps were taken, repeatability tests were performed on 9 systems at a variety of conditions. For batch experiments, the rag layer height was repeatable to ±0.25 cm. The data set of the continuous experiments included 30 pairs of repeats collected over a variety of conditions. It was observed that the absolute error varied systematically but the relative error varied randomly. The relative deviation was 6.4%. The water volume fraction during rag layer growth was repeatable to ±0.020 (The statistical analysis is provided in Appendix C).

3.3.4 Other Design Considerations for Continuous Separation Experiments

The initial design process for the continuous apparatus had to incorporate three key aspects for a successful experiment: 1) constant composition of the emulsion feed; 2) constant emulsion properties; 3) no settling zone. These aspects are described in detail in this section.

1. Constant composition of emulsion feed. The pump feed point was located in the emulsion phase at approximately the same height as the impeller, and was kept constant throughout the experiment. Some coalescence inevitably occurred during the residence time between the beaker and the separator feed point, as shown in Figure 3.9. This means that the volume fraction of emulsified water entering the separator was less than in the beaker and could possibly vary through out the experiment. The fraction of emulsified water at the feed outlet was measured at two different times in two different runs at the same experimental conditions and was found to be same (details are provided in Appendix A). These results show that the fraction of emulsified water at the feed outlet does not change with time. Similarly, the free water at the feed outlet was found to be constant. When modeling the coalescence rate in the separator, this measured amount of emulsion was used in all the calculations.

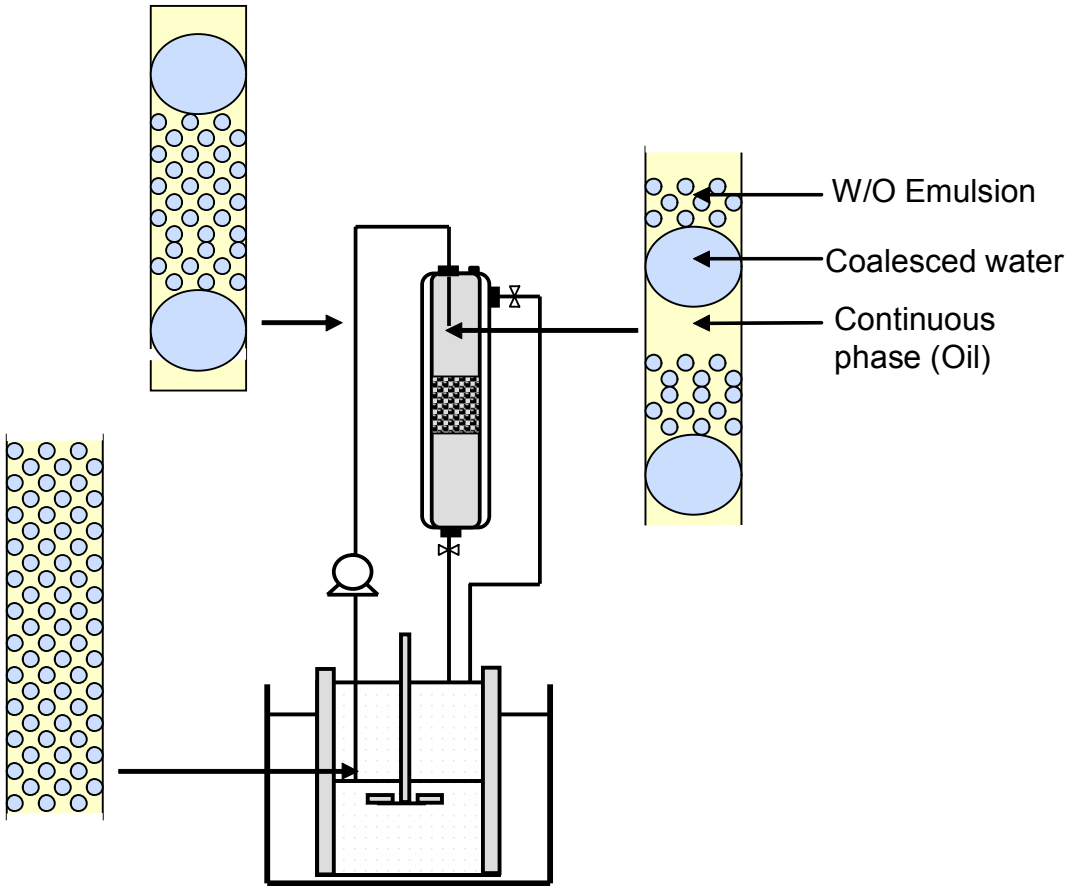

Figure 3.9 Schematic representation of the emulsion path from the beaker to the separator.

2. Constant emulsion properties. The coalescence rate depends in part on the size distribution of the emulsified water droplets. The size of the droplets depends on the shear conditions and the surfactant concentration. The shear conditions were held constant but the surfactant concentration in the beaker can change during the course of an experiment as some of the emulsion remains in the rag layer in the separator. As shown in Figure 3.10, the volume of fluid in the system is large relative to the volume of the emulsion layer. In other words, the amount of surfactant bound up in the rag layer was small relative to the total amount of surfactant. Hence, the concentration of surfactant in

the emulsion preparation beaker was not expected to vary significantly as the rag layer grew. Therefore, the size distribution of the emulsion was also expected to be nearly constant over the course of an experiment. Unfortunately, the droplets were too unstable to measure size distributions with a microscope and in-situ techniques were not available; hence direct confirmation was not possible.

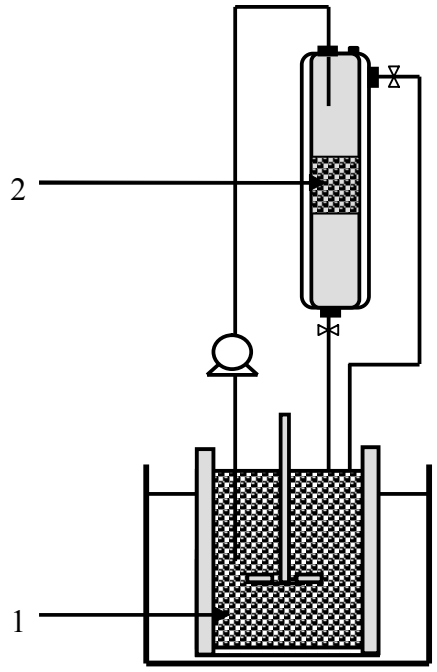

Figure 3.10 Relative volume of the emulsion in the system. 1- Initial emulsion in the system, 2- Emulsion layer in the separator.

3. Negligible settling zone. The purpose of this research was to examine coalescence rates rather than settling rates. The model emulsion systems in continuous experiments were designed for fast settling and slow coalescence, as shown in Figure 3.11. The emulsion was tailored to form large enough droplets for rapid settling, but with a slow enough coalescence rate to observe rag layer growth. The variables manipulated to control the settling rate and coalescence rate were the surfactant type, concentration,

solvent ratio, stirring rate, temperature and flow rate. Several conditions were tested until an appropriate emulsion was obtained (details are provided in Appendix B). The optimal conditions were 80 ppm of nonyphenol ethoxylate (NEO-10, 10 moles of ethylene oxide per mol surfactant) in the aqueous phase, an organic phase of an equivolume mixture of heptane and toluene, a stirring rate of 800 rpm, a temperature of 45°C, and a flow rate 45 cm^3/min. At these conditions, the emulsion was observed to settle to the interface within a few seconds and the rag layer decayed in approximately 40 minutes.

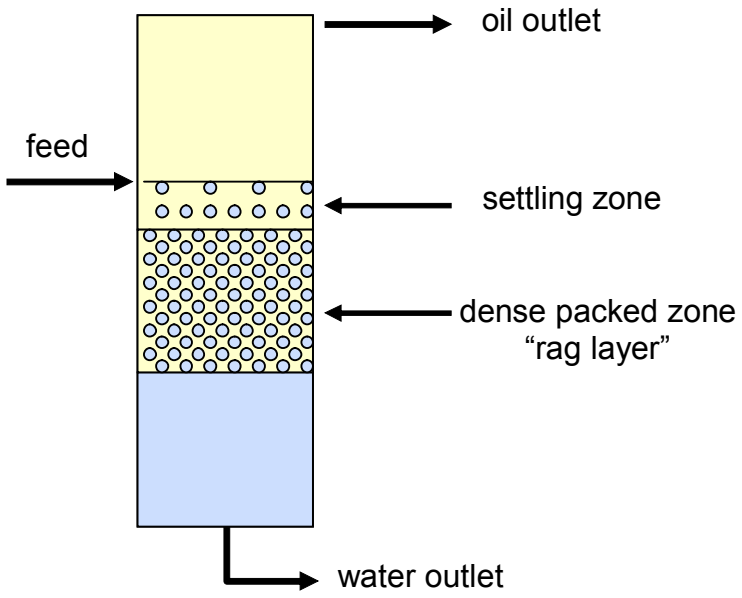

Figure 3.11 Schematic representation of the settling and rag layer zones.

CHAPTER 4
RAG LAYER MODEL

A model was developed for rag layer growth in batch and continuous emulsion separation systems. The model is based on a water mass balance on the rag layer, and the water in the feed emulsion is expressed as an influx into the rag layer and the water efflux from the rag layer is attributed solely to coalescence, which is treated as a reaction term. The mass of water in the interface is obtained from the balance between the emulsion influx and the coalescence rate. The balance provides a relationship between rag layer height over time, the feed and coalescence rates. This chapter provides the derivations of both the batch and continuous balances. The tests performed to validate the models are also presented.

4.1 Batch Settling Model

The evolution of the rag layer during a batch settling experiment is shown in Figure 4.1. As mentioned in Chapter 3, the experiments were designed so that the water droplets formed a continuous network within the beaker. Hence, there was no settling and the rag layer height depended only on the coalescence rate and, to a lesser extent, compaction.

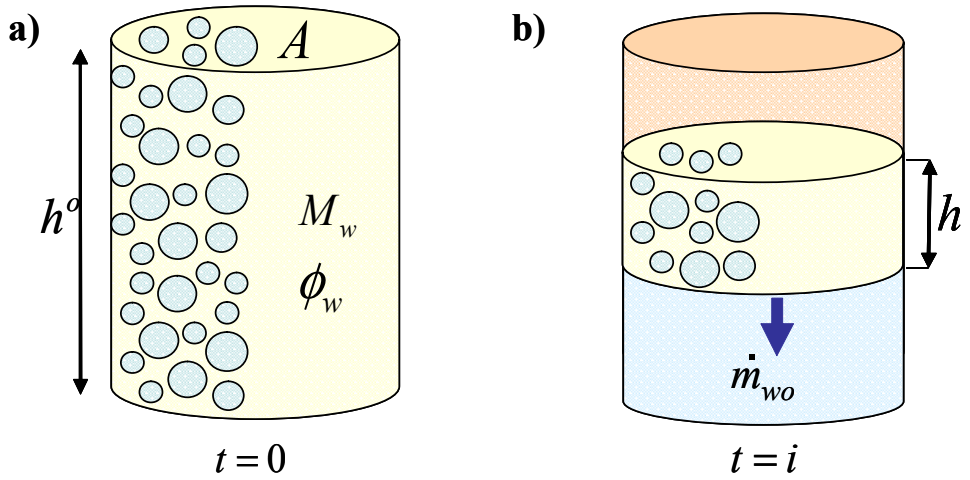

Figure 4.1 Schematic of a simplified material balance on a rag layer in batch experiment. a) initial rag layer at time zero and b) rag layer after some coalescence has occurred at time t = i.

Since there is no water entering the rag layer through settling, the mass balance on the water in the rag layer reduces to:

$$\frac{dM_w}{dt} = -\dot{m}_{wo} \qquad \textbf{Equation 4.1}$$

where M_w is the mass of water in the rag and $\dot{m}_{wo}$ is the mass flow rate of free water exiting the rag layer. The mass of water in the rag layer is given by:

$$M_w = \rho_w \phi_w A h \qquad \textbf{Equation 4.2}$$

where ρ_w is the density of water, ϕ_w is the volume fraction of water in the rag layer, A and h are the area and height of the rag layer, respectively. Note, if there is no compaction then ϕ_w is constant; otherwise it must be modified accordingly. The experimental results

indicated that the water volume fraction in the rag layer was approximately constant after the first minutes of the batch experiments.

The mass flow rate of water released from the rag layer is solely from coalescence. Here coalescence is defined as the rate at which water is released from the rag layer into the free water layer; that is, macroscopic coalescence. This is related to but not to be confused with the microscopic coalescence rate between pairs of water droplets. It was assumed that the rag layer was uniform with microscopic coalescence occurring at the same rate throughout the rag layer at any given time. In this case, the macroscopic coalescence rate is proportional to the volume of water in the rag layer and is given by:

$$\dot{m}_{wo} = -k(t)\rho_w \phi_w A h \qquad \textbf{Equation 4.3}$$

where $k(t)$ is the "coalescence" rate coefficient and is a function of time. It must be determined experimentally and the following relationship was found to adequately fit the data:

$$k(t) = k_o + (k_s - k_o)(1 - \exp\{-ct\}) \qquad \textbf{Equation 4.4}$$

where k_o and k_s are the initial and steady state coalescence rates and c is a constant.

Eqs. 4.2 and 4.3 are substituted into Eq. 4.1 to obtain,

$$\rho_w \phi_w A \frac{dh}{dt} = -k(t)\rho_w \phi_w A h \qquad \textbf{Equation 4.5}$$

Eq. 4.5 simplifies to:

$$\frac{dh}{dt} = -k(t)h \qquad \textbf{Equation 4.6}$$

Eq. 4.6 can also be expressed in terms of dimensionless height h/h_o, where h_o is the total height of the liquid column, as follows:

$$\frac{d\left(h/h_o\right)}{dt} = -k(t)\frac{h}{h_o} \qquad \textbf{Equation 4.7}$$

4.2 Continuous Model

The material balance for the continuous experiment is the same as for the batch experiment with the addition of water influx into the rag layer, as shown in Figure 4.2.

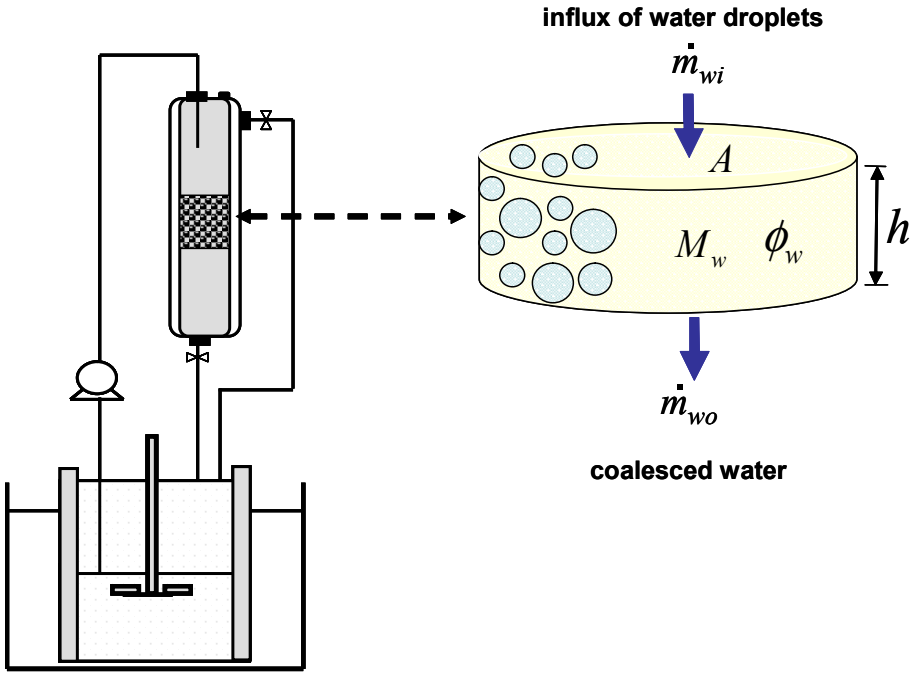

Figure 4.2 Schematic of a simplified material balance on a rag layer in a continuous system.

The rate at which water enters the rag layer is given by:

$$\dot{m}_{wi} = \rho_w \phi_w^o \dot{V}_{in} \qquad \textbf{Equation 4.8}$$

where $\phi_w°$ is the fraction of emulsified water in the feed outlet to the separator and $\dot{V}_{in}$ is the volumetric flow rate of the feed. The material balance is simplified as before to obtain:

$$\frac{dh}{dt} = \frac{\phi_w{}^o}{\phi_w} \frac{\dot{V}_{in}}{A} - k(t)h$$

Equation 4.9

4.3 Validation of Model Assumptions

The following assumptions were made in the model derivation that required confirmation:

1. The volume fraction of water in rag layer is constant (and its value must be determined)
2. The volume fraction of emulsified water in the feed to the separator is constant (and its value must be determined). Free water is assumed to pass immediately to the free aqueous phase below the rag layer.

The tests performed to confirm these assumptions and the methodology to determine the volume fraction of water in the rag layer and the volume fraction of water in the emulsion feed are discussed below.

4.3.1 Water Volume Fraction in the Rag Layer

Batch Tests: To calculate the volume fraction of water in the rag layer during batch experiment, the rag layer was allowed to coalescence until no significant rag remained. The volume fraction of water present in the rag layer was originally 0.5. The water volume fraction in the rag layer at any time is simply the volume of resolved water divided by the original rag layer volume. An example of the water volume fraction in the rag layer during a batch experiment is plotted versus time in Figure 4.3.

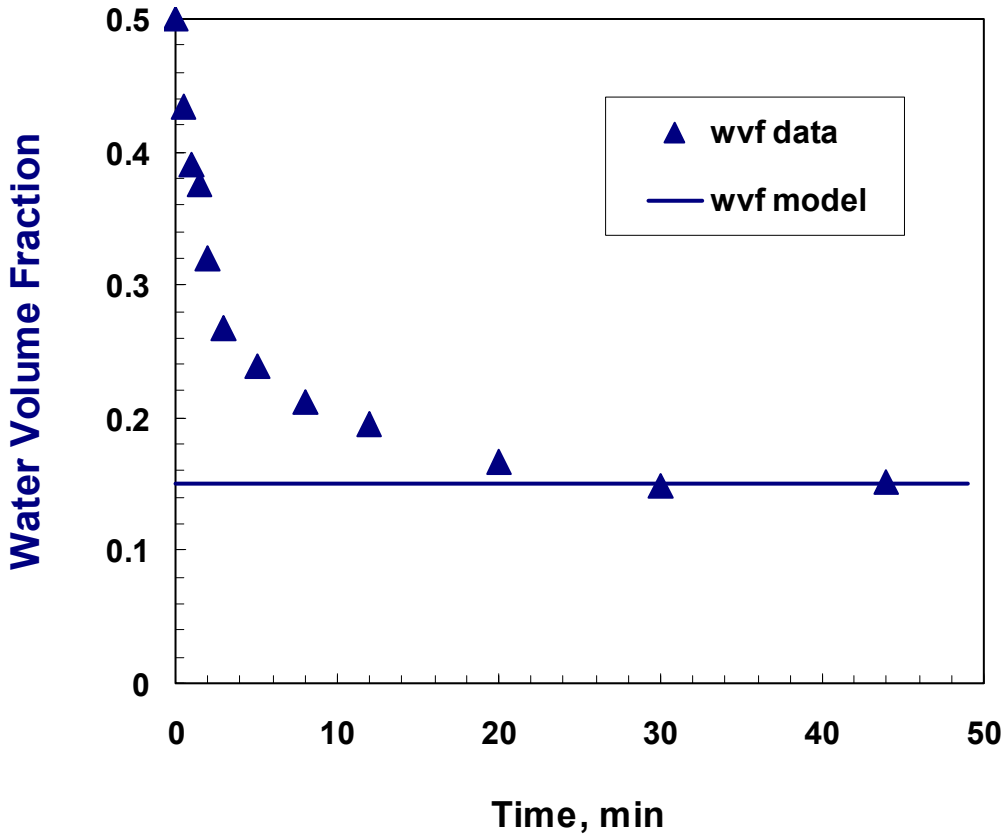

Figure 4.3 Water volume fraction in the rag lager during batch experiment.

Figure 4.3 shows that the water volume fraction in the rag layer decreases significantly over the first 10 minutes of the experiment and only becomes constant after approximately 15 minutes. This result was observed in all of the batch experiments and was unexpected because the continuous organic phase is expected to drain from the

coalescing emulsion so that the water volume fraction would remain constant or increase. It is probable that large water droplets rapidly coalesced and drained to the free water phase at early times leaving water free pockets in the emulsion layer, reducing the average water volume fraction. Hence, the assumption of water volume fraction constant is only valid after the first ten to fifteen minutes of the batch experiment.

Therefore, an alternate approach was devised to determine the coalescence rates for the batch experiments using a mass balance on the free water layer:

$$\frac{dM_{fw}}{dt} = -\dot{m}_{wo} \qquad \textbf{Equation 4.10}$$

or:

$$\rho_w A \frac{dh_{fw}}{dt} = -k(t)\rho_w \phi_w(t) A h \qquad \textbf{Equation 4.11}$$

which, after normalization, simplifies to:

$$\frac{d\left(h_{fw}/h_o\right)}{dt} = -k(t)\phi_w(t)\frac{h}{h_o} \qquad \textbf{Equation 4.12}$$

where subscript *fw* denotes the free water layer and the water volume fraction in the rag layer is now a function of time. As long as the water volume fraction in the emulsion layer can be determined, the effective coalescence rate in the compacting emulsion layer can be determined from the measured heights of the rag and free water layers using Eq. 4.12. Once the coalescence rate is known, the height of the rag layer can be calculated for confirmation using Eq. 4.7.

Continuous Tests: To calculate the water fraction in the rag layer present in the separator, the continuous experiment was run for a given time. Then the inlet and outlet flow rates

were stopped and the volume of the rag layer was measured at that time. The rag layer was then allowed to coalescence until no rag layer remained. The amount of water originally present in the rag layer was determined from the change in volume of the resolved water layer in the separator. The volume fraction of water in the rag layer is simply the volume of resolved water divided by the original rag layer volume.

The experiment was run for 3 minutes of continuous operation. After the rag layer had disappeared the water and oil were re-emulsified and the experiment run for 5 minutes of continuous operation. This procedure was repeated to collect data at 3, 5, 10, 15, and 25 minutes of continuous operation. In Figure 4.4, the rag layer volume is plotted versus time for each run and the measured water volume fractions are also indicated. The measured water volume fraction ranged from 0.33 to 0.38 indicating that the water fraction in the separator rag layer was almost constant over time at approximately 0.36 ±0.02.

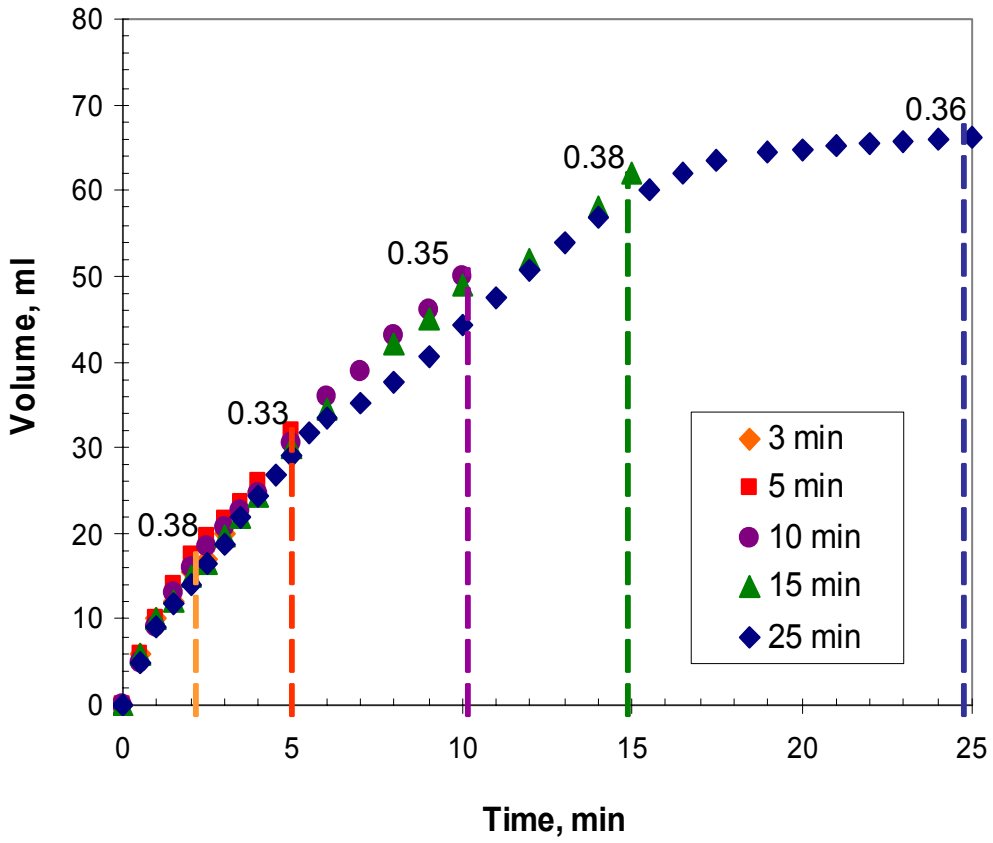

Figure 4.4 Water fraction in the rag lager during growth until steady-state.

To confirm the above water fraction value, the experiment was repeated with a new solution at the same conditions and the water fraction was found to be approximately 0.35, within 0.01 of the original experiment. One more experiment was performed changing the surfactant concentration from 80ppm to 40ppm. This time the water fraction in the separator rag layer was measured at 0.28 (details are provided in Appendix A). Hence, the volume fraction of water in the rag layer is approximately constant for any given system but should be determined for each system.

Decay Tests: To calculate the volume fraction of water in the rag layer during decay experiments, a continuous experiment was run until a steady state rag layer height was established and then the flow rate to the separator was stopped. After the flow was stopped, the rag layer was allowed to coalescence until no significant rag remained just as for a batch experiment. The water volume fraction in the rag layer at any time is simply the difference between the original water volume in the rag layer and the free water resolved at that time divided by the height of the rag layer at that time.

Figure 4.5 presents an example of the water volume fraction in the rag layer during a decay experiment is plotted versus time for 80 ppm NEO-10 system. The measured water volume fraction ranged from 0.27 to 0.36 indicating that the water fraction in the separator rag layer during decay was almost constant over time at approximately 0.31 ±0.04 for 80 ppm NEO-10 system. Several experiments were performed changing the surfactant concentration or flow rate and in all cases with water volume fraction was almost constant although the average value was different for different systems (details are provided in Appendix A). Hence, the volume fraction of water in the rag layer decay experiment is approximately constant for any given system but must be determined for each system.

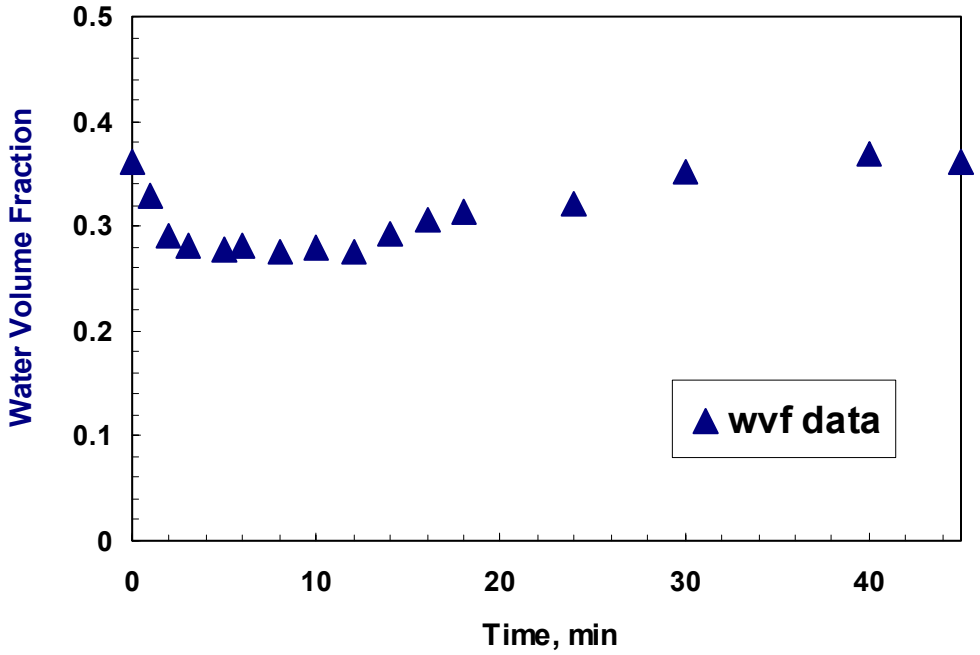

Figure 4.5 Water volume fraction in the rag lager during decay experiment.

4.3.2 Water Volume Fraction in the Feed

The feed inlet was located in the beaker so that the total water content of the feed was the same as the water content of the emulsion (50 vol%). However, some coalescence was expected between the beaker and the outlet of the feed tubing inside the separator (Points 1 and 2 in Figure 4.6).

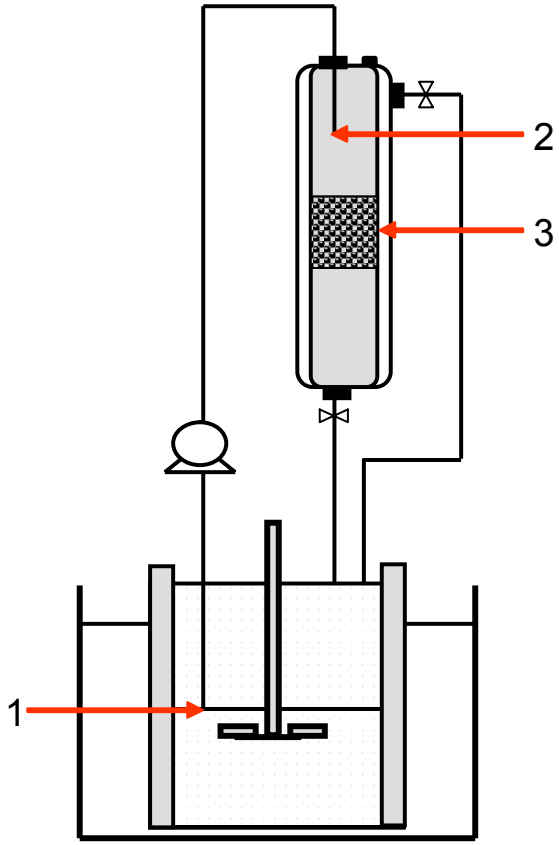

Figure 4.6 Water fraction at different points in the continuous apparatus.

Two experiments were devised in order to determine the water volume fraction at Point 2:

1. At a given point of time during the continuous experiment, the water outlet was shut off but the feed and oil outlets were left open. The amount of free water released from the rag layer was measured for 30 seconds. In this case, the resolved water comes, both from the free water in the feed and from coalescence of the coalescence of emulsified water in the rag layer.
2. At the same given point of time during a repeat of the continuous experiment, the feed and both outlets were shut off. The amount of free water released from the rag layer was measured for same period of time as first experiment. In this case,

the resolved water comes only from the coalescence of emulsified water in the rag layer.

Given the total volume of water resolved and the volume of emulsified water resolved over the same time interval, the fraction of emulsified water at the feed outlet was calculated for a given flow rate (details are provided in Appendix A). The emulsified water volume fraction in the feed was 0.15 for 80 ppm NEO-10. One more experiment was performed changing the surfactant concentration from 80 ppm to 40 ppm. This time the emulsified water volume fraction in the feed rag layer was found to be 0.064. This experiment was repeated after 30 seconds and the water volume fraction was 0.067 indicating that emulsified water fraction in the feed outlet does not change with time for a given experimental condition. However, the emulsified water fraction must be determined for each system.

CHAPTER 5
RESULTS AND DISCUSSION

The objectives of this study were: 1. to design a continuous emulsion separator to examine rag layer growth; 2. to model rag layer growth for model emulsions. The design of the apparatus was presented in Chapter 3, hence Chapter 5 will focuse on testing the model with the following two hypotheses:

1. Coalescence rates from batch and decay experiments can be determined and used to predict rag layer growth in a continuous separator.
2. Given coalescence rates for a given emulsion in a continuous separator, rag layer growth at other flow rates or separator geometries can be predicted for the same emulsion

The methodology is as follows:

1. measure batch and decay rag layer heights and determine coalescence rates
2. measure rag layer growth in the continuous separator
3. attempt to model the separator results based on the batch and decay coalescence rates (consider different surfactant type and concentration)
4. attempt to model rag layer growth at different flow rates and separator geometries

This chapter is divided into three main parts. In the first part, the results of the batch and decay experiments are presented. In the second part, the results for the continuous separator are presented. In the third part, the effects of flow rate and geometry on continuous separator performance are discussed.

5.1 Batch and Decay Experiments

The change in the rag and free water layer dimensionless heights during a typical batch experiment are presented in Figure 5.1. There is a rapid release of free water from the rag layer over the first 5 minutes followed by a much slower release over the next 40 minutes. The initial rapid coalescence is probably a combination of disengagement of some poorly emulsified free water and the coalescence of relatively large water droplets. The water volume fraction in the rag layer was not constant for the batch experiments and therefore the free water height data was fitted to the measured rag and free water heights using Eq. 4.12. Euler's method was employed with time step ranging from 30 seconds to 1 minute for this and all other cases. Then, the rag layer height was calculated from the fitted coalescence rate constants and Eq. 4.4. The fitted coalescence rate constants are provided in Table 5.1.

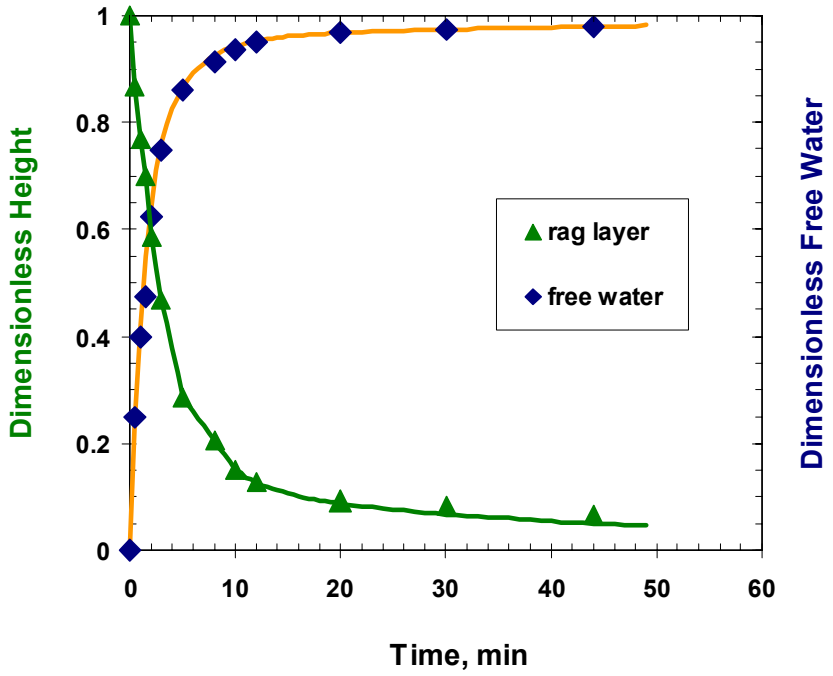

Figure 5.1 Dimensionless rag and free water heights for a batch experiment on a water-in-oil emulsion (50 vol% water) prepared an organic phase of 50:50 heptane:toluene and an aqueous phase of 80 ppm NEO-10 in water emulsified at 800 rpm and 45°C. Symbols are data; lines are model.

Table 5.1 Model parameters for the batch and decay experiments. Dispersion with 80 ppm of NEO-10 at 45°C with a mixing speed of 800 rpm. Flow rate before decay = 45 cm^3/min.

	Batch Model	Decay Model
Water volume fraction in the rag layer (ϕ_w)	*	0.36
Initial coalescence rate (k_o)	0.5	0.27
Steady state coalescence rate (k_s)	0.02	0.02
Coalescence rate constant (c)	0.19	0.25

* water volume fraction is variable and all measured values were used

Figure 5.2 shows a typical decay experiment; that is, how the steady state rag layer coalesces and disappears after the flow to the continuous separator is stopped. As with the batch experiment, there is a period of rapid coalescence followed by slow coalescence. However, unlike the batch experiment, the water volume fraction was approximately constant during the decay experiment (details are provided in Appendix A). Therefore, the rag layer height data were fitted using Eq. 4.4 based on the height of the rag layer only and the height of the water layer was simultaneously fitted using the predicted rag layer height and Eq. 4.7.

The decay experiment was first modeled with the same coalescence parameters used to model the batch experiment (Figure 5.1). The model predicted the final rag layer shrinkage rate well but significantly over-predicted the initial shrinkage rate. Therefore, the initial coalescence rate was decreased to better fit the data and the final constants are provided in Table 5.1. The results demonstrate that a slowly accumulated rag usually coalesces more slowly than a rag layer formed instantaneously. The instantaneous rag includes all of the droplets in the emulsion and therefore has the same size distribution of droplets as the emulsion. In a slowly accumulating rag, at least some of the larger, less stable droplets or pockets of free water have had time to coalesce and/or drain and

therefore the drop size distribution may be skewed towards smaller droplets with a lower average coalescence rate. Note, the coalescence rates at low surfactant concentration are similar in both cases possibly because these are unstable emulsions, the droplets have a low residence time in the continuously formed rag layer, and therefore the rag layer is similar to an instantaneously formed rag layer.

Batch experiments are not a good predictor for continuous rag layer growth probably because the drop size distribution in an instantaneously formed rag layer is different than in a gradually accumulated rag layer. Hence, the hypothesis that coalescence rates from batch experiments can be used to predict rag layer growth in a continuous separator is not valid for coalescence rates determined using the current rag layer growth model.

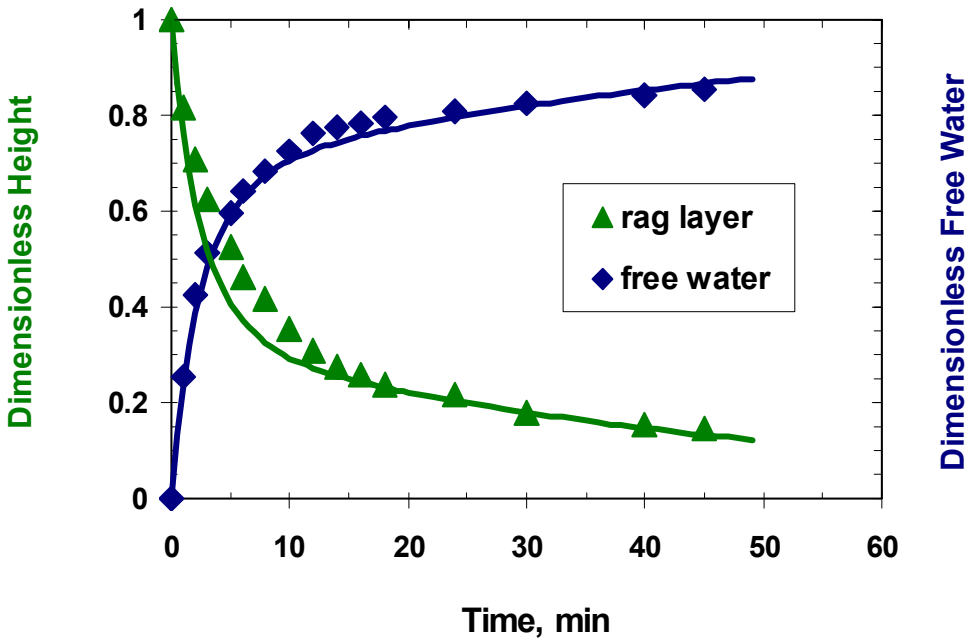

Figure 5.2 Dimensionless rag and free water heights for a decay experiment of the steady state rag layer after the separator flow rates are stopped. Flow rate before decay = 45 cm³/min and ϕ_w=0.36. Symbols are data; lines are model.

Table 5.2 Model parameters for the batch and decay experiments. Dispersion with 40, 60 or 80 ppm of NEO-10 at 45°C with a mixing speed of 800 rpm. Flow rate before decay = 45 cm³/min.

	40 ppm		60 ppm		80 ppm	
	Batch	Decay	Batch	Decay	Batch	Decay
ϕ_w	*	0.28	*	0.32	*	0.36
k_o, min^{-1}	0.59	0.70	0.525	0.55	0.50	0.27
k_s, min^{-1}	0.02	0.02	0.01	0.013	0.02	0.02
c, min^{-1}	0.15	2.0	0.15	0.70	0.19	0.25

Table 5.3 Model parameters for the batch and decay experiments. Dispersion with 80 ppm of different type of surfactant (NEO-10, NEO-10 or AOT) at 45°C with a mixing speed of 800 rpm. Flow rate before decay = 45 cm³/min.

	NEO-10		NEO-15		AOT	
	Batch	Decay	Batch	Decay	Batch	Decay
ϕ_w	*	0.36	*	0.47	*	0.47
k_o, min^{-1}	0.50	0.27	0.37	0.20	0.32	0.20
k_s, min^{-1}	0.02	0.02	0.01	0.016	0.01	0.016
c, min^{-1}	0.19	0.25	0.18	0.3	0.18	0.27

* water volume fraction is variable and all measured values were used

5.2 Rag Layer Growth in the Continuous Separator

The coalescence rate constants obtained from the decay experiments were used to predict rag layer growth in the continuous separator. A constant water volume fraction was assumed for all of the calculations.

Figure 5.3 shows the growth of a rag layer in a continuous experiment performed with the same emulsion used in the previous batch and decay experiments (Figures 5.1 and 5.2). The feed flow rate was 45 cm^3/min and the volume fraction of water in the emulsion feed was found to be 0.15 (see Section 4.3.2).The rag layer reached a steady state height of approximately 6 cm and the water volume fraction in the rag layer was approximately constant at 0.36.

To model the rag layer growth rate, the final coalescence rate was set equal to the initial coalescence rate of the decay experiment ($k_s = 0.27$ min^{-1}). This constant was sufficient to match the steady state condition. It was found that a rapid initial coalescence rate ($k_0 =$ 1.2 min^{-1}) was required to match the early data. This initial coalescence rate could not be determined from the batch or decay experimental data.

Note that, if the final coalescence rate was set to the initial coalescence rate of a batch experiment, the data could not be well fitted, Figure 5.3. Hence, the rag layer growth rate in the continuous separator could not be predicted from the data of simple batch experiments. While the decay experiments did not provide sufficient information to predict the early rag layer growth, the steady state rag layer height depends only on the final coalescence rate (k_s) which could be determined from the decay experiment.

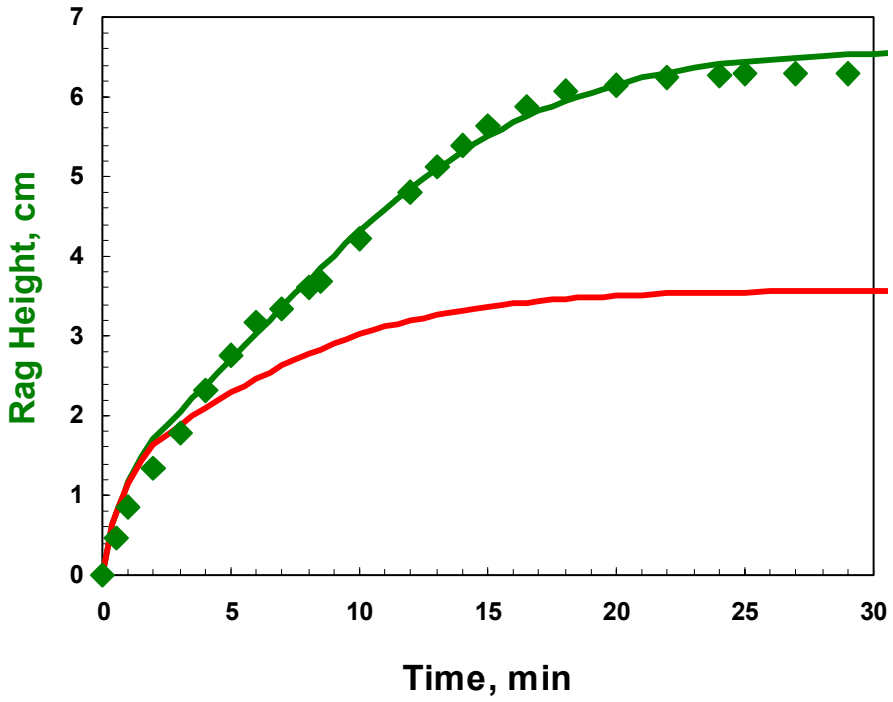

Figure 5.3 The growth of the rag layer in a continuous experiment for a water-in-oil emulsion (50 vol% water) prepared by an organic phase of 50:50 heptane:toluene and an aqueous phase of 80 ppm NEO-10 in water emulsified at 800 rpm and 45°C. Flow rate = 45 cm³ /min and ϕ_w=0.36. Symbols are data; lines are model.

The effect of NEO-10 surfactant concentration on rag layer growth is shown in Figure 5.4. As expected, increasing the surfactant concentration reduces the coalescence rate giving larger steady state rag layer heights. The data was fitted using the constants provided in Table 5.4. In all cases, the final coalescence rate was set equal to the initial coalescence rate of the respective decay experiment. In all cases, the decay experiments did not provide sufficient information to predict the initial coalescence rate, k_0, and in some cases, the value for the decay constant, c, had to be adjusted as well. Again, the steady state rag layer height depends only on the final coalescence rate and therefore could be predicted from the decay experiment data but not from the batch experiments.

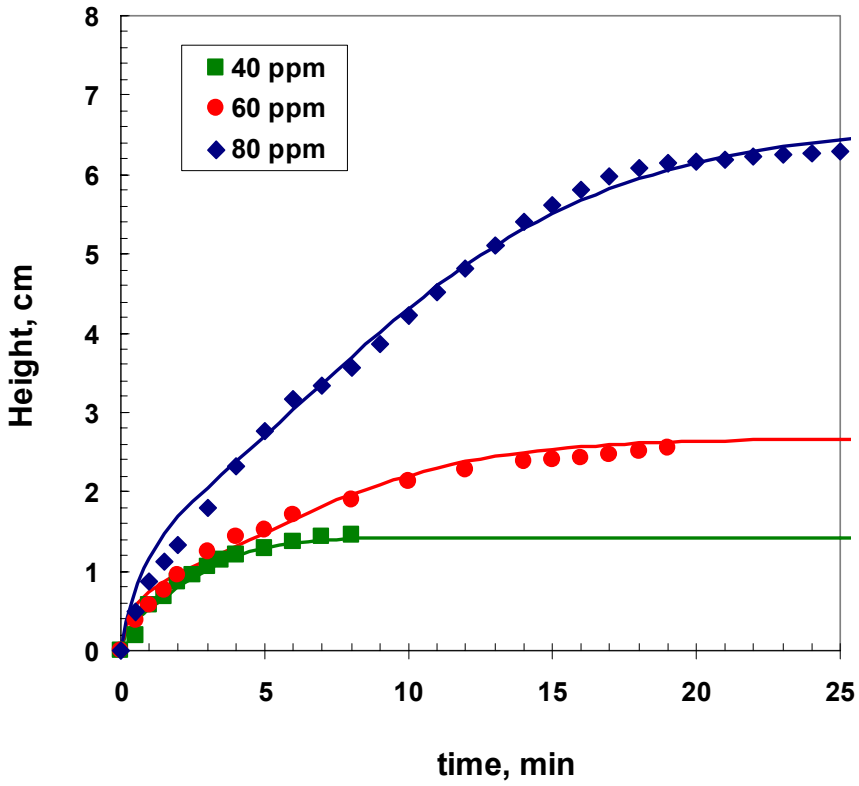

Figure 5.4 Rag layer growth versus time at different NEO-10 concentration. Temperature = 45 ^{o} C, stirring speed = 800 rpm and flow rate = 45cm^3/min. Symbols are data; lines are model.

Table 5.4 Model parameters for the decay and continuous (45cm³/min) experiments. Dispersion with 40, 60 or 80 ppm of NEO-10 at 45°C with a mixing speed of 800 rpm.

	40 ppm		60 ppm		80 ppm	
	Decay	Continuous	Decay	Continuous	Decay	Continuous
ϕ°_{w}	-	0.065	-	0.11	-	0.15
ϕ_{w}	0.28	0.28	0.32	0.32	0.36	0.36
k_o , min^{-1}	0.70	2.5	0.55	2.0	0.27	1.2
k_s , min^{-1}	0.02	0.70	0.013	0.55	0.02	0.27
c , min^{-1}	2.0	1.0	0.7	0.3	0.25	0.25

Figure 5.5 shows the results of three different types of surfactant (NEO-10, NEO-15 and AOT) using the same concentration (80 ppm) and operating conditions. It was found that surfactants NEO-15 and AOT produced a more stable emulsion and hence a larger rag layer. The rag layer grew rapidly in both cases and overflowed the system. Hence, it was not possible to measure a steady-state height for the NEO-15 and AOT. Time did not permit repeating the experiments at lower surfactant concentrations to observe a steady state condition. Nonetheless, the data is sufficient to illustrate the effect of different surfactants.

The data were fitted using the constants given in Table 5.5. As before, the fraction of emulsified water in the feed and the water volume fraction in the rag layer were measured. The final coalescence rate was set equal to the initial coalescence rate from the respective decay experiment. The initial coalescence rate and decay constant were adjusted to fit the data.

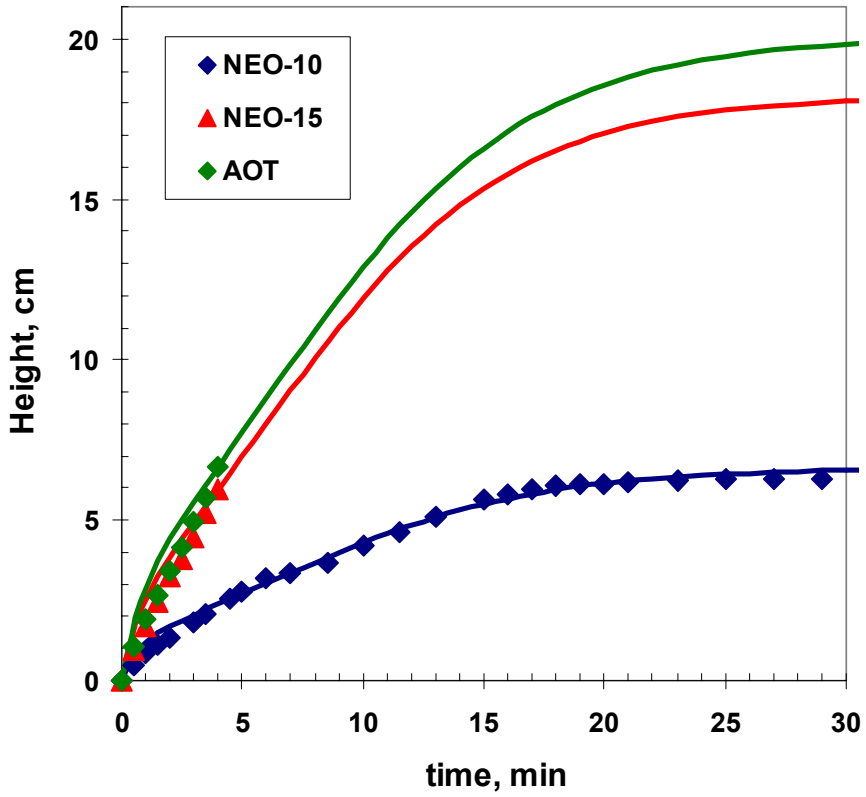

Figure 5.5 Rag layer growth versus time for different surfactants each at 80 ppm concentration, 45°C, 800 rpm stirring speed, and 45 cm³ /min flow rate. Symbols are data; lines are model.

Table 5.5 Model parameters for the decay and continuous (45cm³/min) experiments. Dispersion with 80 ppm of NEO-10, NEO-15 or AOT at 45°C with a mixing speed of 800 rpm.

	NE0-10		NEO-15		AOT	
	Decay	Continuous	Decay	Continuous	Decay	Continuous
ϕ°_{w}	-	0.15	-	0.40	-	0.44
ϕ_{w}	0.36	0.36	0.47	0.47	0.47	0.47
k_o , min^{-1}	0.27	1.2	0.20	1.0	0.20	1.0
k_s , min^{-1}	0.02	0.27	0.016	0.20	0.016	0.20
c , min^{-1}	0.25	0.25	0.30	0.30	0.27	0.30

5.3 Effect of Flow Rate and Geometry on Rag Layer in a Continuous Separator

The continuous rag layer growth could not be modeled using the coalescence rates from the batch and decay experiment data. The next test was to determine if the rag layer growth could be predicted at different flow rates and separator geometry based on the coalescence rates determined in a continuous experiment with the same emulsion.

Effect of flow rate:

Flow rates between 40 and 50 cm^3/min were examined for 80 ppm NEO-10 system. At flow rates below 40 cm^3/min, no significant rag layer formation was observed. Most of the emulsified water coalesced into the free water in the tubing between the beaker and the separator. At flow rates above 50 cm^3/min, the rag layer grew rapidly and overflowed the separator within a few minutes.

Figure 5.6 shows the rag layer growth for flow rates of 40, 45, and 50 cm^3/min. As expected, the rag layer grew more rapidly and reached higher steady state heights as the flow rate increased. Higher emulsion feed rate at a fixed coalescence rate creates larger rag layers.

To model the rag layer growth in the continuous separator, the final coalescence rate was set to the initial coalescence rate found for the relevant decay experiment. The water volume fractions in the rag layer and in the feed were measured, as reported in Table 5.6. The coalescence rate parameters determined previously were used to predict the 40 and 50 cm^3/min flow rate data, Figure 5.6. The predictions are in reasonable agreement with the data and an even better agreement is obtained if the decay constant, c, is adjusted from 0.25 to 0.30 for all three flow rates, Figure 5.7. These results demonstrate that the effect of changing flow rate can be predicted if the coalescence rate is known.

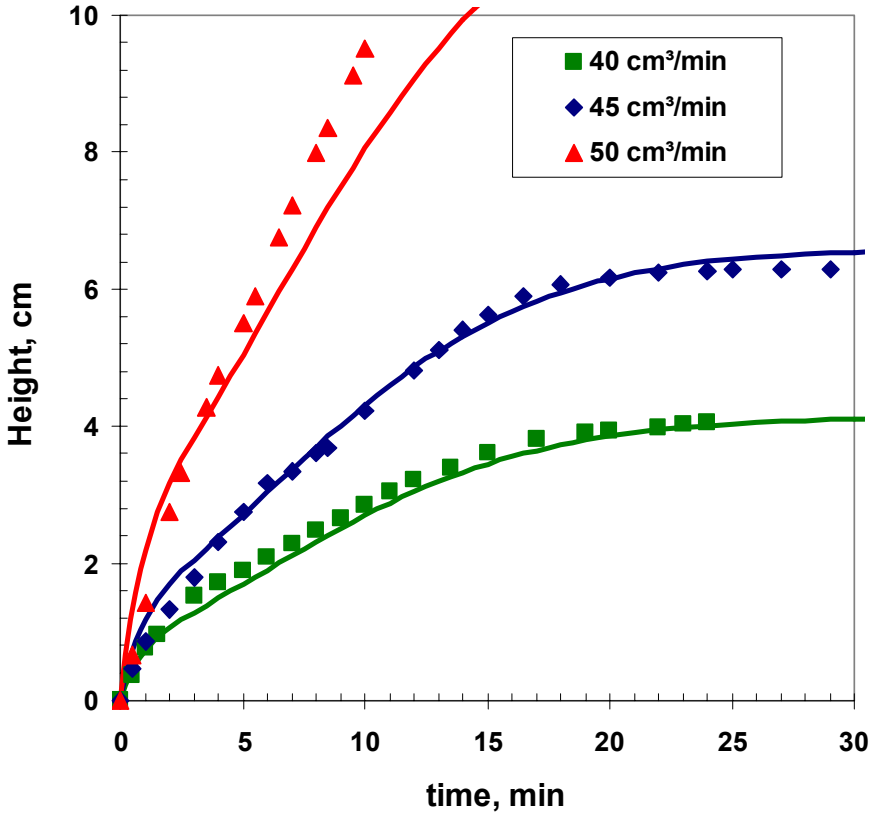

Figure 5.6 Rag layer growth at different flow rates for 80 ppm NEO-10 at 45°C, 800 rpm stirring speed. Model parameters from 45 cm³/min only. Symbols are data; lines are model.

Table 5.6 Model parameters for the effect of flow rate on the rag layer growth. Dispersion with 80 ppm of NEO-10 at 45°C with a mixing speed of 800 rpm.

	40 cm³/min		45 cm³/min		50 cm³/min	
	Decay	Continuous	Decay	Continuous	Decay	Continuous
ϕ°_{w}	-	0.094	-	0.15	-	0.28
ϕ_{w}	0.32	0.32	0.36	0.36	0.4	0.4
k_o, min^{-1}	0.27	1.2	0.27	1.2	0.27	1.2
k_s, min^{-1}	0.02	0.27	0.02	0.27	0.02	0.27
c, min^{-1}	0.25	0.25	0.25	0.25	0.2	0.25

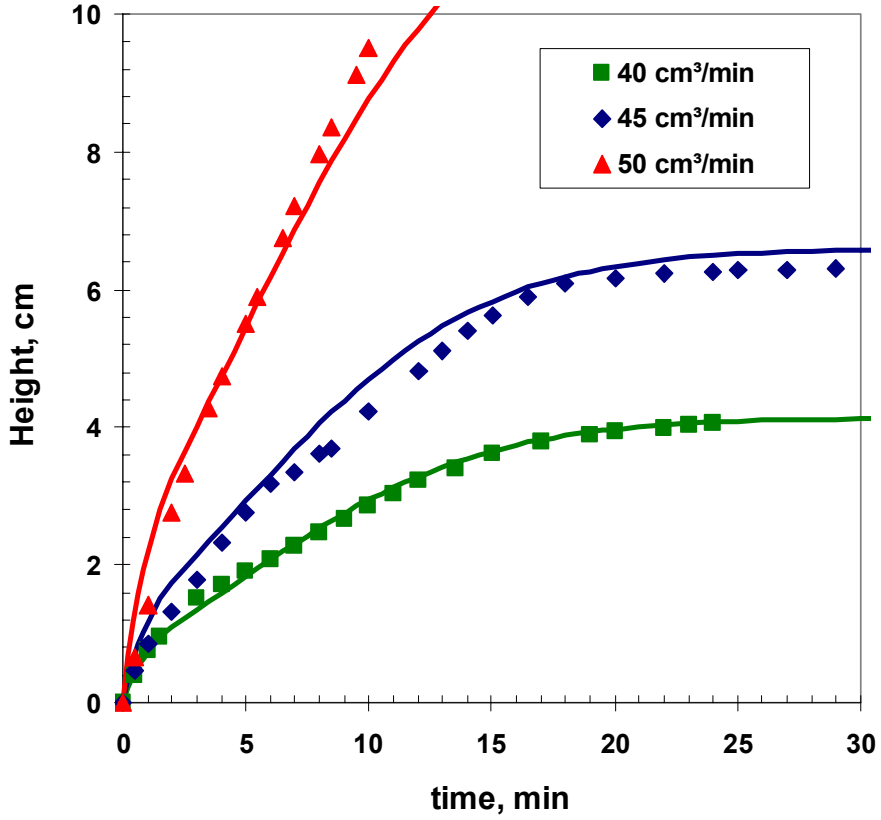

Figure 5.7 Rag layer growth at different flow rates for 80 ppm NEO-10 at 45°C, 800 rpm stirring speed. Decay constant adjusted from 0.25 to 0.30. Symbols are data; lines are model.

Effect of geometry:

The effect of geometry was investigated for the 80 ppm NEO-10 emulsion. A new separator was installed with a cross sectional area of 14.4 cm² (separator volume of 500 ml) compared with the previous separator which had an area of 10.5 cm² (separator volume of 250 ml). Figure 5.8 shows the growth in rag layer height result for the two different separator areas with the same flow rate of 45 cm³/min A new separator was installed with a cross sectional area of 14.4 cm² (separator volume of 500 ml) compared with the previous separator which had an area of 10.5 cm² (separator volume of 250 ml). The rag layer growth data for the smaller separator was fitted previously, Figure 5.3. The

same coalescence parameters were used to model the data for the larger separator, Figure 5.8. The predicted rag layer height is significantly higher than the data. The data was repeated twice with the same results. Therefore, the model is not correctly accounting for the effect of the area of the separator. It is probable that the coalescence rate of droplet with the free water interface is higher than with another droplet. Hence, the model assumptions are not correct. It is recommended to replace the current coalescence term with an expression based on the interfacial area. In its current form, the proposed rag layer model is adequate to predict the change in rag layer height with a change in flow rate. However, it cannot predict rag layer growth in another separator or predict rag layer growth in continuous separation from batch experiments. The latter deficiency may be corrected when the effect of the interfacial area is correctly accounted for.

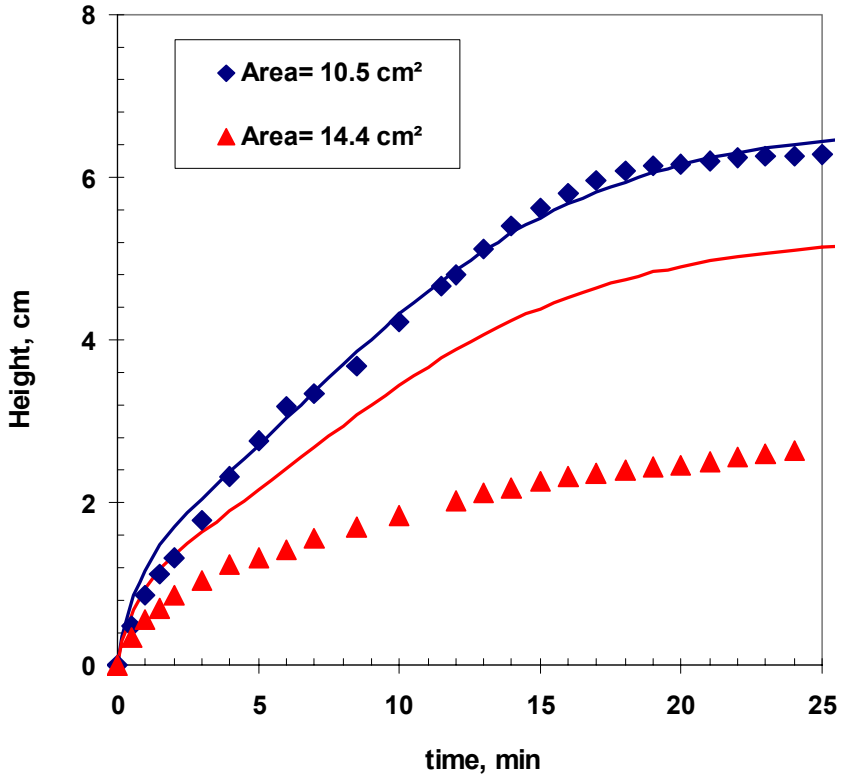

Figure 5.8 Rag layer growth for two different cross sectional areas of the separator. Dispersion with 80 ppm NEO-10 at 45°C, 45 cm³/min flow rate, and 800 rpm stirring speed. Symbols are data; lines are model.

Table 5.7 Model parameters for the decay and continuous ($45 cm^3/min$) experiments at two different cross sectional areas with 80 ppm of NEO-10 at 45^oC and a mixing speed of 800 rpm.

	$10.5\ cm^2$		$14.4\ cm^2$	
	Decay	Continuous	Decay	Continuous
ϕ°_w	-	0.15	-	0.15
ϕ_w	0.36	0.36	0.33	0.33
k_o, min^{-1}	0.27	1.2	0.27	1.2
k_s, min^{-1}	0.02	0.27	0.01	0.27
c, min^{-1}	0.25	0.25	0.42	0.25

CHAPTER 6

CONCLUSIONS AND RECOMMENDATIONS

6.1 Thesis Conclusions

The main objective of this work was the design and methodology for using a continuous separator to study rag layer growth. For a given model emulsion system a methodology was establish to measure coalescence rates within the rag layer. Based on batch and decay coalescence rates a model was developed and tested which related the rag layer growth to coalescence. The rag layer model was also tested to assess the effects of a different surfactant and surfactant concentration. The predictive capability of the model was tested with different flow rates and separator geometries with the same emulsion system.

The conclusions from this study and recommendations for future work are presented below.

Batch and decay experiments:

- It was found that during the batch and decay experiment there is a period of rapid coalescence followed by slow coalescence.

- The water volume fraction in the rag layer was not constant for the batch experiments. Therefore, the model was based on the growth of the free water layer rather than the rag layer.

- The water volume fraction during the decay experiments was approximately constant with time. In this case, the rag layer was modeled directly.

- The initial coalescence rate of the decay experiment was usually lower than the corresponding batch experiment. It appears that a slowly accumulating rag layer coalesces more slowly than a rag formed instantaneously. Therefore, coalescence rates from batch experiments are not a good predictor for continuous rag layer growth.

Rag Layer Growth in the Continuous Separator:

- The rate at which the model emulsion released water to the free water layer in both batch and continuous experiments change over time.

- The water volume fraction during the rag layer growth is approximately constant with time.

- Steady state rag layer height depends only on the final coalescence rate (k_s) which could be determined from the decay experiment but not from the batch experiment.

- Increasing the surfactant concentration reduces the coalescence rate resulting in larger steady state rag layer heights.

- It was found that surfactants NEO-15 and AOT follow the same general trends as the NEO-10. However they resulted in a more stable emulsion and hence a larger rag layer.

- The continuous rag layer growth could not be modeled using the coalescence rates from the batch and decay experimental data. However, the steady state rag layer height could be predicted from the decay experimental data.

Effect of flow rate and separator geometries:

- As the flow rate increased, the rag layer grew more rapidly and reached higher steady state heights. Higher emulsion feed rate at a fixed coalescence rate creates larger rag layers.

- The proposed rag layer model can be used to predict the change in rag layer height with a change in flow rate.

- In the small separator, the rag layer grows more rapidly and reaches a higher steady state height. At the same volumetric flow rate, the mass flux of the emulsion is higher in the smaller diameter separator giving a higher rag layer. The model was not able to predict the effect of changing the separator diameter. It is possible that the coalescence occurs primarily at the water-oil interface rather than throughout the rag layer. If so, the model must be revised.

6.2 Recommendations for Future Studies

- It is recommended that the current model be modified to account for the effect of the area of the separator. The current coalescence rate expression could be replaced with an expression based on the interfacial area. It is probable that the coalescence rate of a droplet with the free water interface is higher than with another droplet. Such modification may improve the prediction of the effect of the area of the separator.

- From the present work, a baseline of rag layer growth rates was established. It is recommended to assess the effect of solids on these rag layers including the size, type, and wettability of the solids; for example, coarse sand, fine sand, clays, and iron sulfides. The effect of different chemical additives or combinations of additives could also be tested.

- It is recommended to assess model systems more closely related to petroleum emulsions; for example, solutions of asphaltenes in toluene and heptane or solvent diluted bitumen. Finally, diluted oil sand froths could be investigated and the interpretation guided by the model system results.

REFERENCES

Binks B. and Horozov T. (2006) Colloidal particles at liquid interfaces. Cambridge University.

Binks BP. (1998) Emulsions-Recent Advances in Understanding. Modern Aspects of Emulsion Science. U.K.: The Royal Society of Chemistry: 1-47.

Chen, F., Finch, J.A., Xu, Z., and Czarnecki, J. (1999). Wettability of Fine Solids Extracted from Bitumen Froth, *Journal of Adhesion Science and Technology*, 13 (10), 1209-1224.

Czarnecki, Jan; Moran, Kevin; Yang, Xiaoli. (2007). On the "Rag Layer" and diluted bitumen froth dewatering, *Canadian Journal of Chemical Engineering*, v 85, n 5, 748-755.

Dalingaros, W., Jeelani, S. A. K. and Hartland, S. (1987). Prediction of steady-state dispersion height in the diseneating section of an extraction column from batch settling data. *Canadian Journal of Chemical Engineering*, in press.

Dean, J.A. (1999). Lange's Handbook of Chemistry, McGraw-Hill, 15th Edition.

Farn R. (2006). Chemistry and technology of surfactants. Blackwell Pub.1-14

Gafonova O. and Yarranton W.H. (2001). The Stabilization of Water-in-Hydrocarbon Emulsions by Asphaltenes and Resins. *Journal of Colloid and Interface Science,* 241, 469–478.

Gu, G., Zhang L. Xu, Z., Nandakumar, K., and Masliyah, J.H. (2007). Novel Bitumen Froth Cleaning Device and Rag Layer Characterization, *Energy & Fuels*, 21, 3462–3468.

Hartland S. (1979). Effect of gravity on the drainage of thin films in two-dimensional dense-packed dispersions. *Chemical Engineering Science*, v 34, n 4, p 485-491.

Hartland, S. and Jeelani, S. A. K. (1985). Relationship between models for predicting steady-state dispersion height from batch settling data. *Inst. Chem. Engr*, Symp. Series No. 94, II, 21 l-223.

Hartland, S. and Jeelani, S. A. K. (1987). Choice of Model for Predicting the dispersion height in liquid/liquid gravity settlers from batch settling data. *Inst. Chemical Engineering Science*, Vol. 42, No.8, pp, 1927-1938.

Hartland, S. and Jeelani, S. A. K. (1988). Prediction of Sedimentation and Coalescence Profiles in a Decaying Batch Dispersion. *Chemical Engineering Science*. Vol. 43, pp. 2421-2429.

Hepler, L.G. (1994). Alberta oilsands: Industrial procedures for extraction and some recent fundamental research, AOSTRA Technical publication No. 14.

Hirasaki G., Jiang T., and Miller C. (2007). Diluted Bitumen Water-in-Oil Emulsion Stability and Characterization by Nuclear Magnetic Resonance (NMR) Measurements. Institut Francüais du Petrole (IFP). *Energy & Fuels*, 21, 1325-1336.

Hirasaki G., Jiang T, Miller C., and Moran K (2008). Using Silicate and pH Control for Removal of the Rag Layer Containing Clay Solids Formed during Demulsification. Department of Chemical and Biomolecular Engineering, Rice University, *Energy Fuels,* 22, 4158– 4164.

Holmberg K. (2003). Novel surfactants: preparation, applications, and biodegradability CRC Press.

Ivanov I.B. (1998). Thin Liquid Films: Fundamentals and Applications.

James Swarbrick (2007). Encyclopaedia of Pharmaceutical Technology, 2007, 1554-1564.

Jeelani, S. A. K. and Hartland, S. (1985). Prediction of steady state dispersion height from batch settling data. *A.I.Ch.E. J.* 31, 71 l-720.

Jeelani, S. A. K. and Hartland, S. (1986a) Prediction of dispersion height in liquid/liquid gravity settlers from batch settling data. *Chem. Engng Res. Des*. 64, 450-460.

Jeelani, S. A. K. and Hartland, S. (1986b). Scale-up of industrial gravity settlers from batch settling data.

Jeelani, S.A.K. and Hartland, S. (1993). The continuous separation of liquid/liquid dispersions. *Chemical Engineering Science*, Vol. 48, No. 2. p. 239-254.

Kankaanpaan T. (2007). CFD Procedure for Studying Dispersion Flows and Design optimization of The Solvent Extraction Settler. Doctoral thesis. Department of Materials Science and Powder Metallurgy. Helsinki University of Technology.

Khadim, M.A., and Sarbar, M.A. (1999). Role of Asphaltene and Resin in Oil Field Emulsions, *Journal of Petroleum Science and Engineering*, 23 (3-4), 213-221.

Kitchener, J.A., Musselwhite, A.(1968). The Theory of Stability of Emulsions, Emulsion Fundamentals Science , P. Sherman, Ed., Academic Press, London.

Liu, J., Xu, Z., and Masliyah, J. (2004). Role of Fine Clays in Bitumen Extraction From Oil Sands, *AIChE Journal*, 50 (8), 1917-1927.

Manning F., and Thompson R. (1995). Oilfield Processing of Petroleum: Crude oil. Tulsa, Okla. PennWell.

Masliyah, J.H. (1994). Electrokinetic Transport Phenomena. AOSTRA Technical Publications Series 12, Alberta Oil Sands Information Services Calgary.

McCabe, W.L., Smith, J.C., and Harriott, P. (1985). Unit Operations of Chemical Engineering, McGraw-Hill International Editions, Fourth Edition, Singapore.

Mizrahi, J, and Barnea, E. (1973). Compact settler gives efficient separation of liquid/liquid dispersions, Process engineering, Vol. 1, p. 60-65.

Moran, K. and Czarnecki, J. (2006). Towards a Better Understanding of Rag Layer Emulsion Stability", Oil sands 2006, Edmonton, Alberta, February 22-24.

Ponisseril Somasundaran (2006). Encyclopedia of surface and colloid science CRC Press, 2006, 2435-2444.

Richardson, J.F.; Zaki,W.N. (1954). Sedimentation and fluidisation: Part I. Trans. Inst. Chem. Eng. 32. pp. 35f.

Richardson, J.F., and Zaki, W.N. (1997). Sedimentation and Fluidization: Part I, Process Safety and Environmental Protection: Transactions of the Institution of Chemical Engineers, Part B, 75, S82-S100.

Romanova, U.G., Yarranton, H.W., Schramm, L.L., and Shelfantook, W.E. (2004). Investigation of Oil Sands Froth Treatment, *Canadian Journal of Chemical Engineering*, 82 (4), 710-721.

Romanova, U.G., Valinasab, M., Stasiuk, E.N., Yarranton, H.W., Schramm, L.L., and Shelfantook, W.E. (2006). The Effect of Oil Sands Bitumen Extraction Conditions on Froth Treatment Performance, *Journal of Canadian Petroleum Technology*, 45 (9), 36-45.

Rosen M. (2004). Surfactants and interfacial phenomena. John Wiley and Sons.

Salamone, Joseph. (1996). Polymeric Materials Encyclopedia. CRC Press.

Saadatmand, M. (2007). Personal communication, University of Calgary.

Saadatmand, M. (2008). Investigation of Rag Layers from Oil Sands Froth. M.Sc. Thesis. University of Calgary, Calgary, 2008.

Stasiuk, E.N. (2009). Personal communication, University of Calgary.

Schramm L & Kutay S. (2000). Emulsions and Foams in the Petroleum Industry. In: Schramm L (ed) Surfactants: Fundamentals and Applications in the Petroleum Industry. U.K.: Cambridge University Press.

Schramm L, Stasiuk E & Marangoni G. (2003). Surfactants and their Applications. In: Anonymous Annu. Rep. Prom.Chem., Sect. C.

Schramm, L. (2005). Emulsions, Foams, and Suspensions Fundamentals and Applications, Wiley-VCH Verlag GmbH & Co. KGaA, Weinheim.

Schulman, J.H., and Leja J. (1954). Trans Faraday Soc. 50 (1), 598.

Sjoblom J, Aske N, Auflem IH, Brandal O, Havre TE, Saether O, Westvik A, Johnsen EE & Kallevik H. (2003). Our current understanding of water-in-crude oil emulsions. Recent

characterization techniques and high pressure performance. *Adv Colloid Interface Sci.* 100-102: 399-473.

Somusundurum S., and Huung L. (1998). Thermodynamics of adsorption of surfactants at solid-liquid interface. Lungmuir Center for Colloids und Interfaces.

Stechemesser H and B. Dobiáš. (2005). Coagulation and flocculation, CRC Press, 151-156

Swarbrick J. (2007). Encyclopedia of Pharmaceutical Technology, Informa Health Care, 2 556 - 1559

Sztukowski DM, Jafari M, Alboudwarej H & Yarranton HW. (2003). Asphaltene self association and water-in-hydrocarbon emulsions. *Journal of Colloid and Interface Science*, 265(1): 179-186.

Sztukowski DM & Yarranton HW. (2005). Oilfield solids and water-in-oil emulsion stability. *Journal of Colloid Interface Science,* 285(2): 821-833.

Tambe D., and Sharma M. (1993). Factors Controlling the Stability of Colloids-Stabilized Emulsions. *Journal of Colloids and Interfaces Science*, 157, 244-253.

Tropea C., Yarin A., Foss J. (2007). Springer handbook of experimental fluid mechanics 687-689

Vaclavik V. and W. Christian. (2007). Essentials of Food Science. Springer.

Urrutia P. (2006). Predicting Water-in-Oil Emulsion Coalescence from Surface Pressure Isotherms. M.Sc. thesis. Deparment of Chemical and Petroleum Engineering, University of Calgary, Calgary, Alberta.

Yarranton HW, Alboudwarej H & Jakher R. (2000). Investigation of Asphaltene Association with Vapor Pressure Osmometry and Interfacial Tension Measurements. *Ind Eng Chem Res*, 39(8): 2916-2924.

Yarranton HW, Sztukowski DM & Urrutia P. (2007). Effect of interfacial rheology on model emulsion coalescence. I. Interfacial rheology. *Journal of Colloid and Interface Science*, 310(1): 246-252.

Yarranton HW. (2005). Asphaltene self-association. *J Dispersion Sci Technol,* 26(1): 5-8.

Yarranton HW. (1997). Asphaltene Solubility and Asphaltene Stabilized Water-in-Oil Emulsions. Doctoral thesis. Department of Chemical and Materials Engineering, University of Alberta. Edmonton, Alberta.

APPENDIX A

WATER VOLUME FRACTION IN THE RAG LAYER

A.1 Water Volume Fraction during Rag Layer Growth

Table A.1 Water volume fraction in the rag lager during growth until steady-state. Dispersion with 80 ppm of NEO-10 at 800 rpm and 45°C. Flow rate = 45 cm^3 /min.

NEO-10 model system	Time min	Data 1 wvf	Data 2 wvf
80 ppm			
	3	0.38	0.37
	5	0.33	0.36
	10	0.35	0.32
	15	0.38	0.35
	22	0.36	0.35
	Average	**0.36**	**0.35**

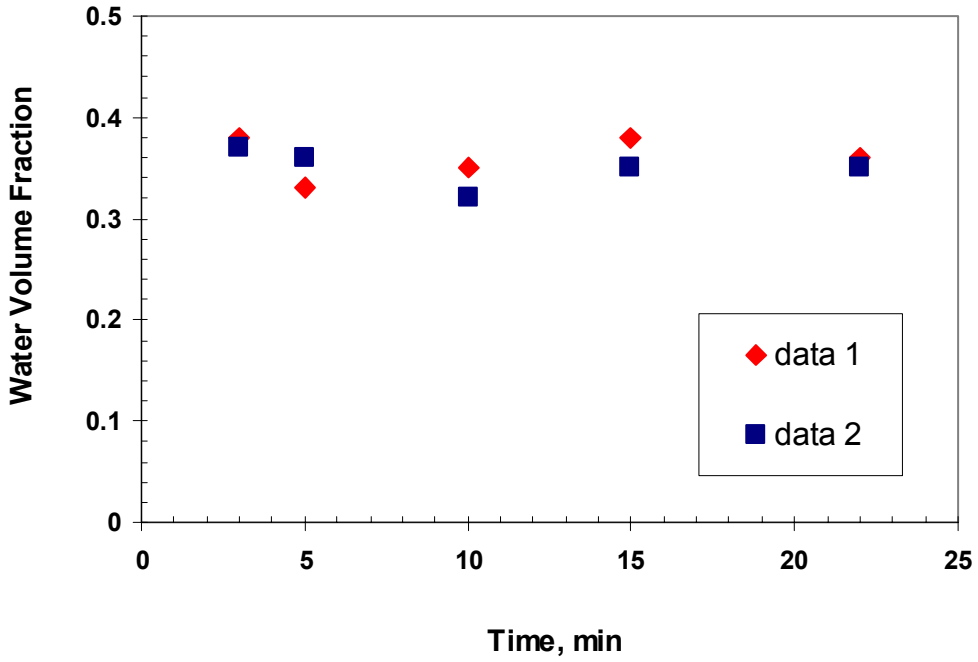

Figure A.1 Water volume fraction in the rag lager during growth until steady-state. Dispersion with 80 ppm of NEO-10 at 800 rpm and 45°C. Flow rate = 45 cm³ /min.

Table A.2 Water volume fraction in the rag lager during growth until steady-state. Dispersion with 40 ppm of NEO-10 at 800 rpm and 45°C. Flow rate = 45 cm³ /min.

NEO-10 model system	Time min	Data No. 1 wvf	Data No. 2 wvf
40 ppm			
	3	0.3	0.32
	5	0.26	0.28
	8	0.28	0.27
	Average	**0.28**	**0.29**

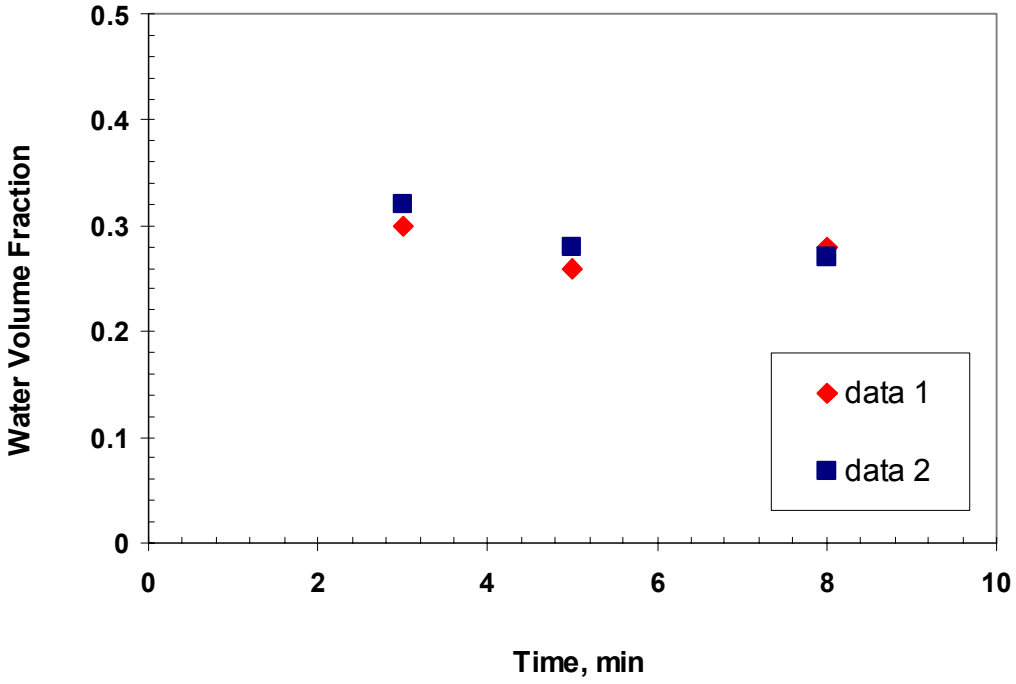

Figure A.2 Water volume fraction in the rag lager during growth until steady-state. Dispersion with 40 ppm of NEO-10 at 800 rpm and 45°C. Flow rate = 45 cm^3 /min.

A.2 Water Volume Fraction in the feed

Table A.3 Water volume fraction in the feed. Dispersion with 80 ppm of NEO-10 at 800 rpm and 45°C. Flow rate = 45 cm³ /min. Test 1.

time, sec	rag	ϕ_w	rag wtr	cumulative tot wtr	cumulative free wtr	cumulative coalescence	cumulative % emul feed
90	14	0.36	5.04	0	0	0	0
100	15	0.36	5.4	2.36	2	0.7	17.97
110	16.2	0.36	5.832	5.592	4.8	1.3	14.96
120	17	0.36	6.12	9.08	8	1.6	11.81
							14.91%

Table A.4 Water volume fraction in the feed. Dispersion with 80 ppm of NEO-10 at 800 rpm and 45°C. Flow rate = 45 cm³ /min. Test 2.

time, sec	rag	ϕ_w	rag wtr	cumulative tot wtr	cumulative free wtr	cumulative coalescence	cumulative % emul feed
120	15.4	0.36	5.544	0	0	0	0
130	16.2	0.36	5.832	2.388	2.1	0.8	18.22
140	17.2	0.36	6.192	5.648	5	1.6	15.92
150	18	0.36	6.48	9.136	8.2	2	12.85
							15.66%

Table A.5 Water volume fraction in the feed. Dispersion with 40 ppm of NEO-10 at 800 rpm and 45°C. Flow rate = 45 cm³ /min. Test 1.

time, sec	rag	ϕ_w	rag wtr	cumulative tot wtr	cumulative free wtr	cumulative coalescence	cumulative % emul feed
90	7	0.28	1.96	0	0	0	0
100	7.8	0.28	2.184	3.524	3.3	0.4	7.08
110	8.3	0.28	2.324	7.264	6.9	0.7	5.86
120	9.6	0.28	2.688	10.428	9.7	0.9	6.24
							6.4%

Table A.6 Water volume fraction in the feed. Dispersion with 40 ppm of NEO-10 at 800 rpm and 45°C. Flow rate = 45 cm³ /min. Test 2.

time, sec	rag	ϕ_w	rag wtr	cumulative tot wtr	cumulative free wtr	cumulative coalescence	cumulative % emul feed
120	8.8	0.28	2.464	0	0	0	0
130	9.4	0.28	2.632	3.568	3.4	0.5	7.49
140	9.9	0.28	2.772	7.308	7	0.9	6.61
150	10.6	0.28	2.968	10.604	10.1	1.1	6.05
							6.7%

Table A.7 Water volume fraction in the feed. Dispersion with 80 ppm of NEO-10 at 800 rpm and 45°C. Flow rate = 40 cm³ /min.

time, sec	rag	ϕ_w	rag wtr	cumulative tot wtr	cumulative free wtr	cumulative coalescence	cumulative % emul feed
120	10.4	0.32	3.328	0	0	0	0
130	11.3	0.32	3.616	3.388	3.1	0.6	10.48
140	12	0.32	3.84	7.312	6.8	1.2	9.37
150	12.8	0.32	4.096	10.568	9.8	1.6	8.96
							9.6%

A.3 Water Volume Fraction during decay

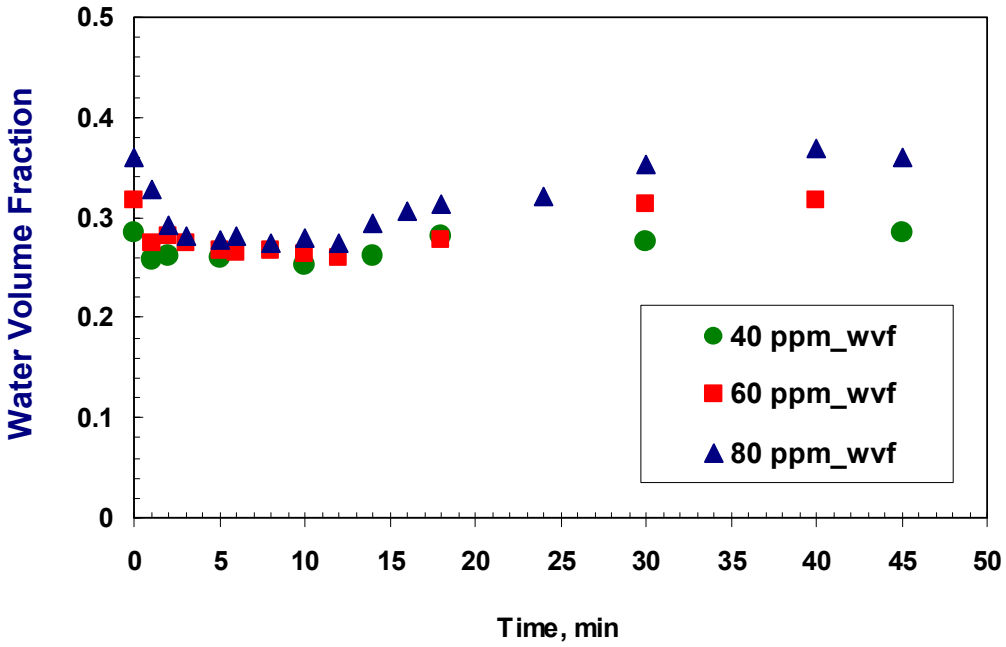

Figure A.3 Water volume fraction during decay at different concentration of NEO-10. Dispersion with a temperature of 45°C and a mixing speed of 800 rpm. Flow rate before decay = 45 cm³/min.

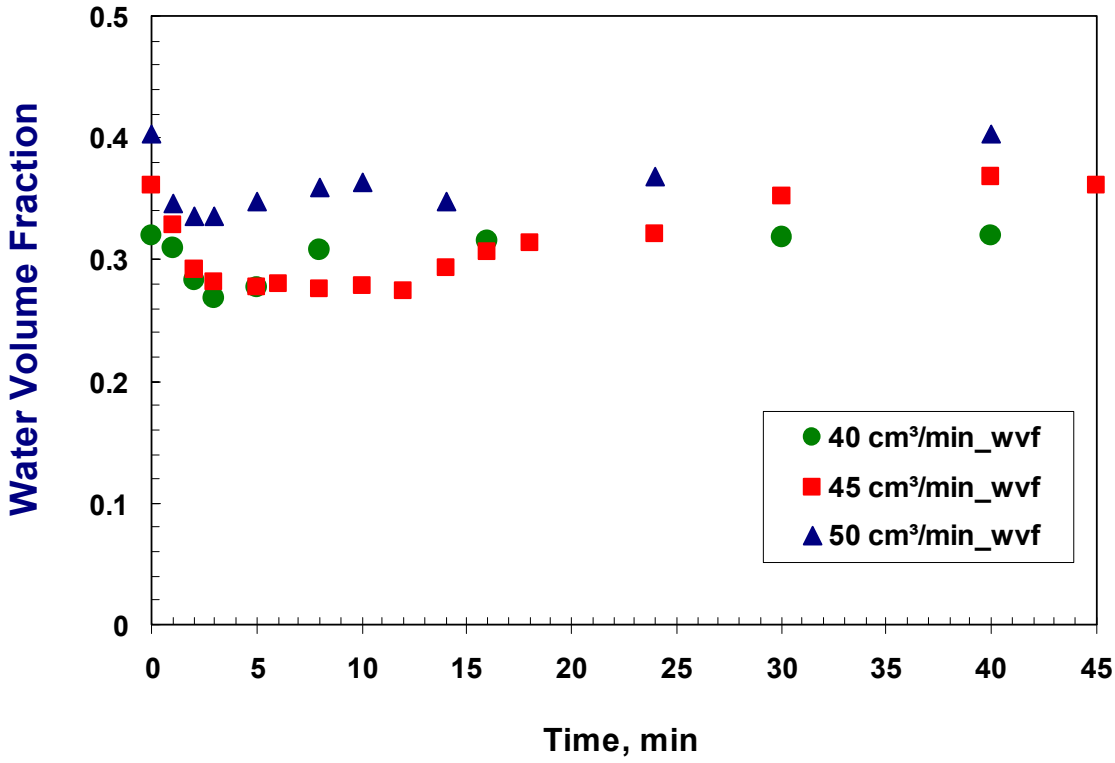

Figure A.4 Water volume fraction during decay at different flow rate. Dispersion with 80 ppm of NEO-10 at 45°C with a mixing speed of 800 rpm. Flow rate before decay = 40, 45 and 50cm³/min.

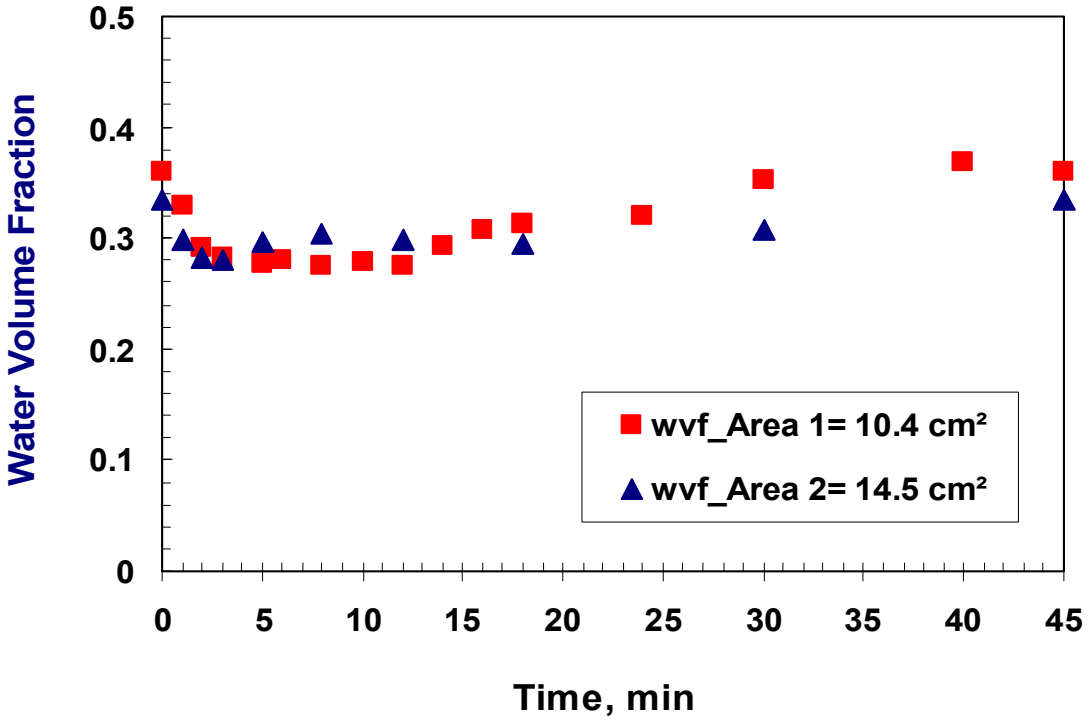

Figure A.5 Water Volume Fraction during decay at two different cross sectional areas (area 1 = 10.5 cm^2 and area 2 = 14.4 cm^2). Dispersion with 80 ppm of NEO-10 at 45°C with a mixing speed of 800 rpm. Flow rate before decay = 45 cm^3/min.

APPENDIX B

VARIABLES FOR THE MODEL EMULSIONS

The variables manipulated to control the settling rate and coalescence rate were the surfactant type, concentration, solvent ratio, temperature and flow rate. Stirring rate constant = 800 rpm. Several conditions were tested until an appropriate emulsion was obtained.

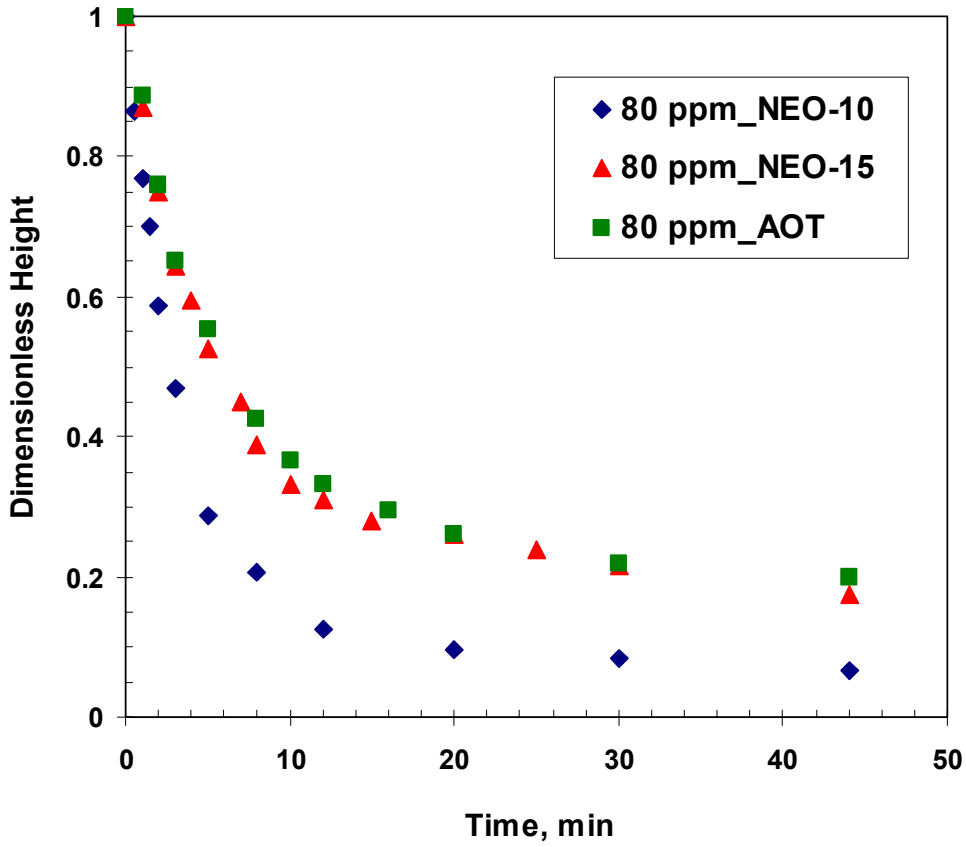

Figure B.1 Dimensionless rag and free water heights for a batch experiment on a water-in-oil emulsion (50 vol% water) prepared an organic phase of 50:50 heptane:toluene and an aqueous phase of 80 ppm NEO-10, NEO-15 or AOT in water emulsified at 800 rpm and 45°C.

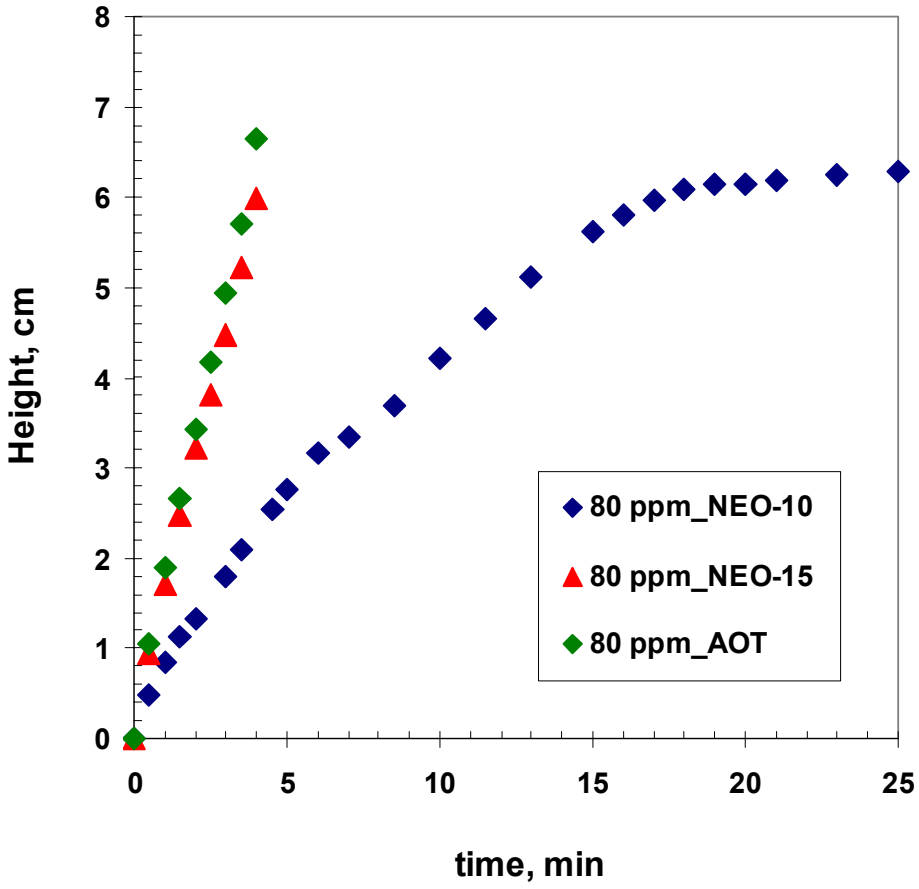

Figure B.2 Rag layer growth versus time. Dispersion with 80 ppm with different surfactants. Temperature = 45 ^{o} C, stirring speed = 800 rpm and flow rate = 45cm^3/min.

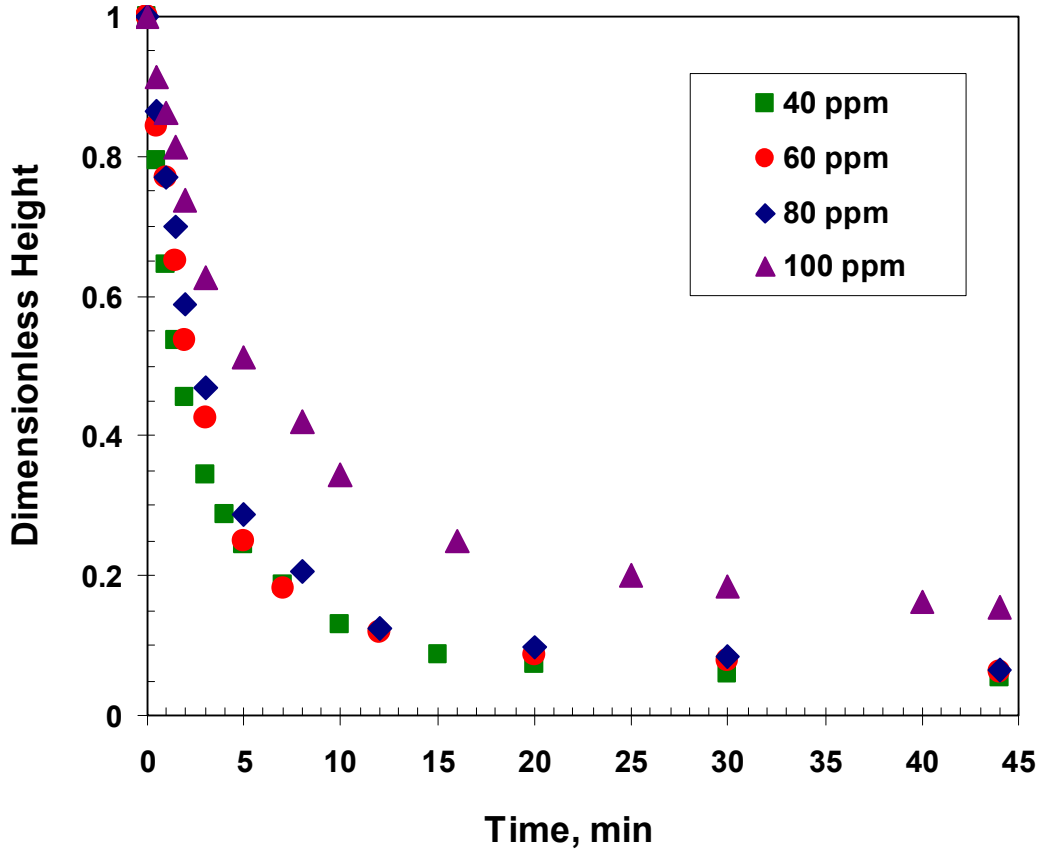

Figure B.3 Dimensionless rag and free water heights for a batch experiment on a water-in-oil emulsion (50 vol% water) prepared an organic phase of 50:50 heptane:toluene and an aqueous phase of 40, 60, 80 or 100 ppm NEO-10 in water emulsified at 800 rpm and 45°C.

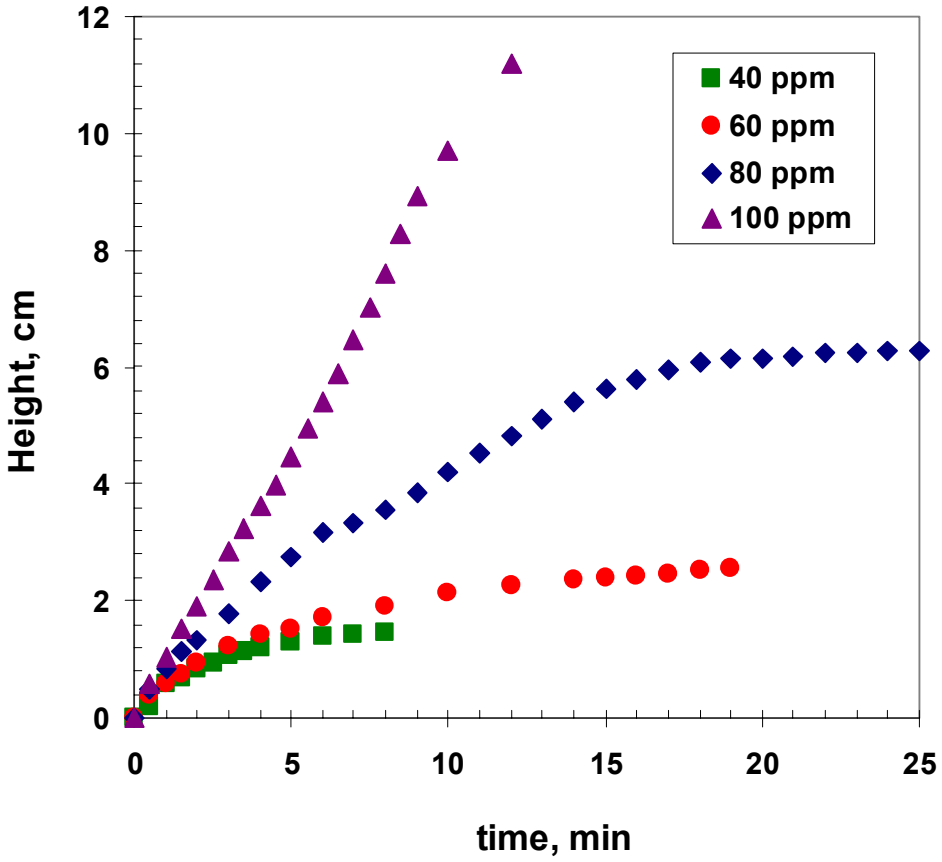

Figure B.4 Rag layer growth versus time. Dispersion at different NEO-10 concentration. Temperature = 45^{o} C, stirring speed = 800 rpm. Flow rate = 45cm^{3}/min.

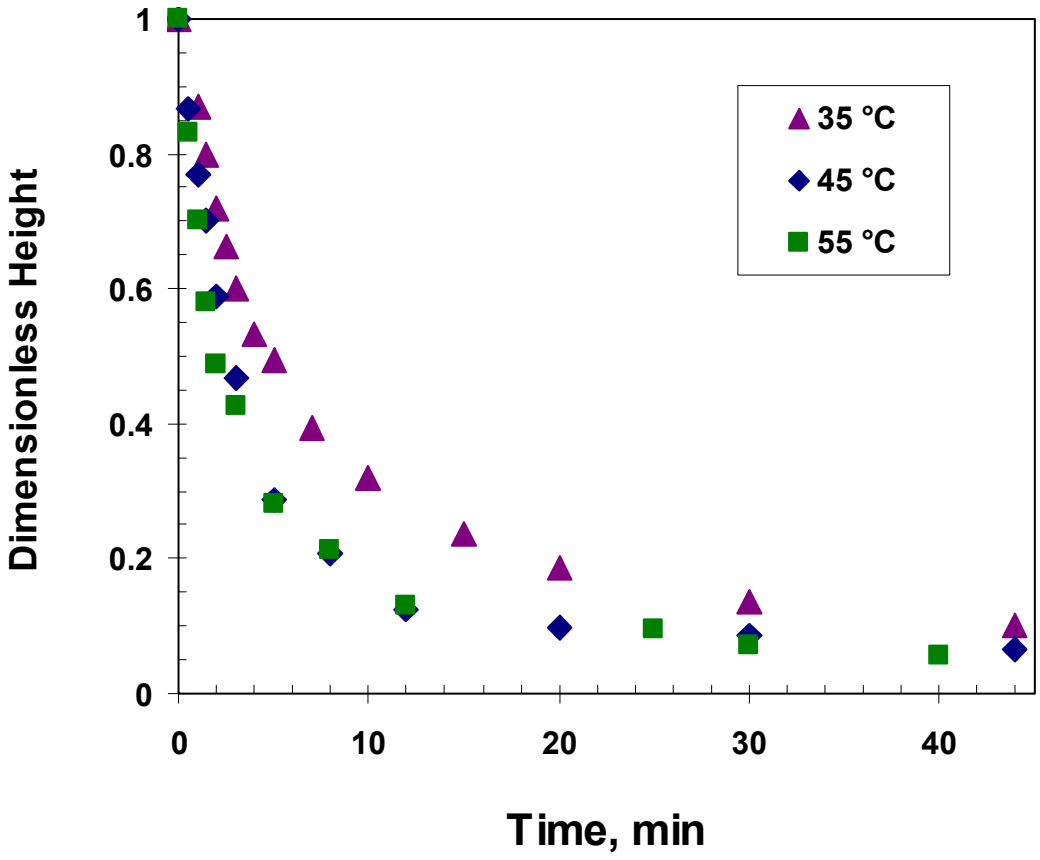

Figure B.5 Dimensionless rag and free water heights for a batch experiment on a water-in-oil emulsion (50 vol% water) prepared an organic phase of 50:50 heptane:toluene and an aqueous phase of 80 ppm NEO-10 in water emulsified at 800 rpm at different temperature.

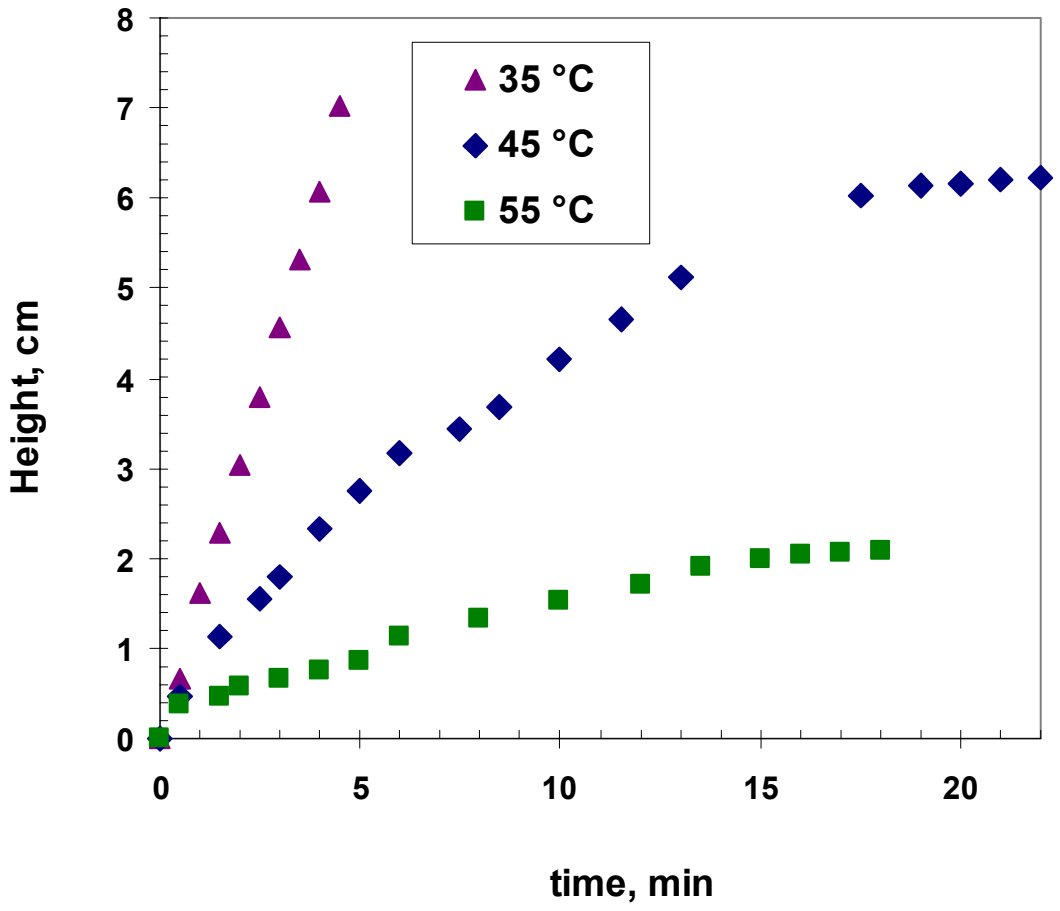

Figure B.6 Rag layer growth versus time. Dispersion with 80 ppm NEO-10 at different temperature, stirring speed = 800 rpm and flow rate = 45cm^3/min.

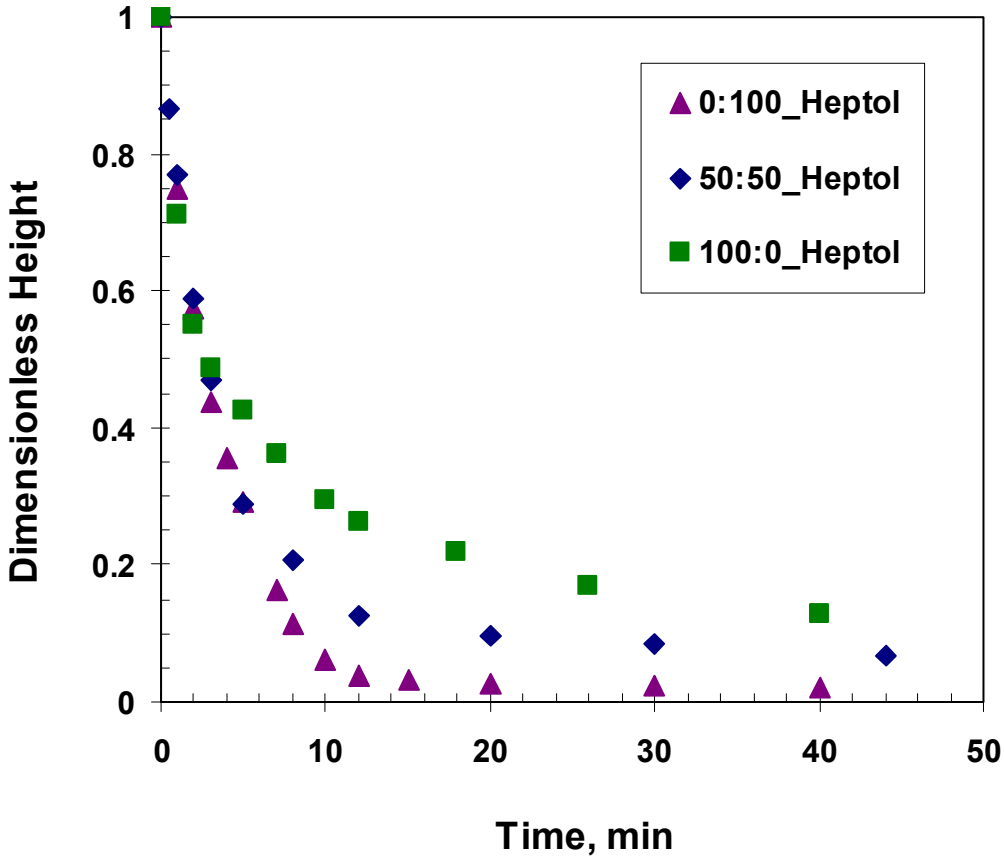

Figure B.7 Dimensionless rag and free water heights for a batch experiment on a water-in-oil emulsion (50 vol% water) prepared an organic phase of 50:50 heptane:toluene and an aqueous phase of 80 ppm NEO-10 in water emulsified at 800 rpm at different temperature.

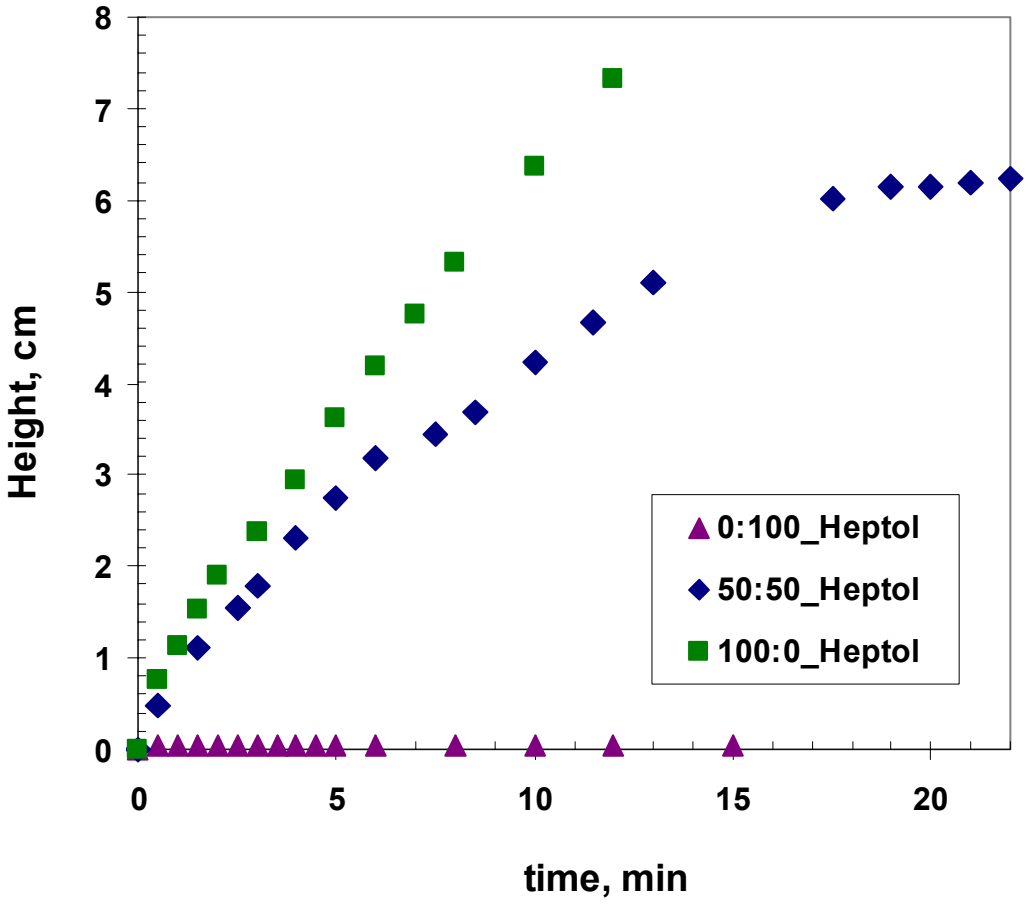

Figure B.8 Rag layer growth versus time. Dispersion with 80 NEO-10 at different solvent ratio. Temperature = 45 ^{o} C, stirring speed = 800 rpm and flow rate = 45cm^{3}/min.

APPENDIX C - ERROR ANALYSIS

The confidence intervals of the data were calculated from the mean, standard deviation and t-distribution for each type set of measurements. The error analysis was divided in three different sections; water volume fraction for batch and continuous experiments, rag layer height for batch experiments, and rag layer height for continuous experiments. A 95% confidence interval was used in all cases.

C.1 Water Volume Fraction

The data set consists of 8 pairs of repeated data (Tables C1 to C3). The mean value for each pair, $\bar{y}_j$, is determined from:

$$\bar{y}_j = \frac{\sum_{i=1}^{n} y_i}{n_j} \qquad \textbf{Equation C.1}$$

where n_j is the number of measurements for each set of repeats (2 in this case), and y_i is a measured value.

It was assumed that the distribution of error was the same for every pair of repeats. The standard deviation, s, was then calculated from the following relation:

$$s = \sqrt{\frac{\sum_{i=1}^{n} \left(y_{ji} - \bar{y}_j\right)^2}{n-1}} \qquad \textbf{Equation C.2}$$

where n is the total number measurements for all sets of repeats (16 in this case). Next, the confidence interval was determined for each pair of repeats as follows:

$$\bar{y}_j - t_{(\alpha/2,\nu)} \frac{s}{\sqrt{n_j}} \le \bar{y}_j \le \bar{y}_j + t_{(\alpha/2,\nu)} \frac{s}{\sqrt{n_j}} \qquad \textbf{Equation C.3}$$

where $\nu = n - 1$ and $\alpha = 1 -$ (%confidence/100); for example, for a 95% confidence, $\alpha/2 = 0.025$. Note that the standard deviation was determined from $n = 16$ measurements

and therefore $v = 15$. The corresponding value of t is 2.13 (Dean, J.A., 1999). Since only a pair of repeats was used in each case, the final confidence interval calculation was based on $n_j = 2$. Since pairs of repeats were used in all cases, the 95% confidence interval is the same in all cases and is ±0.020 volume fraction.

Table C.1 Reproducibility analysis for water volume fraction data during batch experiment for a water-in-oil emulsion (50 vol% water) prepared an organic phase of 50:50 heptane:toluene and an aqueous phase of 80 ppm NEO-10 in water emulsified at 800 rpm and 45°C.

NEO-10 model system	Time (min)	Data 1 wvf	Data 2 wvf	Mean wvf	Standard Deviation
Batch - 80 ppm					
	1	0.39	0.40	0.40	0.008
	3	0.27	0.28	0.27	0.009
	5	0.24	0.26	0.25	0.013
	8	0.21	0.23	0.22	0.015
	12	0.20	0.21	0.21	0.007
	20	0.16	0.18	0.17	0.012
	30	0.15	0.16	0.15	0.008
	44	0.15	0.16	0.15	0.004

Table C.2 Reproducibility analysis for water volume fraction data during rag layer growth in a continuous experiment for a water-in-oil emulsion (50 vol% water) prepared an organic phase of 50:50 heptane:toluene and an aqueous phase of 40 ppm NEO-10 in water emulsified at 800 rpm and 45°C. The flow rate = 45 cm^3 /min.

NEO-10 model system	Time (min)	Data 1 wvf	Data 2 wvf	Mean wvf	Standard Deviation
(40 ppm)					
	3	0.30	0.32	0.31	0.014
	5	0.26	0.28	0.27	0.014
	10	0.28	0.27	0.28	0.007

Table C.3 Reproducibility analysis for water volume fraction data during rag layer growth in a continuous experiment for a water-in-oil emulsion (50 vol% water) prepared an organic phase of 50:50 heptane:toluene and an aqueous phase of 80 ppm NEO-10 in water emulsified at 800 rpm and 45°C. The flow rate = 45 cm^3 /min.

NEO-10 model system	Time (min)	Data 1 wvf	Data 2 wvf	Mean wvf	Standard Deviation
(80 ppm)					
	3	0.38	0.37	0.38	0.007
	5	0.33	0.36	0.35	0.021
	10	0.35	0.32	0.34	0.021
	15	0.38	0.35	0.37	0.021
	20	0.36	0.35	0.36	0.007

C.2 Rag Layer Height in Batch Experiments

The data set included 8 pairs of repeats (Table C.4). The 95% confidence interval was calculated in the same way as for the water volume fractions and is ±0.25 cm.

Table C.4 Reproducibility analysis for rag layer height data during batch experiment for a water-in-oil emulsion (50 vol% water) prepared an organic phase of 50:50 heptane:toluene and an aqueous phase of 80 ppm NEO-10 in water emulsified at 800 rpm and 45°C.

NEO-10 model system	Time (min)	Data 1 cm	Data 2 Cm	Mean cm	Standard Deviation
Batch - 80 ppm					
	1	9.2	9.2	9.2	0.00
	3	5.6	5.5	5.6	0.08
	5	3.5	3.5	3.5	0.03
	8	2.5	2.3	2.4	0.16
	12	1.5	1.4	1.5	0.05
	20	1.9	1.1	1.5	0.61
	30	1.0	0.9	1.0	0.05
	44	0.8	0.7	0.8	0.06

C.3 Rag Layer Height in Continuous Experiments

The data set of the continuous experiments included 30 pairs of repeats collected over a variety of conditions (Tables C.5 to C.9). It was observed that the absolute error varied systematically but the relative error varied randomly. Therefore, the standard deviation of a distribution of relative deviations was determined as follows:

$$s = \sqrt{\frac{\sum_{i=1}^{n} \left(y_{ji} - \bar{y}_j \Big/ \bar{y}_j \right)^2}{n-1}} \qquad \textbf{Equation C.4}$$

Then, the confidence interval was determined for each pair of repeats as follows:

$$\bar{y}_j \left(1 - t_{(\alpha/2,\nu)} \frac{s}{\sqrt{n_j}} \right) \le \bar{y}_j \le \bar{y}_j \left(1 + t_{(\alpha/2,\nu)} \frac{s}{\sqrt{n_j}} \right) \qquad \textbf{Equation C.5}$$

The term $\pm t_{(\alpha/2,\nu)} \frac{s}{\sqrt{n_j}}$ is the 95% confidence interval for a relative deviation and is 6.4%.

Table C.5 Reproducibility analysis for rag layer height data during rag layer growth in a continuous experiment for a water-in-oil emulsion (50 vol% water) prepared an organic phase of 50:50 heptane:toluene and an aqueous phase of 40 ppm NEO-10 in water emulsified at 800 rpm and 45°C. The flow rate into the separator was 45 cm³ /min.

NEO-10 model system	Time (min)	Data 1 cm	Data 2 cm	Mean cm	Standard Deviation
(40 ppm)					
	3	1.1	1.2	1.2	0.02
	5	1.3	1.4	1.4	0.04
	8	1.5	1.5	1.5	0.04

Table C.6 Reproducibility analysis for rag layer height during rag layer growth in a continuous experiment for a water-in-oil emulsion (50 vol% water) prepared an organic phase of 50:50 heptane:toluene and an aqueous phase of 80 ppm NEO-10 in water emulsified at 800 rpm and 45°C. The flow rate into the separator was 45 cm^3 /min.

NEO-10 model system	Time (min)	Data 1 cm	Data 2 cm	Mean cm	Standard Deviation
(80 ppm)					
	1	0.9	1.0	0.9	0.07
	3	1.8	2.1	1.9	0.21
	5	2.8	3.0	2.9	0.20
	8	3.6	4.3	3.9	0.46
	10	4.2	4.8	4.5	0.44
	15	5.6	5.7	5.6	0.02
	20	6.2	5.9	6.0	0.15

Table C.7 Reproducibility analysis for rag layer height data during rag layer growth in a continuous experiment for a water-in-oil emulsion (50 vol% water) prepared an organic phase of 50:50 heptane:toluene and an aqueous phase of 80 ppm NEO-10 in water emulsified at 800 rpm and 45°C. The flow rate = 45 cm^3 /min. Cross sectional area 2= 14.4 cm^2.

NEO-10 model system	Time (min)	Data 1 cm	Data 2 cm	Mean cm	Standard Deviation
Area 2= 14.4 cm2					
	1	0.6	0.6	0.6	0.05
	3	1.0	1.1	1.1	0.05
	5	1.3	1.5	1.4	0.11
	8	1.7	1.8	1.8	0.12
	10	1.8	2.1	1.9	0.15
	15	2.3	2.4	2.4	0.13
	20	2.5	2.6	2.5	0.11
	22	2.6	2.7	2.6	0.07

Table C.8 Reproducibility analysis for rag layer height data during rag layer growth in a continuous experiment for a water-in-oil emulsion (50 vol% water) prepared an organic phase of 50:50 heptane:toluene and an aqueous phase of 80 ppm NEO-10 in water emulsified at 800 rpm and 45°C. The flow rate into the separator was 40 cm^3 /min.

NEO-10 model system	Time (min)	Data 1 cm	Data 2 cm	Mean cm	Standard Deviation
40 cm3/min					
	1	0.8	0.7	0.7	0.07
	3	1.5	1.3	1.4	0.13
	5	1.9	1.7	1.8	0.13
	8	2.5	2.3	2.4	0.13
	10	2.9	2.7	2.8	0.13
	15	3.6	3.7	3.7	0.07
	20	3.9	4.1	4.0	0.10

Table C.9 Reproducibility analysis for rag layer height data during rag layer growth in a continuous experiment for a water-in-oil emulsion (50 vol% water) prepared an organic phase of 50:50 heptane:toluene and an aqueous phase of 80 ppm NEO-10 in water emulsified at 800 rpm and 45°C. The flow rate into the separator was 50 cm^3 /min.

NEO-10 model system	Time (min)	Data 1 cm	Data 2 cm	Mean cm	Standard Deviation
50 cm3/min					
	1	1.4	1.3	1.4	0.07
	3	3.9	3.5	3.7	0.27
	5	5.5	5.4	5.5	0.07
	8	8.0	8.3	8.1	0.20
	10	9.5	10.4	9.9	0.60